U.PORTO

Universidade do Porto
FEUP Faculdade de Engenharia

Dynamical Analysis of Partial Damping Treatments in Laminated Composite Plates

Jaime Filipe dos Santos Correia

Dissertation submitted to
Faculdade de Engenharia da Universidade do Porto
for the degree of:

Mestre em Engenharia Mecânica

Advisor:
Prof. José Dias Rodrigues
(Associate Professor)

Co-Advisor:
Eng. João Pereira Amorim

Laboratório de Vibrações de Sistemas Mecânicos
Departamento de Engenharia Mecânica
Faculdade de Engenharia da Universidade do Porto

Porto, 2021

The work presented in this dissertation was performed at the
Laboratory of Vibrations of Mechanical Systems
Department of Mechanical Engineering
Faculty of Engineering
University of Porto
Porto, Portugal.

Jaime Filipe dos Santos Correia
E-mail: up201605371@edu.fe.up.pt

Faculdade de Engenharia da Universidade do Porto
Departamento de Engenharia Mecânica
Laboratório de Vibrações de Sistemas Mecânicos
Rua Dr. Roberto Frias s/n, Sala M206
4200-465 Porto
Portugal

Abstract

Technological advances and the continuous evolution of industries, such as aeronautics, have enhanced the development of structures and mechanisms where noise and vibration control plays a prominent role in their design.

In this dissertation, a dynamic analysis of composite laminated plates is performed, in which passive vibration control takes place, through integrated partial viscoelastic damping treatments. In addition, a qualitative and quantitative study is also carried out on the influence of different parameters of the structure, with an evaluation of its impact on the efficiency of the applied treatments.

Dynamic analysis is performed through the experimental study of seven plates, previously manufactured. The specimens include rectangular plates with integrated viscoelastic damping treatments, either total and partially distributed. Different viscoelastic materials withstanding composite cure are considered. For this study, these plates were cut and the instrumented halves were analyzed. The code implemented in MATLAB ®, using the Finite Element Method and a Layerwise Theory, generates frequency response functions. An analysis of the correlation between numerical and experimental FRF's is done, in order to observe the influence of the relationship between the length/thickness ratio of the plate, allowing the comprehension of the influence on the effectiveness of partial damping treatments.

Following this, the parametric analysis of the plates takes place. Concerning the viscoelastic strips, the parameters in focus are the width, their thickness, the location of these strips in relation to the middle plane of the plate and their orientation (0° or 90°) in relation to one of the axes of the plate. Concerning the composite layers, their fiber orientations are analyzed as well.

The parameters concerning the viscoelastic strips are appraised in order to study how mode shapes affect the damping capacity that can be obtained for some viscoelastic treatment, as well as understand the effectiveness of a partial damping treatment and what advantages it brings when compared with total treatments. Regarding fiber orientations, a different study is done: a parametric method is used to establish possible stacking sequences that maximize the values already obtained by the manufactured plates. An evolutionary optimization algorithm provides support to the parametric method since this last one was only used before to maximize natural frequencies, instead of loss factors.

Keywords: Layerwise Theory, Vibration Damping, Viscoelastic Damping Treatment, Frequency Response Function, Viscoelastic Materials, Finite Element Method, Dynamical Analysis, Parametric Analysis, Fiber Orientation, Loss Factor, Layerwise Optimization Approach

Resumo

Os avanços tecnológicos e a crescente evolução de indústrias competitivas, como a aeronáutica, potenciaram o desenvolvimento de estruturas e mecanismos onde o controlo de ruído e vibrações assume um papel de destaque no design das mesmas.

Nesta dissertação, é efetuada uma análise dinâmica de placas laminadas compósitas, nas quais é feito o controlo passivo de vibrações através de tratamentos parciais viscoelásticos integrados de amortecimento. Além disso, também é efetuado um estudo qualitativo e quantitativo acerca da influência de diferentes parâmetros da estrutura, com avaliação do seu impacto na eficiência dos tratamentos aplicados. A análise dinâmica é realizada através do estudo experimental de sete placas, previamente analisadas. Incluem-se neste grupo placas retangulares com tratamentos integrados viscoelásticos de amortecimento, sejam total ou parcialmente distribuídos. Diferentes materiais viscoelásticos foram considerados para o fabrico das mesmas. O código implementado em MATLAB®, recorrendo ao Método dos Elementos Finitos e a uma Teoria Layerwise, gera funções de resposta em frequência. É feita uma análise da correlação entre FRF's numéricas e experimentais, com vista à observação da influência da relação entre o comprimento/largura e a espessura da placa, de modo a perceber os seus efeitos na eficácia dos tratamentos parciais integrados de amortecimento.

De seguida, tem lugar a análise paramétrica das placas. No que diz respeito às tiras viscoelásticas, os parâmetros em análise são a sua largura, a sua espessura, a localização destas placas em relação ao plano médio da placa, a sua orientação (0° ou 90°) em relação a um dos eixos da placa. No que toca às camadas de material compósito, é apresentada uma análise acerca da orientação das fibras destas camadas.

Os parâmetros respeitantes às tiras viscoelásticas são analisados de modo a aferir de que modo as formas naturais influenciam o fator de perda que é possível obter para um dado tratamento viscoelástico, bem como compreender a efetividade de um tratamento parcial de amortecimento e que vantagens traz em relação aos tratamentos totais. A relação entre a variação do fator de perda e da frequência natural também é discutida com especial interesse. Quanto à orientação das fibras, é feito um estudo de otimização distinto, onde um método paramétrico é utilizado para estabelecer possíveis sequências de empilhamento que maximizem os valores já obtidos pelas placas fabricadas. Um algoritmo de otimização evolucionário permitirá compreender a efetividade do método paramétrico anterior, já que este apenas é apresentado para maximização de frequências naturais e não para fatores de perda.

Palavras-Chave: Teoria Layerwise, Amortecimento de Vibrações, Funções de Resposta em Frequência, Materiais Viscoelásticos, Método dos Elementos Finitos, Análise Dinâmica, Análise Paramétrica, Fator de Perda, *Layerwise Optimization Approach*.

"Far better it is to dare mighty things, to win glorious triumphs, even though checkered by failure, than to rank with those poor spirits who neither enjoy nor suffer much, because they live in the gray twilight that knows not victory nor defeat."

Theodore Roosevelt

Acknowledgements

I want to thank my advisor, Professor José Dias Rodrigues, for the opportunity to work in an area that I am delighted in, for the trust and all the suggestions in key moments.

To my co-advisor, Professor João Amorim, thank you for all the patience, the conversations and the eye for detail, which was so important during these months. I am also thankful for the availability and enthusiasm on my work.

To my friends, thank you for your kindness, friendship and laughs during the last five years. Your support was always encouraging to face each day we shared. It was incredible to live this unforgettable experience with you all.

To my family: to my uncles and cousins who are always there to cheer up for me; to my godparents, who always were an inspiration to me; and to my grandparents, who will always be my example of strength.

To my parents, thank you for the flexibility, for the support, to make me believe in my dreams and that I was capable of reaching my goals. To my sister, thank you for your peculiar, but full of meaning support, during this journey.

Contents

Abstract i

Resumo iii

Acknowledgements vii

List of Figures xi

List of Tables xiii

List of Symbols xvii

1 Introduction 1
- 1.1 Damping in Structural Engineering . . . 1
- 1.2 Viscoelastic Damping Treatments . . . 2
- 1.3 Optimization of Viscoelastic Treatments . . . 4
  - 1.3.1 Partial Local Treatments . . . 4
- 1.4 Motivation . . . 5
- 1.5 Objectives . . . 6
- 1.6 Organization of the Dissertation . . . 6

2 Structural and Damping Materials 9
- 2.1 Introduction . . . 9
- 2.2 Composite Materials . . . 9
  - 2.2.1 Basic Terminology . . . 9
  - 2.2.2 General Types of Laminate Configurations . . . 10
  - 2.2.3 Symmetric Laminated Plates . . . 11
- 2.3 Viscoelastic Materials . . . 11
  - 2.3.1 Considerations on Temperature and Frequency Dependence . . . 12
  - 2.3.2 Harmonic Load and VEM's Response . . . 13
  - 2.3.3 Complex Modulus . . . 14
  - 2.3.4 Fractional Derivative Model . . . 15

3 Mechanical Model 17
- 3.1 Introduction . . . 17
- 3.2 Classic Thick Plate Theories . . . 18
- 3.3 Layerwise Plate Theory . . . 18
  - 3.3.1 Displacement Field . . . 20
  - 3.3.2 Strain Field . . . 20
  - 3.3.3 Stress Field of Isotropic Materials . . . 23

3.3.4 Stress Field of Orthotropic Materials . . . 24
3.3.5 Strain Energy . . . 25
3.3.6 Kinetic Energy . . . 26
3.4 Finite Element Formulation . . . 28
3.4.1 Discretization . . . 29
3.4.2 Variational Formulation . . . 30
3.4.3 Stiffness and Mass Matrices . . . 30
3.4.4 Coordinate Transformation . . . 31
3.4.5 Assembling with Partial Damping Treatments . . . 31
3.4.6 Shear Locking . . . 32
3.5 Equations of Motion . . . 32
3.6 Modes of Vibration . . . 33
3.7 Frequency Response Functions . . . 33
3.7.1 Direct Frequency Analysis . . . 33
3.7.2 Partial Fraction Expansion . . . 34
3.8 Numerical Validation . . . 34
3.8.1 Influence of the Mesh Size . . . 35
3.8.2 Number of Layers . . . 36

4 Dynamical Analysis of Viscoelastic Damping Treatments 37
4.1 Introduction . . . 37
4.2 Viscoelastic Materials . . . 37
4.3 Specimens Characterization . . . 38
4.4 Experimental Setup and Procedure . . . 41
4.5 Frequency Domain Based Approaches . . . 44
4.6 Correlation Indicator . . . 45
4.7 Reference Plate Results: 254×198 mm . . . 46
4.7.1 Reference Plate . . . 46
4.7.2 SMACWRAP® 0.2 mm Damping Treatment . . . 47
4.7.3 SMACWRAP® 0.1 mm Damping Treatment . . . 48
4.7.4 KRAIBON® 0.5 mm Damping Treatment . . . 50
4.8 Reference Plate Results: 198×126 mm . . . 52
4.9 Influence of Thickness and Damping Materials . . . 54
4.10 Total and Partial Damping Treatments . . . 56
4.10.1 SMACWRAP® 0.2 mm . . . 56
4.10.2 SMACWRAP® 0.1 mm . . . 59
4.10.3 KRAIBON® 0.5 mm . . . 63

5 Parametric Study on the Efficiency of Partial Damping Tratments 69
5.1 Introduction . . . 69
5.2 Configurations and Mesh Parameters . . . 69
5.3 Width and Location - SMACWRAP® 0.2 mm Configurations . . . 71
5.3.1 Width Increase from the Edges to the Center - Configuration 1, E-C 71
5.3.2 Width Increase from Center to the Edges - Configuration 1, C-E . . 72
5.3.3 Discussion and Comparison of Configurations 1, C-E and E-C . . . 74
5.4 Width and Location - SMACWRAP® 0.1 mm Configurations . . . 75
5.4.1 Width Increase from Edges to the Center - Configuration 1, E-C . . 76
5.4.2 Width Increase from Center to the Edges - Configuration 1, C-E . . 78
5.4.3 Discussion and Comparison of both Configurations . . . 80
5.5 Notes and Remarks about Width and Location . . . 81

5.6 Position of the Viscoelastic Strips 83
5.6.1 Width increase 84
5.6.2 Remarks on the Location of Viscoelastic Strips 87
5.7 Influence of Viscoelastic Layer's Thickness 87
5.8 Fiber Orientation 89
5.8.1 Layerwise Optimization Approach 89
5.8.2 Teaching Learning Based Optimization 94
5.9 Optimized Stacking Sequence Analysis 97

6 Conclusion **101**
6.1 Conclusions 101
6.2 Future Work 103

References **105**

A Assembly **109**
A.1 Introduction 109
A.2 Assembly 109

List of Figures

1.1 Free Layer damping treatment. 3
1.2 Constrained Layer Damping treatment. 3
1.3 Integrated Layer Damping treatment. 4
1.4 Partial damping treatment using Free Layer Damping configuration. 5
1.5 Integrated partial damping treatments. 5

2.1 Laminate composite plate. 10
2.2 Local and global coordinate system. 11
2.3 Loss factor and shear storage modulus dependence of temperature (adapted from Nashif et al. [1985]). 12
2.4 Loss factor and shear storage modulus dependence of frequency (adapted from Nashif et al. [1985]). 13
2.5 Lag between stress and strain field (adapted from Moreira [2004]). 13
2.6 Hysteresis loop (adapted from Moreira [2004]). 14

3.1 Deformation profiles according to different theories (adapted from Liew et al. [2019]). 18
3.2 Layerwise model (adapted from Moreira [2004]). 19
3.3 Four-node quadrilateral element in natural coordinate system. 28

4.1 Storage modulus and loss factor of SMACWRAP ST ®. 38
4.2 Storage modulus and loss factor of KRAIBON ®. 38
4.3 Mesh (the lighter area represents the location of the viscoelastic strips). . . 39
4.4 Laminate composite plate. 39
4.5 SMACWRAP ST ® 0.2 mm configurations. 40
4.6 SMACWRAP ST ® 0.1 mm configurations. 40
4.7 KRAIBON ® 0.5 mm configurations. 41
4.8 Suspended Plate. 41
4.9 Instrumented plate. 42
4.10 Excitation of the system. 42
4.11 Laser Doppler Vibrometer System. 43
4.12 FFT spectral analyser. 43
4.13 Diagram of the experimental setup. 44
4.14 Numerical and experimental FRF_{33} for the reference base plate. 46
4.15 LAC for the FRF_{33} of the reference base plate. 46
4.16 Numerical and experimental FRF_{33} for the base plate with SMACWRAP ® 0.2 mm total damping treatment. 47
4.17 LAC for the FRF_{33} for the base plate with SMACWRAP ® 0.2 mm total damping treatment. 47

4.18 Numerical and experimental FRF_{33} for the base plate with SMACWRAP ® 0.2 mm partial damping treatment. 48
4.19 LAC for the FRF_{33} for the base plate with SMACWRAP ® 0.2 mm partial damping treatment. 48
4.20 Numerical and experimental FRF_{33} for the base plate with SMACWRAP ® 0.1 mm total damping treatment. 49
4.21 LAC for the FRF_{33} for the base plate with SMACWRAP ® 0.1 mm total damping treatment. 49
4.22 Numerical and experimental FRF_{33} for the base plate with SMACWRAP ® 0.1 mm partial damping treatment. 50
4.23 LAC for the FRF_{33} for the base plate with SMACWRAP ® 0.1 mm partial damping treatment. 50
4.24 Numerical and experimental FRF_{33} for the base plate with KRAIBON ® 0.5 mm total damping treatment. 51
4.25 LAC for the FRF_{33} for the base plate with KRAIBON ® 0.5 mm total damping treatment. 51
4.26 Numerical and experimental FRF_{33} for the base plate with KRAIBON ® 0.5 mm partial damping treatment. 52
4.27 LAC for the FRF_{33} for the base plate with KRAIBON ® 0.5 mm partial damping treatment. 52
4.28 Numerical and experimental FRF_{33} for the reference base plate. 53
4.29 LAC for the FRF_{33} of the reference base plate. 53
4.30 Numerical and experimental FRF_{63} for the reference base plate. 54
4.31 LAC for the FRF_{63} of the reference base plate. 54
4.32 Experimental point FRF's of the reference plate, KRAIBON ® 0.5 mm configuration and SMACWRAP ® 0.2 mm configuration. 55
4.33 Experimental transfer FRF's of the reference plate, KRAIBON ® 0.5 mm configuration and SMACWRAP ® 0.2 mm configuration. 55
4.34 Numerical and experimental FRF_{33} for SMACWRAP ® 0.2 mm total damping treatment configuration. 56
4.35 LAC for the FRF_{33} with SMACWRAP ® 0.2 mm total damping treatment configuration. 56
4.36 Numerical and experimental FRF_{33} for SMACWRAP ® 0.2 mm partial damping treatment configuration. 57
4.37 LAC for the FRF_{33} with SMACWRAP ® 0.2 mm partial damping treatment configuration. 57
4.38 Numerical and experimental FRF_{63} for SMACWRAP ® 0.2 mm total damping treatment configuration. 58
4.39 LAC for the FRF_{63} with SMACWRAP ® 0.2 mm total damping treatment configuration. 58
4.40 Numerical and experimental FRF_{63} for SMACWRAP ® 0.2 mm partial damping treatment configuration. 59
4.41 LAC for the FRF_{63} with SMACWRAP ® 0.2 mm partial damping treatment configuration. 59
4.42 Numerical and experimental FRF_{33} for SMACWRAP ® 0.1 mm total damping treatment configuration. 60
4.43 LAC for the FRF_{33} with SMACWRAP ® 0.1 mm total damping treatment configuration. 60

4.44 Numerical and experimental FRF_{33} for SMACWRAP® 0.1 mm partial damping treatment configuration. 61
4.45 LAC for the FRF_{33} with SMACWRAP® 0.1 mm partial damping treatment configuration. 61
4.46 Numerical and experimental FRF_{63} for SMACWRAP® 0.1 mm total damping treatment configuration. 62
4.47 LAC for the FRF_{63} with SMACWRAP® 0.1 mm total damping treatment configuration. 62
4.48 Numerical and experimental FRF_{63} for SMACWRAP® 0.1 mm partial damping treatment configuration. 63
4.49 LAC for the FRF_{63} with SMACWRAP® 0.1 mm partial damping treatment configuration. 63
4.50 Numerical and experimental FRF_{33} for KRAIBON® 0.5 mm total damping treatment configuration. 64
4.51 LAC for the FRF_{33} with KRAIBON® 0.5 mm total damping treatment configuration. 64
4.52 Numerical and experimental FRF_{33} for KRAIBON® 0.5 mm partial damping treatment configuration. 65
4.53 LAC for the FRF_{33} with KRAIBON® 0.5 mm partial damping treatment configuration. 65
4.54 Numerical and experimental FRF_{63} for KRAIBON® 0.5 mm total damping treatment configuration. 66
4.55 LAC for the FRF_{63} with KRAIBON® 0.5 mm total damping treatment configuration. 66
4.56 Numerical and experimental FRF_{63} for KRAIBON® 0.5 mm partial damping treatment configuration. 67
4.57 LAC for the FRF_{63} with KRAIBON® 0.5 mm partial damping treatment configuration. 67

5.1 Configuration E-C: direction of width increase, with the upper view of the plate on the left and the generic representation of width from Step 1 to Step N on the right. 70
5.2 Configuration C-E: direction of width increase, with the upper view of the plate on the left and the generic representation of width from Step 1 to Step N on the right. 70
5.3 Location of the viscoelastic strips at the plate. 71
5.4 Stacking sequence and position with SMACWRAP® 0.2 mm strips and Configuration 1, E-C. 71
5.5 Influence of the width increase from the edges to the center. 72
5.6 Stacking sequence and position with SMACWRAP® 0.2 mm strips and Configuration 1, C-E. 72
5.7 Influence of the width increase from center to the edges. 73
5.8 Comparison of loss factor and natural frequency between configurations E-C C-E with SMACWRAP® 0.2 mm strips for the first six modes of vibration. 74
5.9 Comparison between natural frequency and loss factor. 75
5.10 Stacking sequence and position with SMACWRAP® 0.1 mm strips and Configuration 1, E-C. 76
5.11 Influence of the width increase from the edges to the center. 76
5.12 Mode shapes between 41.7% and 66.7% covered area (switches between 50% and 58.3%). 77

5.13 Stacking sequence and position with SMACWRAP ® 0.1 mm strips and Configuration 1, C-E. 78
5.13 Influence of the increase of width from the edges to the center. 78
5.14 Mode shapes between 33.3% and 58.3% covered area (switches between 41.7% and 50%). 79
5.15 Comparison of loss factor and frequency between Configurations E-C and C-E using SMACWRAP ® 0.1 mm for the first six modes of vibration. . . . 80
5.16 Comparison between SMACWRAP ® 0.2 mm (S 0.2) and SMACWRAP ® 0.1 mm (S 0.1) arrangements, in E-C and C-E configurations, in terms of natural frequency and loss factor. 82
5.17 Influence of width increase for viscoelastic strips along the shortest edges. . 85
5.18 Mode shapes between 50% and 87.5% covered area. 86
5.19 Stacking sequence and position of viscoelastic strips. 88
5.20 Thickness evaluation of thickness ratio, $\frac{h_{VEM}}{h_{Hexcel}}$. 88
5.21 Layerwise Optimization Approach for a symmetric six-layered plate. 90
5.22 First step of the first iteration of Layerwise Optimization Approach. 91
5.23 Convergence of loss factor with P_n=200 and 50 iterations. 97
5.24 Comparison between the optimized configuration and the original configuration regarding loss factor. 98
5.25 Comparison between the optimized configuration and the original configuration regarding natural frequency. 98

A.1 Beam with partial damping treatments. 109

List of Tables

3.1 Four node quadrilateral element's shape functions. 29
3.2 Properties of the plate. 35
3.3 Theoretical nondimensionalized frequencies $\bar{\omega}$ of four layer cross-ply laminates [Reddy, 2003]. 35
3.4 Nondimensionalized frequencies $\bar{\omega}$ of four layer cross-ply laminates. 36
3.5 Nondimensionalized frequencies $\bar{\omega}$ of eight layer cross-ply laminates. 36

4.1 SMACWRAP ST ® constitutive model parameters at 24°C. 37
4.2 KRAIBON ® constitutive model properties at 24°C. 38
4.3 Properties of Hexcel 8552 IM7®. 39
4.4 Sensitivity of the transducers. 43

5.1 Covered area on each step for each configuration. 71
5.2 Loss factor of the six modes of vibration for each arrangement. 83
5.3 Loss factor of the six modes of vibration for each arrangement. 87
5.4 VEM thickess on each step. 87
5.5 Maximization of the fundamental natural frequency. 92
5.6 Comparison of loss factors between original stacking sequence and optimal for natural frequency. 92
5.7 Maximization of the loss factor for the first mode of vibration. 93
5.8 Comparison of loss factors between the optimized stacking sequence for maximum natural frequency and optimal stacking sequence for maximum loss factor. 93
5.9 Maximization of the loss factor for the first mode of vibration, with hypothetical layers with mass but no stiffness. 93

List of Symbols

Indices

i	counter
0	reference layer

Identifiers

$()^e$	relative to e-th element of the mesh
$()_k$	refering to k-th layer of the laminate
$()_r$	refering to r-th mode of vibration
$()^{\mathrm{B}}$	relative to bending component
$()^{\mathrm{C}}$	relative to coupling component
$()^{\mathrm{MC}}$	relative to membrane + coupling component
$()^{\mathrm{M}}$	relative to membrane component
$()^{\mathrm{S}}$	relative to shear component

Acronyms

AMT	Abartsumian Multilayered Theory
CFRP	Carbon-Fiber-Reinforced Polymers
CLD	Constrained Layer Damping
ESL	Equivalent Single Layer (theories)
FLD	Free Layer Damping
FRF	Frequency Response Function
HSDT	High-Order Shear Deformation Theory
ICE	Iterative Complex Eigensolution Approach
ILD	Integrated Layer Damping
IMSE	Iterative Modal Strain Energy Approach
LMT	Lekhnitskii Multilayered Theory
LOA	Layerwise Optimization Approach
MSE	Modal Strain Energy Approach
RMT	Reissner Multilayered Theory
TLBO	Teacher Learner Based Optimization
VEM	Viscoelastic materials

Operators

$[\mathcal{L}]$	differential operator
$\ddot{\bullet}$	second time order derivative
δ	virtual work operator
$\dfrac{\partial}{\partial i}$	partial derivative in order to i
$\dfrac{d}{dt}$	time order derivative
$\dot{\bullet}$	first order time derivative
$\Gamma(1-\alpha)$	Gamma function

Scalar variables

α	order of the fractional order derivative
$\alpha(\omega)$	frequency response function in the form of receptance
$\bar{A}(j\omega)$	accelerance phasor
$\bar{V}(j\omega)$	mobility phasor
$\bar{X}(j\omega)$	receptance phasor
β_x, θ_y	rotation around y axis

β_y	symmetric of rotation around x axis
δ_l	lag
η	loss factor
γ	shear strain
λ	shear correction factor
ν	Poisson ratio
Ω	volume unit
ω	frequency
ω_r	natural frequency
Π^{K}	total kinetic energy of the system
Π^{P}	total strain energy of the system
ρ	density
σ	stress
σ^*	complex stress
σ_0	stress amplitude
τ	relaxation time
τ	shear stress
θ	fiber orientation
θ_x	rotation around y axis
ε	strain
ε	strain
ε^*	complex strain
ε_0	strain amplitude
A	area of integration
$A(\omega)$	frequency response function in the form of accelerance
b	width
E	Young modulus
E'	storage modulus
E''	loss modulus
E^*	extensional complex modulus
E_0	static modulus of elasticity
E_∞	dynamic modulus at high frequency
E_{opt}	Optimization error
G	Shear modulus
G^*	complex shear modulus
G_0	relaxed shear modulus
G_∞	dynamic shear modulus at high frequency
h	thickness of the layer
j	imaginary operator $j = \sqrt{-1}$
l	length
Q	plane stress-reduced stiffness
Q^*	complex plane stress-reduced stiffness
t	time
T_g	glass transition temperature
T_s	softening temperature
u	displacement in the x-direction
v	displacement in the y-direction
w	displacement in the z-direction
$Y(\omega)$	frequency response function in the form of mobility
z_k	height of the middle plane of the k-th layer in relation to the middle plane of the reference layer
$X(\omega)$	phase vector of the response

Matrix Variables

$[\bar{K}(\omega, T)]$	stiffness matrix dependent on frequency ω and temperature T
$[\bar{Q}]$	plane stress-reduced stiffness matrix
$[\widehat{\mathcal{B}}]$	modified deformation matrix
$[\widehat{\mathcal{D}}]$	modified constitutive law of the material
$[\mathcal{B}]$	deformation matrix

$[\mathcal{D}]$ constitutive law of the material

$[\mathcal{J}]$ diagonal inertia matrix of the layer

$[\mathcal{N}]$ matrix of coefficients h and z from generalized displacement field

$[\Omega^2]$ diagonal matrix of the square values of natural frequencies

$[\phi]$ normalized modal matrix

$[\mathbf{A}]$ extensional stiffness matrix

$[\mathbf{B}]$ bending-extensional stiffness matrix

$[\mathbf{D}]$ bending stiffness matrix

$[\mathbf{C}]$ coefficient matrix to obtain transverse shear matrix in orthotropic materials

$[\mathbf{J}]$ Jacobian matrix

$[\widehat{J}]$ modified inertia matrix

$[B]$ deformation matrix in the natural coordinate system

$[C]$ coefficient matrix to obtain elasticity matrix in orthotropic materials

$[D]$ constitutive law of the material (bending)

$[G]$ constitutive law of the material (transverse shear)

$[I]$ identity matrix

$[J]$ inertia matrix of the layer

$[K]$ stiffness matrix

$[M]$ mass matrix

$[N]$ shape function matrix

$[T]$ transformation matrix

$[Z(\omega)]$ dynamic stiffness matrix

$\{\phi\}$ i-th mode shape

$\{\sigma\}$ stress field

$\{\varepsilon\}$ strain field

$\{d\}$ generalized displacement field

$\{F(\omega)\}$ phase vector

$\{f(t)\}$ load vector

$\{x(t)\}$ response function

Other Symbols

$1, 2, 3$ coordinate system of laminae

ξ, η natural coordinate system

x, y, z cartesian coordinate referential

Chapter 1

Introduction

1.1 Damping in Structural Engineering

Damping is important to the reduction of the oscillation amplitude of the generated response by a dynamic system, due to an excitation. That is possible because damping promotes the dissipation of the energy proceeding from the excitation. However, damping values need to be under watch, to prevent some possible consequences of its application, such as limitations in the operation or design modifications of the structure to get some space for damping devices [Silva, 2007]. High damping values provide low vibration and noise levels, although low damping levels offer high sensitivity to structures. Usually, thermal energy is the result of the conversion of the dissipated energy at an atomic-scale level, so damping may be considered a macro-scale phenomenon of dissipation [Akay and Carcaterra, 2014].

Some industries, like aeronautics, are currently facing new challenges. The development of several optimization methods throughout the years is bearing fruit. The manufacturing of more efficient structures allows the maximization of the efficiency of the design process. Within design variables, weight is in evidence. The weight of a structure can compromise the costs of its operation. For that reason, weight has been a point of interest in the latest research, to improve efficiency by reducing costs with fuel consumption [Zhu et al., 2018].

However, weight loss brings some concerns. Lightweight structures dissipate residual quantities of energy only by themselves, which does not guarantee damping capacity, compromising vibration and noise control. They need some devices to help in this task [Jones, 2001].

There are three different types of vibration control: active, passive, or hybrid damping. Each one of them has its singular approach.

On the one hand, active damping consists of connecting sensors and actuators to the structure, which measure the response of the system at each period of time. These devices are manufactured with piezoelectric materials, for instance, that generate an electric signal when the structure is submitted to an excitation. This type of damping depends on a power source to get energy, as they usually are more complex (in terms of maintenance) and expensive than passive damping, despite it achieve high-performance levels [Jones, 2001; Preumont, 2018].

On the other hand, passive damping devices are less complex. They work with the vibrations from structures, which provide energy. Thus, there is no need for a power source, which reduces costs. These devices require low maintenance, although it is necessary to pay attention and choose carefully the combinations between the materials of the structure and damping materials. It will influence any choice about the materials to use [Bankar

and Aradhye, 2016; Jones, 2001].

Damping treatments are an example of passive control. These add-on devices do not contribute with an expressive amount of weight to the structure, but energy dissipation is guaranteed. Damping treatments are an option even when the manufacturing process is in a very advanced stage or when changing the design of the structure is not an option [Jones, 2001; Moreira, 2014]. They resort to the inherent ability of some materials to absorb the energy that comes from the vibration of the structure. Passive devices are present within metal structures or composite materials, for instance. Nevertheless, it is important to know the materials' microstructure, since it can affect dissipation and damping. In recent years, the use of smart materials, together with several damping technologies, is rising, as an attempt to discover new damping mechanisms [Chung, 2001; Preumont, 2018].

Finally, hybrid damping is a combination of passive and active damping techniques that tries to amend not only the limited control of active devices, but also the limited effective range of operation of passive devices. It is a way of vibration control as simple as passive damping with some advantages of active damping [Baz, 2019].

1.2 Viscoelastic Damping Treatments

Viscoelastic materials are not efficient as structural materials, due to their low resistance, but they present a great energy dissipation capacity. They are added to the structure in the form of viscoelastic damping treatments, that increase the damping capacity of the structures, by dissipating energy resultant from the strain field that it undergoes [Moreira, 2004].

Viscoelastic materials are usually applied in layers on the surface of the host structure. There are three different configurations: free layer damping (FLD), constrained layer damping (CLD) and integrated layer damping (ILD).

Free Layer Damping In FLD configuration, one VEM layer is applied directly on the surface of the host structure. The tension-compression deformation processes that the host structure goes through generate energy that is mainly dissipated as heat. This process supports the existence of viscoelastic damping.

The efficiency of the damping treatment is influenced by the distance between the viscoelastic layer and the neutral axis of the structure. Therefore, it is easy to see that, if the viscoelastic layer is thin, the provided damping is lower than the one that would be provided if the viscoelastic layer was thicker [Vasques and Cardoso, 2011].

The thickness of the VEM layer is one of the main reasons for the efficiency of damping treatments. It reaches satisfactory values when that thickness is one or two times bigger than the thickness of the host structure. Above that, there are only residual changes in damping and material can be wasted [Moreira, 2014]. However, this assumption is not suitable for lightweight structures, so FLD treatments are not suitable for them. This configuration also adds to the structure stiffness, but mainly mass, which are also two more parameters to have in consideration in the design of the VEM layer. Anyway, it has some advantages, such as its low application costs and easy numeric simulations [Vasques and Cardoso, 2011]. Figure 1.1 shows the configuration of this treatment.

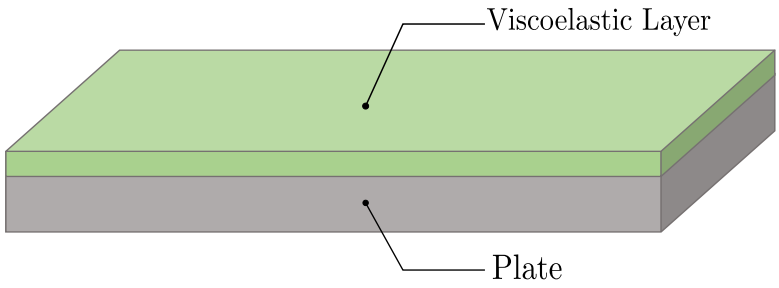


Figure 1.1: Free Layer damping treatment.

Constrained Layer Damping In CLD configurations, one VEM layer is applied directly on the surface of the host structure, in a similar way to FLD configurations. On top of that, there is a thinner and stiffer plate, usually manufactured in the same material of the host structure, however, it is not a part of the structure. This configuration provides high values of shear deformation to the viscoelastic layer during flexural deformation of the host structure [Moreira, 2014].

It means that greater values of damping can be reached when the VEM layer is closer to the neutral plane. The stiffness of the constraining layer (normally, an elastic layer of aluminum or stainless steel) must be higher than the stiffness of the viscoelastic layer, so that the dissipated energy can come from the deformation process. The constraining layer also protects the viscoelastic layer from the external environment.

Thickness is an important parameter, since the efficiency of the process also depends on that parameter. For that reason, it is possible to have smaller values of thickness and, as a result, smaller values of added mass [Vasques and Cardoso, 2011]. Typically, the viscoelastic layer is no thicker than 0.5 mm[Moreira, 2004]. This configuration is illustrated in Figure 1.2.

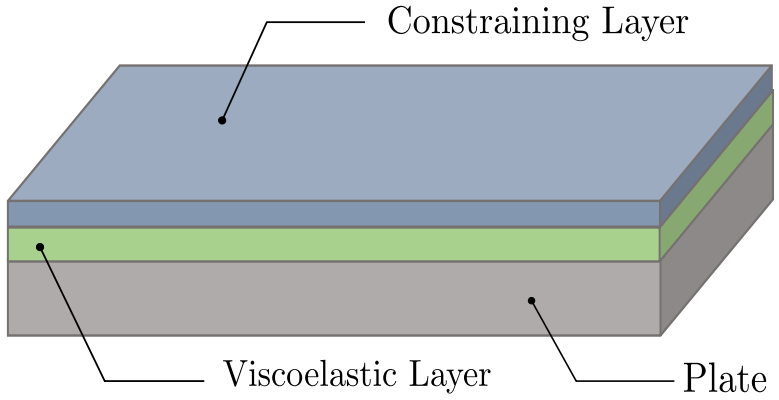


Figure 1.2: Constrained Layer Damping treatment.

Integrated Layer Damping The Integrated Layer Damping treatment, represented in Figure 1.3, is based on the application of a viscoelastic material in the core layer of a sandwich structure, which maximizes damping capacity. The dissipative layer assumes a central position in the sandwich structure, so it can have small thickness values and provide a substantial amount of damping [Vasques and Cardoso, 2011].

While FLD and CLD assume a corrective procedure character, being usually applied after the design of the structure, ILD treatments must be considered in the design of the

sandwich structure, to their production [Moreira, 2004].

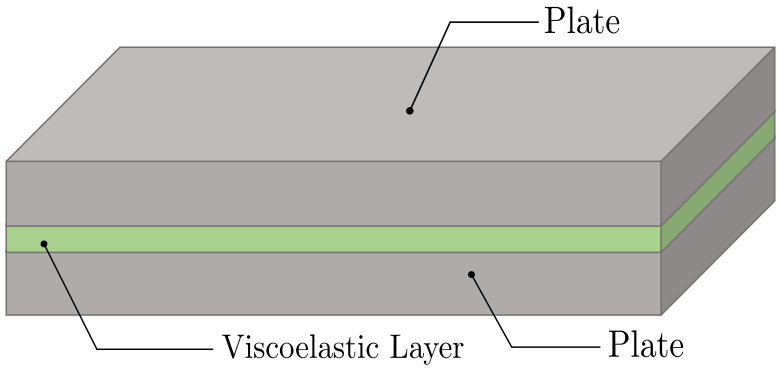


Figure 1.3: Integrated Layer Damping treatment.

1.3 Optimization of Viscoelastic Treatments

It is usual to apply viscoelastic layers across the entire surface of the structure. However, it is possible to optimize viscoelastic damping treatments, without extra costs and reducing changes in the structures. For example, in FLD and CLD treatments, the application of layers in some previously known locations (instead of covering the entire surface with VEM) is a good way of reducing waste and costs.

In fact, in FLD treatments, optimizing a damping treatment consists in redesign the covered area, bearing in mind that smaller areas may provide smaller values of added mass for the same values of efficiency. In CLD treatments, it is recommended some research on maximizing shear deformation energy, but it is possible to say that the lower the thickness of the viscoelastic layer, the higher the shear deformation values.

Therefore, thickness is an important design variable for the optimization of viscoelastic treatments, studied by several numerical methods, parametric studies or experimental procedures, together with materials, optimal covered area, among others [Moreira, 2014].

1.3.1 Partial Local Treatments

Noise and vibrations are undesired effects and may occur in the structure as a consequence of some processes. Hence, damping devices are required and viscoelastic damping treatments are a good option. However, material and money can be wasted, as covering the entire surface may be a disadvantage.

In order to reduce costs and material wasting (which allows the control of added mass too), it is possible to apply partial damping treatments. Thus, only specific locations of the host structure are covered, without affecting the efficiency of the treatment [Granger and Ross, 2009].

This is illustrated in Figure 1.4 for a FLD treatment. Comparing with Figure 1.1, only a part of the plate's surface is covered with a VEM layer, based on some established criteria that define this area as the most appropriate to apply a viscoelastic layer.

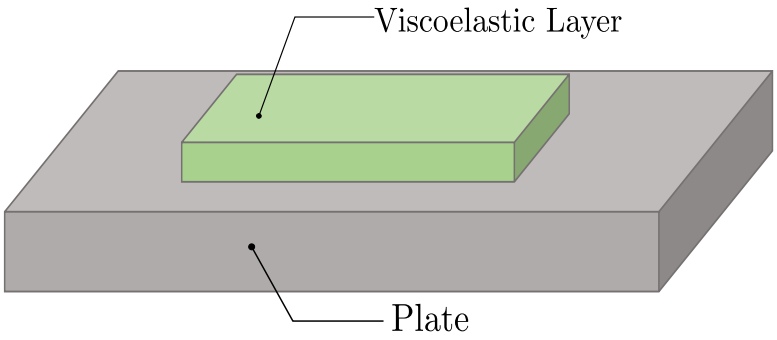


Figure 1.4: Partial damping treatment using Free Layer Damping configuration.

1.4 Motivation

Over the last decades, different industries have tried to build new structures based on lightweight structures. These are more exposed to the effects of vibration, so damping became an important tool to combat those effects. Several industries, such as the aircraft industry, need structures that dissipate energy. The focus on lightweight structures requires the application of damping devices, since they dissipate a very low amount of energy, with partial damping treatments as an efficient way to achieve such objectives.

Viscoelastic damping treatments, an external source of damping, are an example of passive damping devices with an interesting growth in a wide range of industries. These devices provide enough damping to minimize the effects of vibrations, without adding a significant amount of mass to the lightweight structures. In particular, the integrated partial damping treatments are in the limelight, when it comes to the design of a structure that needs vibration and noise control. As previously said, these configurations must be included in the project design of the structure, instead of FLD and CLD, which is a corrective procedure, applied after the assembling of the entire structure. It is interesting for the engineer since there is room to maneuver in terms of the design of this treatment. When the structure is already assembled, the design will have an impact on the efficiency of the viscoelastic damping treatment without any prediction of such scenario.

Furthermore, viscoelastic materials do not offer stiffness to the structure, instead, their contribution is on mass. As such, ILD configurations allow the introduction of damping without compromise the stiffness of the structure. It is important to mention that a viscoelastic layer presents a stiffness that is from an order of magnitude three times lower when compared to a CFRP. Replacing a CFRP layer by a VEM layer strongly influences the stiffness of the structure. Thereby, the application of integrated partial treatments - see Figure 1.5 - is the way to the needful equilibrium between stiffness and vibration damping control.

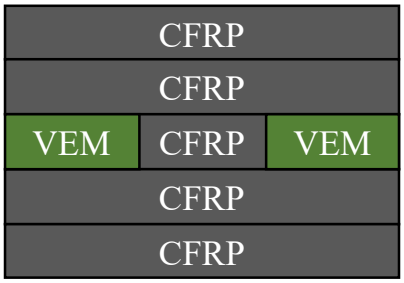


Figure 1.5: Integrated partial damping treatments.

The influence of both geometrical and material properties is also a point of interest. An efficient stacking sequence can provide a good damping capacity to the viscoelastic core, without covering the entire area of the structure. Bearing that in mind, the dynamical analysis of the current plates, along with the prediction of possible improved plates concerning the viscoelastic core and the stacking sequence are the purpose of this work.

1.5 Objectives

The principal purpose of the present work is to study the viability of viscoelastic materials as a damping tool in laminate composite plates and how this damping solution can be optimized, namely in partial damping treatments. Results are validated through several experimental modal analysis of laminate composite plates with different partial damping treatments. Thus, the aimed objectives for this work are the following ones:

- Understand the different viscoelastic treatments and how their optimization can take place.
- Study the fundamental principles of viscoelasticity, the effects of temperature and frequency (this one mainly) in the dynamic properties of viscoelastic materials, as well as viscoelastic constitutive modeling as a tool of describing the behavior of the material along with frequency.
- Implement and validate an algorithm in MATLAB ®, based on a quadrangular four-node plate element, using a Layerwise Theory.
- Develop a dynamical analysis based on experimental results, to determine the Frequency Response Functions (FRF) of laminated composite plates with total and partial damping, to establish comparisons.
- Study the influence of several singular parameters in the behavior of the viscoelastic damping treatments, to evaluate and possibly improve the efficiency of partial damping treatments, such as the width and location of the viscoelastic strips, the orientation of the viscoelastic layer (0° or 90°) in order to one of the axes of the plate, their thickness and, finally, the stacking sequence of the orthotropic plate.

1.6 Organization of the Dissertation

The dissertation begins with an introduction, in Chapter 1, to damping treatments. These treatments assume several shapes and sizes, through their different types of damping treatments. A brief discussion about the optimization of partial treatments and their advantages happens at the end, finishing with some objectives and contents of this thesis

In Chapter 2, the characterization of composite and viscoelastic materials is the purpose. There are some explanations about some basic terminology concerning both types of materials. Particularly to viscoelastic materials, the effects of temperature and frequency, two main parameters in characterizing such materials. Extensional and shear moduli have here the first introduction, as well as loss factor.

Chapter 3 begins with the presentation of all the aspects regarding the Layerwise Theory considered in this work: the assumptions that the theory presents, the displacement, stress, and strain fields, and the formulation of the principal matrices, such as stiffness and mass matrices. The characterization of the finite element formulation is also in this

chapter, and the considerations taking place with the presence of shear locking. Following this, some aspects of Frequency Response Functions and Modal Analysis are presented. Finally, some validation tests are presented to the evaluation of the code.

The results from the experimental dynamical analysis on the specimen plates are in Chapter 4. The chapter starts with the information about the materials and the experimental setup, followed by some previous results and a comparison between the different damping treatments. Following this, a similar analysis occurs, considering the specimen plates used in this work. The aim is to check whether the behavior of the treatments registers any change, as well as discuss the viability of each damping treatment.

In Chapter 5, a parametric analysis takes place, in order to study the efficiency of the viscoelastic damping treatments. The influence of several parameters is analyzed for the first six modes of vibration, to understand their influence on the final performance of the plates. Besides the width, position, location, and thickness of the viscoelastic strips, also fiber orientation is studied, but with a closer look. Regarding only one mode of vibration (in this case, the first one), the Layerwise Optimization Approach carries out an iterative process to find out which stacking sequence provides improved values of loss factor. The Teaching Learning Based Optimization method validates the accuracy of the results obtained with the Layerwise Optimization Approach.

A final reflection about the developed work is performed in Chapter 6, where some conclusions are listed. Some suggestions of work and research for the future are also enumerated.

Chapter 2

Structural and Damping Materials

2.1 Introduction

Over the years, vibration control has been crucial in the minimization of the effects of high amplitudes of oscillations or fatigue failure problems. Three types of approaches can be considered: passive, active and hybrid control.

Passive damping treatments commonly resort to viscoelastic materials, providing effectiveness in the control of high-frequency excitations. The benefits of this type of materials are visible in the success of these treatments.

The use of integrated partial damping treatments in a sandwich structure with both composite and viscoelastic materials requires its correct characterization.

In the current chapter, the presentation of the materials used for the plates of this work takes place. The mechanical behavior of these materials and the representation of their mechanical properties are tackled. Concerning laminated composite materials, some basic concepts and laminate configurations are presented. Regarding viscoelastic materials, the dependence on external factors such as the frequency of the excitation or the temperature is also a point of interest.

2.2 Composite Materials

Composite materials are responsible to mostly provide stiffness to the structure. They are also good to improve strength, resistance to corrosion, fatigue life, among others. However, their damping capacity is low. Thereby, they will only confer a weight reduction to the structure.

2.2.1 Basic Terminology

Fiber reinforced composite materials are usually manufactured with two materials: the fibers, which are the reinforcement materials; and the matrix, the base material.

Such materials present themselves in different types and they can be either metallic or non metallic:

- Fibrous composites: composites with fibers of one material and the matrix from another material;
- Laminated composites: layers of different materials.

A fiber reinforced laminated composite plate presents many laminates, which are groups of laminae, a sheet of composite material, stacked together to achieve specific

properties. Each lamina presents a specific stacking sequence, which is the sequence of the several fiber orientations of the composite.

2.2.2 General Types of Laminate Configurations

Fiber reinforced composite materials can be formed by multiple layers which present a fiber orientation value, bound together at a matrix - see Figure 2.1. If a laminate is ply-oriented, it can take one of five configurations:

- symmetric laminate: each $+\theta$ ply has a $+\theta$ ply at its symmetric location, considering the middle plane of the plate;
- cross-ply laminate: they are similar to symmetric laminate plies, however, θ only takes values of 0° or 90°;
- angle-ply laminate: the plies have alternating orientations;
- antisymmetric laminate: each $+\theta$ ply has a -θ ply at its symmetric location, considering the middle plane of the plate;
- balanced laminate: in this type of laminates, for every $+\theta$ ply (except $\theta = 0°$ or $\theta = 90°$), there is a layer, whose orientation is the symmetric value.

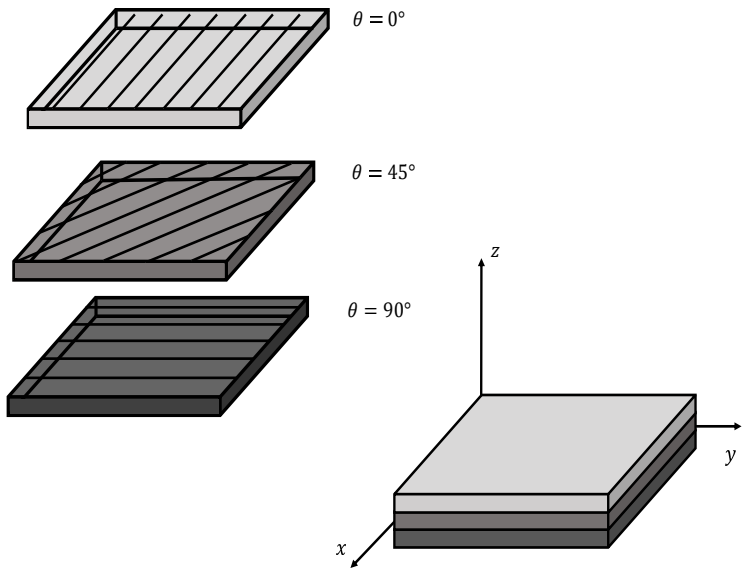


Figure 2.1: Laminate composite plate.

The directions 1, 2 and 3 define the lamina coordinate system, as Figure 2.2 shows.

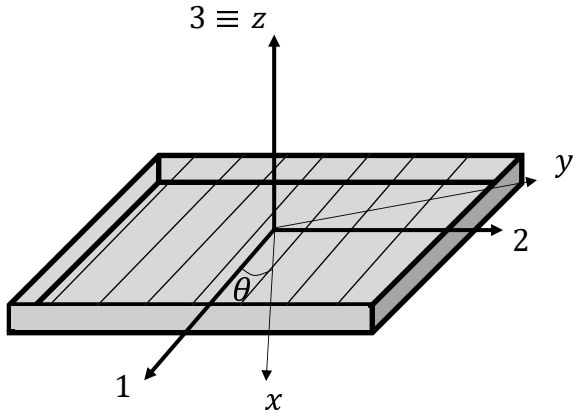


Figure 2.2: Local and global coordinate system.

2.2.3 Symmetric Laminated Plates

The constitutive law is composed by four submatrices, with different components:

$$\begin{bmatrix} [\mathbf{A}] & [\mathbf{B}] \\ [\mathbf{B}] & [\mathbf{D}] \end{bmatrix} \tag{2.1}$$

where

$$A_{ij} = \sum_{k=1}^{N} \bar{Q}_{ij}^{(k)} (z_{k+1} - z_k) \tag{2.2a}$$

$$B_{ij} = \frac{1}{2} \sum_{k=1}^{N} \bar{Q}_{ij}^{(k)} (z_{k+1}^2 - z_k^2) \tag{2.2b}$$

$$D_{ij} = \frac{1}{3} \sum_{k=1}^{N} \bar{Q}_{ij}^{(k)} (z_{k+1}^3 - z_k^3) \tag{2.2c}$$

Equations 2.2a, 2.2b and 2.2c are formed by extensional stiffness, bending-extensional stiffness and bending stiffness coefficients, respectively.

Symmetric laminate composite plates present some advantages. They are easier to analyze than other laminates which present bending-extension coupling. Due to the symmetry of the material coefficients, $\bar{Q}_{ij}$, distances z and thicknesses, in relation to the middle plane of the laminate for all the layers, the coupling stiffness matrix is zero. Besides that, symmetric laminates do not bend with the thermally induced contractions that come from the cooling, after the curing process [Reddy, 2003].

2.3 Viscoelastic Materials

Viscoelastic materials are polymeric-based materials that dissipate mechanical energy, during a cyclic deformation, in the form of heat. They are used mainly in damping treatments, whose efficiency relies on the capability of dissipating energy to the environment [Moreira, 2004].

Once viscoelastic materials are polymers, they are chains of molecules that may suffer some sort of deformation when a force or pressure is applied to them. This pressure causes

a frictional contact between molecules or chains of molecules, producing mechanical energy dissipated as heat [Hazard, 2007].

These materials are homogeneous and isotropic, just like steel or aluminum, for instance. Despite that, the mechanical properties of viscoelastic materials depend on frequency and temperature, because of their polymeric constitution. A third parameter that might interest for some analysis is the deformation amplitude [Moreira, 2004].

2.3.1 Considerations on Temperature and Frequency Dependence

Temperature plays an important role in the behavior of polymers. In fact, among several factors associated with the environment surrounding the material, temperature is the most influential one.

According with Nashif et al. [1985], viscoelastic materials can exhibit three distinct behaviors, depending on the range of temperatures they are subjected to: the glassy region, the transition region and the rubbery region. Figure 2.3 shows the distribution of these regions with temperature.

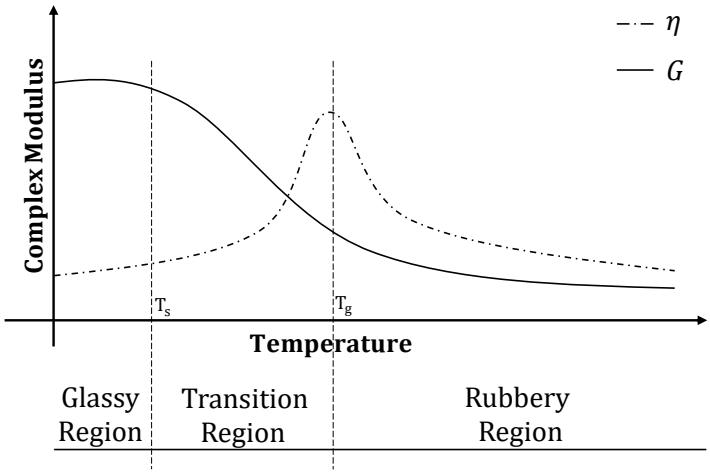


Figure 2.3: Loss factor and shear storage modulus dependence of temperature (adapted from Nashif et al. [1985]).

In the first zone, the glassy region, temperatures are low, being the stiffness of the material high. Also in this area, the shear storage modulus reaches its maximum value and the decreasing variation with temperature is almost undetectable. The loss factor is low, although slight temperature variations induce a sharp rise in this parameter.

In the second zone, modulus decreases faster as temperatures go up, while the loss factor reaches its maximum value at T_g, the glass transition temperature.

The third zone presents a plateau area, where minor variations, with temperature, are registered. Low modulus and low values of loss factor are also pointed.

Besides temperature, frequency plays an important role in the properties of viscoelastic materials. As frequency rises, the modulus increases, although in both glassy and rubbery regions, that behavior is moderated [Nashif et al., 1985]. Figure 2.4 allows a better analysis of frequency effects on both shear storage modulus and loss factor.

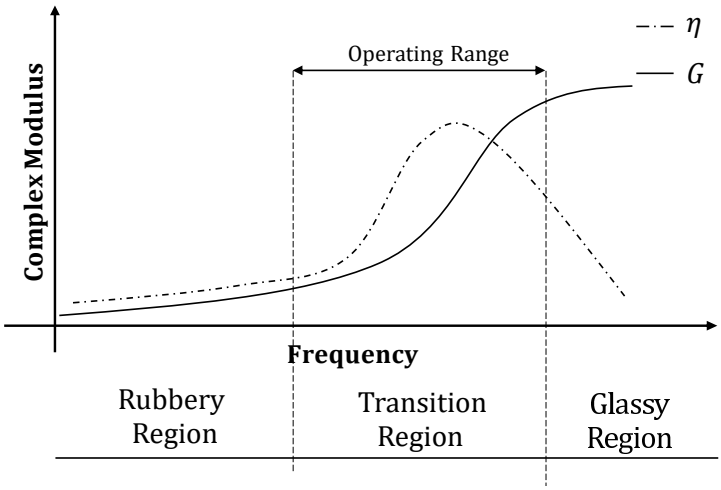


Figure 2.4: Loss factor and shear storage modulus dependence of frequency (adapted from Nashif et al. [1985]).

2.3.2 Harmonic Load and VEM's Response

When a harmonic load is applied on a viscoelastic material, the resultant strain (and stress) are also harmonic with the same frequency. This is also verified in an elastic material, however, in a viscoelastic material, the resultant strain lags by an angle, δ_l, concerning the stress field, as shown in Figure 2.5.

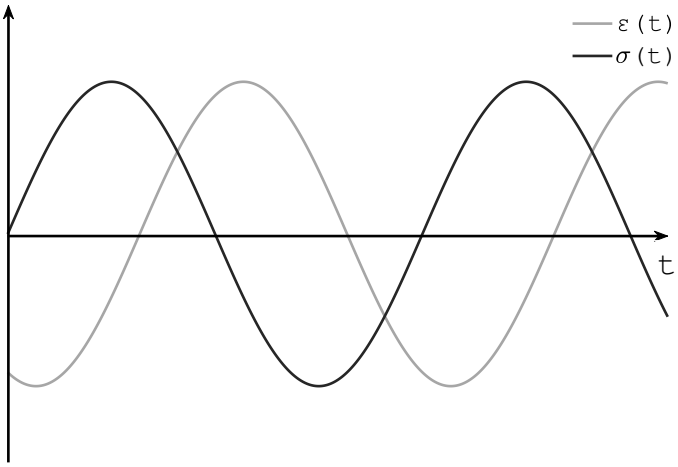


Figure 2.5: Lag between stress and strain field (adapted from Moreira [2004]).

The representation of the stress as a function of the strain is represented in Figure 2.6, by a hysteresis loop. Here, the angle between its larger axis and x-axis is proportional to the stiffness of the material, while the ratio between the smaller axis and the bigger axis is an indicator of the damping capacity of the material.

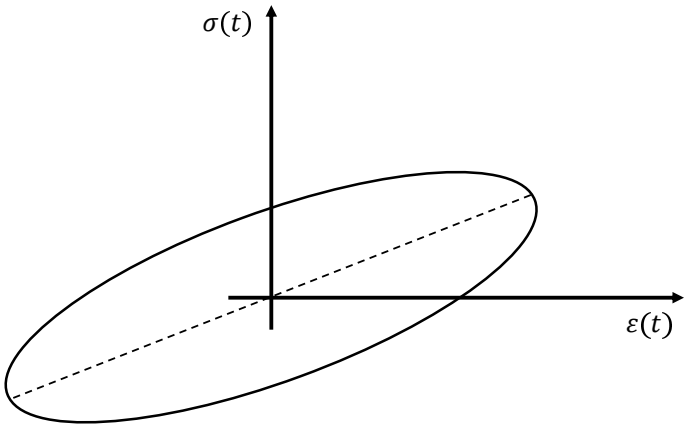


Figure 2.6: Hysteresis loop (adapted from Moreira [2004]).

Therefore, for a harmonic load applied in a viscoelastic material, the stress field is:

$$\sigma(t) = \sigma_0 \sin(\omega t) \tag{2.3}$$

and the material presents a strain field as:

$$\varepsilon(t) = \varepsilon_0 \sin(\omega t - \delta_l) \tag{2.4}$$

2.3.3 Complex Modulus

The strain and stress relationship can also be expressed by complex quantities, since it turns the previous calculus process easier. The previous expressions are now written as:

$$\sigma = \sigma_0 e^{j\omega t} \tag{2.5}$$

and

$$\varepsilon = \varepsilon e^{j\omega t - \delta_l} \tag{2.6}$$

For isotropic materials, Hooke's law says that stress is proportional to strain by a constant, the Young Modulus. Thus, despite being complex and frequency-dependent quantities, stress and strain can be expressed as the following expression indicates:

$$\sigma(j\omega) = E^*(j\omega)\varepsilon(j\omega) \tag{2.7}$$

Being $E^*(j\omega)$ the extensional modulus, a complex quantity that can be expressed in terms of its real and imaginary parts:

$$E^*(j\omega) = E'(\omega) + jE''(\omega) \tag{2.8}$$

The first quantity of the second term, $E'(\omega)$, is the extensional storage modulus that quantifies the stored and recoverable energy. The second quantity, $E''(\omega)$, is the loss modulus, which informs about the lost energy and dissipation effects. From these two quantities, it is possible to define the loss factor as the ratio between the effects related to the dissipation of energy and the amount of recoverable energy:

$$\eta(\omega) = \frac{E''(\omega)}{E'(\omega)} \tag{2.9}$$

The extensional modulus can be established by knowing both the storage modulus and the loss factor:

$$E^*(j\omega) = E' \left[1 + j\eta(\omega)\right] \tag{2.10}$$

These last equations are also available for the determination of shear modulus, $G^*(j\omega)$:

$$E^*(j\omega) = 2G^*(j\omega)[1 + \nu(j\omega)] \tag{2.11}$$

or

$$G^*(j\omega) = \frac{E^*(j\omega)}{2[1 + \nu(j\omega)]} \tag{2.12}$$

The Poisson ratio will be considered as a real and constant quantity since frequency-dependence is out of consideration.

2.3.4 Fractional Derivative Model

The properties of viscoelastic materials are frequency-dependent, as previously mentioned. Taking it into account, the mathematical forms that describe the behavior of the mechanical system should be identified. Many simple models describe qualitatively the dynamic behavior of the system, however, these models only consider the real component of that behavior, which can lead to some inaccuracy between experimental and theoretical models. The reason for such error is in the stress-strain relationship, which is usually defined by a linear differential equation of integer order that has to be generalized and rewritten. Integer order derivatives are replaced by fractional-order ones, which is an advantage since they describe the real dynamic behavior and are simple to use and to understand [Pritz, 1996].

The fractional derivative model with four parameters describes the behavior of a system in a large frequency range, being a sort of interpolation between the viscous and the elastic behavior of the material.

According to Riemann-Liouville definition, the α order derivative of a function $f(t)$, $f^{(\alpha)}(t)$ is defined as:

$$\frac{\partial^\alpha f(t)}{\partial t^\alpha} = f^{(\alpha)}(t) = \frac{1}{\Gamma(1-\alpha)} \frac{d}{dt} \left[\int_0^t \frac{f(\tau)}{(t-\tau)^\alpha} \mathrm{d}\tau \right] \quad 0 \leq \alpha \leq 1 \tag{2.13}$$

The Gamma function $\Gamma(1-\alpha)$ is determined by:

$$\Gamma(1-\alpha) = \int_0^\infty x^{-\alpha} e^{-x} \, \mathrm{d}x \tag{2.14}$$

The following equation represents the Zener model, where both stress and strain are obtained with the same fractional order of derivation, leading to:

$$\sigma(t) + \tau^\alpha \frac{\partial^\alpha \sigma(t)}{\partial t^\alpha} = E_0 \varepsilon(t) + E_\infty \tau^\alpha \frac{\partial^\alpha \varepsilon(t)}{\partial t^\alpha} \tag{2.15}$$

Now, it is possible to apply the Fourier transform to Equation 2.15:

$$E^* = \frac{E_0 + E_\infty (j\omega\tau)^\alpha}{1 + (j\omega\tau)^\alpha} \tag{2.16}$$

Storage and loss moduli are now functions of characteristic parameters (besides α): E_0, the dynamic modulus at zero frequency; E_∞, the limit value of the dynamic modulus at high frequencies; and τ, the relaxation time of the material [Agirre, 2011].

Thereby, stress is given by:

$$\sigma^* = E^*(j\omega)\varepsilon^* \tag{2.17}$$

It is also possible to write an equivalent equation for shear modulus, G^*:

$$G^* = \frac{G_0 + G_\infty(j\omega\tau)^\alpha}{1 + (j\omega\tau)^\alpha} \tag{2.18}$$

Chapter 3

Mechanical Model

3.1 Introduction

In plates with a viscoelastic core, many phenomena determine which deformation theories are appropriate to represent their mechanical behavior correctly. There are four groups of deformation theories: three-dimensional elasticity theories, Equivalent Single-Layer theories, Zig-Zag theories and Layerwise theories.

Liew et al. offer an interesting perspective about these groups of theories. The three-dimensional theories treat the plate as a general solid, but their computational cost is too high to be affordable. The second possibility is the group of ESL theories, where classical laminated theory, First-Order Shear Deformation theories (FSDT) and High-Order Shear Deformation theories (HSDT) are included. All of them take a 3D problem and reduce it into a 2D problem. Although Zig-Zag theories consider the existence of an interface between layers, the accuracy of transverse stresses is in question [Liew et al., 2019].

These theories don't meet all the requirements. Layerwise theories are another type of theories that compile, in a bi-dimensional element, the information of a tridimensional mesh, considering interfaces and transverse stresses. The structure is divided into several layers and, in this work, for each layer, Reissner-Mindlin hypotheses are assumed [Moreira, 2004].

There are two groups of layerwise theories, depending on the variables that are considered: the displacement-based layerwise theories and the mixed layerwise theories. The first one considers displacements as the only variables of the problem. Each layer has its displacement variables, by imposing compatibility conditions at the interfaces of the layers. The second group of theories considers transverse stress and displacements as variables, within Reissner's mixed variational principles. Layerwise theories can have a considerable computational cost, depending on the number of layers (directly related to the number of necessary displacement fields) [Liew et al., 2019].

Each theory has its deformation profile, as Figure 3.1 shows. For example, ESL has a linear profile, since the plate has one displacement field, but Layerwise theories provide a linear profile to each layer. In the end, summing the displacement fields of all layers, the profile assumes a zig-zag shape. It is important to know the restrictions related to the characterization of the profile, to choose the best theory.

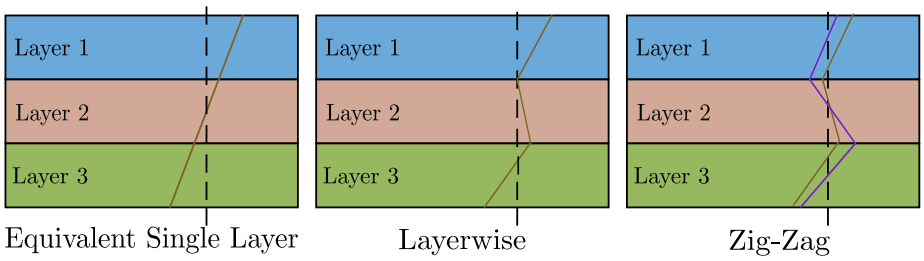


Figure 3.1: Deformation profiles according to different theories (adapted from Liew et al. [2019]).

This chapter presents an explanation of the Layerwise theory applied in this work so that a solid basis for finite element formulation can be guaranteed. The presentation of the layerwise formulation begins with the displacement field and then, the strain and the stress fields. Each layer will have different fields and their formulation varies according to the material (if it is isotropic or orthotropic). The calculus of strain energy and kinetic energy will facilitate the implementation of a variational principle to calculate stiffness and mass matrices.

3.2 Classic Thick Plate Theories

The Layerwise Theory establishes that each layer of a plate structure can be modeled under assumptions based on thick plates theories, such as Reissner-Mindlin theory. The middle plane of the base layer is the reference plane to define the displacement field of the entire plate [Xu et al., 2016].

In the case of thick plates, the theory of Reissner-Mindlin is the most common applied theory. It results from the application of the Kirchhoff hypothesis with a slight change, which gives tools to solve problems with first-order shear deformation assumptions. It also can be applied on thin plates. Those assumptions are [Oñate, 2013]:

- The out-plane displacements of the points that belong to the middle plane of the plate are too small when compared with plate's thickness.
- There is no in-plane shear deformation at the middle plane of the plate;
- the normal stress, σ_{zz} is negligible (plane stress state);
- a straight line, normal to the undeformed middle plane, remains straight in the deformed plane, but it is not possible to say that it will remain normal to the deformed plane.

3.3 Layerwise Plate Theory

The layerwise plate formulation is based on some assumptions [Akoussan et al., 2016; Xu et al., 2016]:

- All points on a normal to the plates have the same transverse displacement, $w(x, y, t)$, which depends on time, t;
- There is no slip at the interfaces of two layers;

- Displacement must be C^0 along the interfaces;
- Elastic layers are modeled with first shear deformation theories (but some viscoelastic layers can also be modeled with high shear deformation theories);
- Linear approaches of elasticity and viscoelasticity are considered;
- Each layer introduced in a treatment adds two degrees of freedom to the nodes of the treated elements;
- Elastic and viscoelastic materials are treated as isotropic and homogeneous in the whole structure, while each layer of fiber reinforced composite materials are orthotropic materials. Viscoelastic materials present frequency dependent properties, such as Young Modulus or Shear Modulus.

In layerwise formulation, the reference layer presents five different displacements: two in-plane displacements, u and v, one out-of-plane displacement, w, and two rotations. There are two rotations per each extra layer, in comparison with Reissner-Mindlin's theory. It means that, for a viscoelastic treatment, each layer has its rotation field, independent from any other displacement, thereafter, the number of degrees of freedom (that starts in five) increases in two units per each added layer - two extra rotations β_k^x and β_k^y, as Figure 3.2 shows [Moreira, 2004].

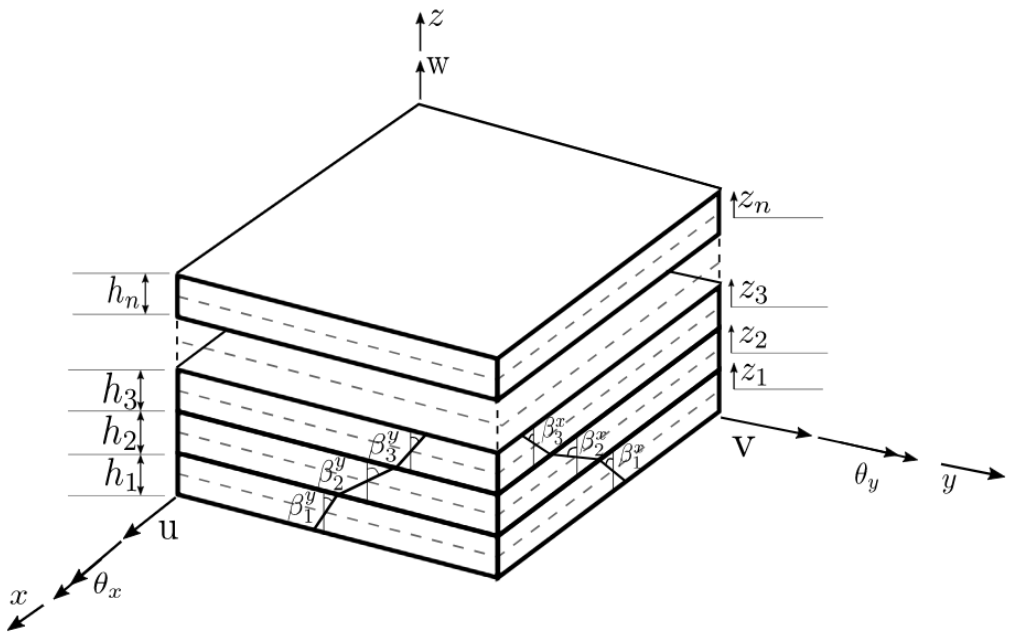


Figure 3.2: Layerwise model (adapted from Moreira [2004]).

It is important to note that:

$$\beta^y = -\theta_x \tag{3.1a}$$

$$\beta^x = \theta_y \tag{3.1b}$$

All the elastic layers are modeled with first order shear deformation theories. Thus, it is possible to observe a zig-zag behavior in the displacement field, along with the thickness of the layer. That behavior is assumed by many theories and is a pattern for the axial displacements in the laminate across its thickness. The interlaminar equilibrium of the

transverse stresses, together with the anisotropy of properties along with the thickness of the plate, creates a discontinuity of the first derivative in displacement field and stress field functions, which is called the "Zig-Zag" effect. Multiple theories have been proposed, being divided into three groups: Lekhnitskii Multilayered Theory (LMT), Abartsumian Multilayered Theory (AMT) and Reissner Multilayered Theory (RMT) [Demasi, 2013; Oñate, 2013].

3.3.1 Displacement Field

Before applying a load, a vertical line can be defined between a point in the k-th layer of the plate and a corresponding point at the bottom layer. That way, the displacement field is obtained with the sum of the displacements of each point on the respective layer. For that reason, continuity of displacements has to be assumed at the interfaces. Therefore, the linear displacements of a point in the k-th layer can be written as [Moreira, 2004]:

$$\{u\}_k = \begin{Bmatrix} u_k \\ v_k \\ w_k \end{Bmatrix} = \begin{Bmatrix} u_0 + \frac{h_1}{2}\beta_1^x + \sum_{j=2}^{k-1} h_j\beta_j^x + \frac{h_k}{2}\beta_k^x + z_k\beta_k^x \\ v_0 + \frac{h_1}{2}\beta_1^y + \sum_{j=2}^{k-1} h_j\beta_j^y + \frac{h_k}{2}\beta_k^y + z_k\beta_k^y \\ w_0 \end{Bmatrix} \tag{3.2}$$

For each layer, $z_k \in \left[-\frac{h_k}{2}, \frac{h_k}{2}\right]$. It is also possible to define the displacement field in a matrix form through some generalized concepts. First, all the displacements can be placed in a vector, $\{d\}$:

$$\{d\} = \{u_0, v_0, w_0, \beta_1^x, \beta_1^y, ..., \beta_k^x, \beta_k^y, ..., \beta_n^x, \beta_n^y\}^{\mathrm{T}} \tag{3.3}$$

Rewriting the displacement field as written in 3.2, but in the matrix form:

$$\{u\}_k = [\mathcal{N}]_k \{d\} \tag{3.4}$$

where $[\mathcal{N}]_k$ contains the coefficients h and z of each term that exists for the k-th layer:

$$[\mathcal{N}]_k = \left[\begin{array}{cccccccccc|ccc} 1 & 0 & 0 & \frac{h_1}{2} & 0 & \dots & h_j & 0 & \dots & \frac{h_k}{2}+z_k & 0 & 0 & \dots & 0 \\ 0 & 1 & 0 & 0 & \frac{h_1}{2} & \dots & 0 & h_j & \dots & 0 & \frac{h_k}{2}+z_k & 0 & \dots & 0 \\ 0 & 0 & 1 & 0 & 0 & \dots & 0 & 0 & \dots & 0 & 0 & 0 & \dots & 0 \end{array}\right] \tag{3.5}$$

3.3.2 Strain Field

The strain field of the k-th layer is given by

$$\{\varepsilon\}_k = [\mathcal{L}] \{u\}_k \tag{3.6}$$

It is composed by six different components:

$$\{\varepsilon\}_k = \{\varepsilon_k^{xx}, \varepsilon_k^{yy}, \gamma_k^{xy}, \gamma_k^{xz}, \gamma_k^{yz}\}^{\mathrm{T}} \tag{3.7}$$

These components can be calculated as expressed from Equation 3.8a to Equation 3.8e

$$\varepsilon_k^{xx} = \frac{\partial u_k}{\partial x} \tag{3.8a}$$

$$\varepsilon_k^{yy} = \frac{\partial v_k}{\partial y} \tag{3.8b}$$

$$\gamma_k^{xy} = \frac{\partial u_k}{\partial y} + \frac{\partial v_k}{\partial x} \tag{3.8c}$$

$$\gamma_k^{xz} = \frac{\partial u_k}{\partial z} + \frac{\partial w_k}{\partial x} \tag{3.8d}$$

$$\gamma_k^{yz} = \frac{\partial v_k}{\partial z} + \frac{\partial w_k}{\partial y} \tag{3.8e}$$

$\left[\mathcal{L}\right]$ is a differential operator defined by:

$$\left[\mathcal{L}\right] = \begin{bmatrix} \frac{\partial}{\partial x} & 0 & 0 \\ 0 & \frac{\partial}{\partial y} & 0 \\ \frac{\partial}{\partial y} & \frac{\partial}{\partial x} & 0 \\ \frac{\partial}{\partial z} & 0 & \frac{\partial}{\partial x} \\ 0 & \frac{\partial}{\partial z} & \frac{\partial}{\partial y} \end{bmatrix} \tag{3.9}$$

Applying the differential operator from 3.9 to the displacement field:

$$\varepsilon_k^{xx} = \varepsilon_k^{xx,\mathrm{M}} + \varepsilon_k^{xx,\mathrm{C}} + \varepsilon_k^{xx,\mathrm{B}} \tag{3.10a}$$

$$\varepsilon_k^{xx} = \frac{\partial u_0}{\partial x} + \frac{h_1}{2}\frac{\partial \beta_1^x}{\partial x} + \sum_{j=2}^{k-1}\left[h_j \frac{\partial \beta_j^x}{\partial x}\right] + \frac{h_k}{2}\frac{\partial \beta_k^x}{\partial x} + z_k \frac{\partial \beta_k^x}{\partial x}$$

$$\varepsilon_k^{yy} = \varepsilon_k^{yy,\mathrm{M}} + \varepsilon_k^{yy,\mathrm{C}} + \varepsilon_k^{yy,\mathrm{B}} \tag{3.10b}$$

$$\varepsilon_k^{yy} = \frac{\partial v_0}{\partial y} + \frac{h_1}{2}\frac{\partial \beta_1^y}{\partial y} + \sum_{j=2}^{k-1}\left[h_j \frac{\partial \beta_j^y}{\partial y}\right] + \frac{h_k}{2}\frac{\partial \beta_k^y}{\partial y} + z_k \frac{\partial \beta_k^y}{\partial y}$$

$$\gamma_k^{xy} = \gamma_k^{xy,\mathrm{M}} + \gamma_k^{xy,\mathrm{C}} + \gamma_k^{xy,\mathrm{B}} \tag{3.10c}$$

$$\gamma_k^{xy} = \frac{\partial u_0}{\partial y} + \frac{\partial v_0}{\partial x} +$$
$$+ \frac{h_1}{2}\frac{\partial \beta_1^x}{\partial y} + \sum_{j=2}^{k-1}\left[h_j \frac{\partial \beta_j^x}{\partial y}\right] + \frac{h_k}{2}\frac{\partial \beta_k^x}{\partial y} + \frac{h_1}{2}\frac{\partial \beta_1^y}{\partial x} + \sum_{j=2}^{k-1}\left[h_j \frac{\partial \beta_j^y}{\partial x}\right] + \frac{h_k}{2}\frac{\partial \beta_k^y}{\partial x} +$$
$$+ z_k \frac{\partial \beta_k^y}{\partial x} + z_k \frac{\partial \beta_k^x}{\partial y}$$

$$\gamma_k^{xz} = \beta_k^x + \frac{\partial w_0}{\partial x} \tag{3.10d}$$

$$\gamma_k^{yz} = \beta_k^y + \frac{\partial w_0}{\partial y} \tag{3.10e}$$

Each component of the strain field results from the sum of the contribution of one or more different phenomena. Thereby, Equations 3.10 are the sum of membrane component, coupling component, bending and transverse shear component contributions, dividing the strain field into three different parts:

$$\{\varepsilon\}_k = \left\{ \{\varepsilon\}_k^{\mathrm{M}} + \{\varepsilon\}_k^{\mathrm{C}} ; \{\varepsilon\}_k^{\mathrm{B}} ; \{\gamma\}_k^{S} \right\}^{\mathrm{T}} \tag{3.11}$$

The deformation matrix of the k-th layer, $[B]_k$, is now able to be defined, as strain field is known:

$$\{\varepsilon\}_k = [\mathcal{L}] [\mathcal{N}]_k \{d\} \tag{3.12}$$

with

$$[\mathcal{B}]_k = [\mathcal{L}] [\mathcal{N}]_k \tag{3.13}$$

It is possible to consider $[\mathcal{B}]_k$ as the assemble of three submatrices:

$$[\mathcal{B}]_k = \begin{bmatrix} [\mathcal{B}]_k^{\mathrm{MC}} \\ [\mathcal{B}]_k^{\mathrm{B}} \\ [\mathcal{B}]_k^{\mathrm{S}} \end{bmatrix} \tag{3.14}$$

The submatrices described in Equation 3.14 are:

- $[\mathcal{B}]^{\mathrm{MC}}$ is the coupling and membrane matrix, defined by:

$$[\mathcal{B}]_k^{\mathrm{MC}} = \left[\begin{array}{cccccccccccc:c} \frac{\partial}{\partial x} & 0 & 0 & \frac{h_1}{2}\frac{\partial}{\partial x} & 0 & \cdots & h_j\frac{\partial}{\partial x} & 0 & \cdots & \frac{h_k}{2}\frac{\partial}{\partial x} & 0 & \\ 0 & \frac{\partial}{\partial y} & 0 & 0 & \frac{h_1}{2}\frac{\partial}{\partial y} & \cdots & 0 & h_j\frac{\partial}{\partial y} & \cdots & 0 & \frac{h_k}{2}\frac{\partial}{\partial y} & [0] \\ \frac{\partial}{\partial y} & \frac{\partial}{\partial x} & 0 & \frac{h_1}{2}\frac{\partial}{\partial y} & \frac{h_1}{2}\frac{\partial}{\partial x} & \cdots & h_j\frac{\partial}{\partial y} & h_j\frac{\partial}{\partial x} & \cdots & \frac{h_k}{2}\frac{\partial}{\partial y} & \frac{h_k}{2}\frac{\partial}{\partial x} & \end{array} \right] \tag{3.15}$$

- The second submatrix is $[\mathcal{B}]_k^{\mathrm{B}}$, which defines the bending part of $[\mathcal{B}]_k$:

$$[\mathcal{B}]_k^{\mathrm{B}} = \left[\begin{array}{ccccccccccc:c} 0 & 0 & 0 & 0 & 0 & \cdots & 0 & 0 & \cdots & z_k\frac{\partial}{\partial x} & 0 & \\ 0 & 0 & 0 & 0 & 0 & \cdots & 0 & 0 & \cdots & 0 & z_k\frac{\partial}{\partial y} & [0] \\ 0 & 0 & 0 & 0 & 0 & \cdots & 0 & 0 & \cdots & z_k\frac{\partial}{\partial y} & z_k\frac{\partial}{\partial x} & \end{array} \right] \tag{3.16}$$

- The last submatrix is $[\mathcal{B}]_k^{\mathrm{S}}$, related to transverse shear:

$$[\mathcal{B}]_k^{\mathrm{S}} = \left[\begin{array}{ccccccccccc:c} 0 & 0 & \frac{\partial}{\partial x} & 0 & 0 & \cdots & 0 & 0 & \cdots & 1 & 0 & \\ 0 & 0 & \frac{\partial}{\partial y} & 0 & 0 & \cdots & 0 & 0 & \cdots & 0 & 1 & [0] \end{array} \right] \tag{3.17}$$

3.3.3 Stress Field of Isotropic Materials

As well as in the strain field, the stress field of the k-th layer is represented by five different stress components:

$$\{\sigma\}_k = \{\sigma_k^{xx}, \sigma_k^{yy}, \tau_k^{xy}, \tau_k^{xz}, \tau_k^{yz}\}^{\mathrm{T}} \tag{3.18}$$

Another similar concept is the one that divides the stress field in three different parts, each one concerning a different type of contribution: membrane stress, coupling stress, bending stress or transverse shear stress:

$$\{\sigma\}_k = \left\{\{\sigma\}_k^{\mathrm{M}} + \{\sigma\}_k^{\mathrm{C}}; \{\sigma\}_k^{\mathrm{B}}; \{\tau\}_k^{\mathrm{S}}\right\}^{\mathrm{T}} \tag{3.19}$$

Each type of material has its own way of defining the stress field, depending on the nature of its properties. In fact, the relationship between strain field and stress field is given by the constitutive law of the layer's material, $[\mathcal{D}]_k$. It is assumed that all materials are either isotropic or orthotropic.

Elastic Material

The aforementioned stress field of a generic k-th layer is obtained by the multiplication of the constitutive law of the material by the strain field of the k-th layer:

$$\{\sigma\}_k = [\mathcal{D}]_k \{\varepsilon\}_k \tag{3.20}$$

It is possible to define $[\mathcal{D}]_k$ matrix from the assembly of submatrices, regarding different effects:

$$[\mathcal{D}]_k = \begin{bmatrix} [D]_k^{\mathrm{MC}} & [0] & [0] \\ & [D]_k^{\mathrm{B}} & [0] \\ sym & & [G]_k^{\mathrm{S}} \end{bmatrix} \tag{3.21}$$

where $[D]_k^{\mathrm{MC}}$,$[D]_k^{\mathrm{B}}$ and $[G]_k^{\mathrm{S}}$ are defined for a homogeneous isotropic material, as established in the following terms:

$$[D]_k^{\mathrm{MC}} = [D]_k^{\mathrm{B}} = [D]_k = \frac{E_k}{1-\nu^2} \begin{bmatrix} 1 & \nu_k & 0 \\ \nu_k & 1 & 0 \\ 0 & 0 & \dfrac{1-\nu_k}{2} \end{bmatrix} \tag{3.22}$$

$$[G]_k^{\mathrm{S}} = [G]_k = \frac{E_k}{2(1+\nu_k)} \begin{bmatrix} 1 & 0 \\ 0 & 1 \end{bmatrix} \tag{3.23}$$

The parameters E_k and ν_k represent the Young Modulus and the Poisson ratio, respectively, of the material of the k-th layer [Moreira, 2004].

Viscoelastic Material

The properties of the viscoelastic material depend on frequency and become complex quantities, as explained in Chapter 2. In spite of that, its constitutive law remains the same [Xu et al., 2016]:

$$\begin{Bmatrix} \sigma^{xx} \\ \sigma^{yy} \\ \tau^{xy} \\ \tau^{xz} \\ \tau^{yz} \end{Bmatrix} = \begin{bmatrix} Q_{11}^*(j\omega) & Q_{12}^*(j\omega) & 0 & 0 & 0 \\ Q_{21}^*(j\omega) & Q_{22}^*(j\omega) & 0 & 0 & 0 \\ 0 & 0 & Q_{44}^*(j\omega) & 0 & 0 \\ 0 & 0 & 0 & Q_{55}^*(j\omega) & 0 \\ 0 & 0 & 0 & 0 & Q_{66}^*(j\omega) \end{bmatrix} \begin{Bmatrix} \varepsilon^{xx} \\ \varepsilon^{yy} \\ \gamma^{xy} \\ \gamma^{xz} \\ \gamma^{yz} \end{Bmatrix} \tag{3.24}$$

$$Q^*_{11}(j\omega) = \frac{E^*_x(j\omega)}{(1-\nu_{xy}\nu_{yx})} \tag{3.25a}$$

$$Q^*_{12}(j\omega) = \frac{\nu_{xy}E^*_y(j\omega)}{(1-\nu_{xy}\nu_{yx})} \tag{3.25b}$$

$$Q^*_{22}(j\omega) = \frac{E^*_y(j\omega)}{(1-\nu_{xy}\nu_{yx})} \tag{3.25c}$$

$$Q^*_{44}(j\omega) = G^*_{yz}(j\omega) \tag{3.25d}$$

$$Q^*_{55}(j\omega) = G^*_{zx}(j\omega) \tag{3.25e}$$

$$Q^*_{66}(j\omega) = G^*_{xy}(j\omega) \tag{3.25f}$$

3.3.4 Stress Field of Orthotropic Materials

In an orthotropic structure, each lamina has its coordinate system with some fiber orientation. Constitutive matrices are associated with a transverse isotropic lamina and defined in the lamina's coordinate system:

$$\left[C\right]_k = \begin{bmatrix} Q_{11} & Q_{12} & 0 \\ Q_{21} & Q_{22} & 0 \\ 0 & 0 & Q_{66} \end{bmatrix} = \begin{bmatrix} \dfrac{E_1}{(1-\nu_{12}\nu_{21})} & \dfrac{\nu_{21}E_1}{(1-\nu_{12}\nu_{21})} & 0 \\ \dfrac{\nu_{21}E_1}{(1-\nu_{12}\nu_{21})} & \dfrac{E_2}{(1-\nu_{12}\nu_{21})} & 0 \\ 0 & 0 & G_{12} \end{bmatrix} \tag{3.26}$$

$$\left[\mathbf{C}\right]_k = \begin{bmatrix} G_{13} & 0 \\ 0 & G_{23} \end{bmatrix} \tag{3.27}$$

This coefficients $Q^{(k)}_{ij}$, are defined with the engineering constants of the k-th layer. However, for an orthotropic material, stress field has to be defined in the laminate coordinates:

$$\{\sigma\}^{(k)} = [\bar{Q}]^{(k)} \{\varepsilon\}^{(k)} \tag{3.28}$$

Defining θ as the angle between 1 and x, the transformation matrices are:

Transformation matrix for $[D]_k$

$$\left[T\right] = \begin{bmatrix} \cos^2(\theta) & \sin^2(\theta) & -\sin(2\theta) \\ \cos^2(\theta) & \sin^2(\theta) & \sin(2\theta) \\ \dfrac{1}{2}\sin(2\theta) & -\dfrac{1}{2}\sin(2\theta) & \cos^2(\theta)-\sin^2(\theta) \end{bmatrix} \tag{3.29}$$

Transformation matrix for $[G]_k$

$$\left[T\right] = \begin{bmatrix} \cos(\theta) & -\sin(\theta) \\ \sin(\theta) & \cos(\theta) \end{bmatrix} \tag{3.30}$$

From the matrices 3.26,3.27,3.29 and 3.30, it is finally possible to establish the constitutive law of an orthotropic material [Moreira, 2004]:

$$[D]_k = \left[T\right] \left[C\right]_k \left[T\right]^{\mathrm{T}} \tag{3.31}$$

$$[G]_k = \left[T\right]\left[\mathbf{C}\right]_k\left[T\right]^{\mathrm{T}} \tag{3.32}$$

Relationships between Young Modulus and Poisson ratio can be written as follows:

$$\frac{\nu_{21}}{E_2} = \frac{\nu_{12}}{E_1} \tag{3.33a}$$

$$\frac{\nu_{31}}{E_3} = \frac{\nu_{13}}{E_1} \tag{3.33b}$$

$$\frac{\nu_{23}}{E_2} = \frac{\nu_{32}}{E_3} \tag{3.33c}$$

With three Young Moduli and three Shear Moduli, it is possible to define six Poisson ratios, in spite of three of them are dependent on the other three. Thus, there are twelve constants, but only nine of them are independent [Gürdal et al., 1999].

E_1 and E_2 are the Young Moduli in 1 and 2 directions, respectively; v_{21} relates the deformation in direction 1 with the one in direction 2. Other Poisson ratios are defined in the same way. Finally, G_{13}, for instance, is the shear transverse modulus, a parameter that characterizes the angle between 1 and 3. The other shear moduli are defined in a similar way [Moreira et al., 2005].

3.3.5 Strain Energy

The strain energy of a plate is given by:

$$\Pi^{\mathrm{P}} = \frac{1}{2}\int_{\Omega}\left\{\varepsilon\right\}^{\mathrm{T}}\left\{\sigma\right\}\mathrm{d}\Omega \tag{3.34}$$

It is established that shear strain is not zero in thick plates and that shear stress are constant. Therefore, it is considered a shear correction factor for shear stress calculus, since stress uniform distribution is not a good representation of those, that is not real [Oñate, 2013]. Shear correction factor minimizes the error in numerical calculus and it is applied in the shear constitutive matrix, to improve the obtained approximated values. The shear correction factor, λ, in the case of rectangular plates, is $\dfrac{5}{6}$

The total stored energy of a system with n-layers is calculated with the energetic contribution of each layer:

$$\Pi^{\mathrm{P}} = \sum_{k=1}^{n}\Pi_k^{\mathrm{P}} \tag{3.35}$$

Replacing in second term by Equation 3.34:

$$\Pi^{\mathrm{P}} = \sum_{k=1}^{n}\frac{1}{2}\int_{\Omega_k}\left\{\varepsilon\right\}_k^{\mathrm{T}}\left\{\sigma\right\}_k\mathrm{d}\Omega_k \tag{3.36}$$

Now, introducing stress field formulation:

$$\Pi^{\mathrm{P}} = \sum_{k=1}^{n}\frac{1}{2}\int_{\Omega_k}\left\{\varepsilon\right\}_k^{\mathrm{T}}\left[\mathcal{D}\right]_k\left\{\varepsilon\right\}_k\mathrm{d}\Omega_k \tag{3.37}$$

Equation 3.36 can also be divided in the sum of bending component and shear component, as expressed in 3.38:

$$\Pi^{\mathrm{P}} = \frac{1}{2}\int_{\Omega_k} \{\varepsilon_{\mathrm{B}}\}_k^{\mathrm{T}} [D]_k \{\varepsilon_{\mathrm{B}}\}_k \,\mathrm{d}\Omega_k + \frac{\lambda h}{2}\int_{\Omega_k} \{\varepsilon_{\mathrm{S}}\}_k^{\mathrm{T}} [G]_k \{\varepsilon_{\mathrm{S}}\}_k \,\mathrm{d}\Omega_k \tag{3.38}$$

The application of previous equations and the transformation of the integral over the volume in a double integral over the thickness, z_k, of the k-th layer and its area, A, allows easier ways of using this formulation, resulting in Equation 3.39:

$$\Pi^{\mathrm{P}} = \sum_{k=1}^{n} \frac{1}{2}\int_A \int_{z_k} \{d\}^{\mathrm{T}} [\mathcal{B}]_k^{\mathrm{T}} [\mathcal{D}]_k [\mathcal{B}] \{d\} \,\mathrm{d}z_k \mathrm{d}A \tag{3.39}$$

The integral over the thickness implies some changes in the deformation matrix and the constitutive law. However, it is possible to exclude the thickness of the k-th layer from this calculus, multiplying the bending deformation matrix by the inverse of the thickness:

$$[\widehat{\mathcal{B}}]_k = \begin{bmatrix} [\widehat{\mathcal{B}}]_k^{\mathrm{MC}} \\ \hdashline \frac{1}{z_k}[\widehat{\mathcal{B}}]_k^{\mathrm{B}} \\ \hdashline [\widehat{\mathcal{B}}]_k^{\mathrm{S}} \end{bmatrix} \tag{3.40}$$

The constitutive law of the material is also affected by the integration over the thickness:

$$[\widehat{\mathcal{D}}]_k = \begin{bmatrix} h_k \left[D\right]_k & [0] & [0] \\ & \frac{h_k^3}{12}\left[D\right]_k & [0] \\ sym. & & h_k \left[G\right]_k \end{bmatrix} \tag{3.41}$$

Finally, computing over the thickness:

$$\Pi^{\mathrm{P}} = \sum_{k=1}^{n} \frac{1}{2}\int_l \{d\}^{\mathrm{T}} [\widehat{\mathcal{B}}]_k^{\mathrm{T}} [\widehat{\mathcal{D}}]_k [\widehat{\mathcal{B}}] \{d\} \, b\mathrm{d}l \tag{3.42}$$

3.3.6 Kinetic Energy

The kinetic energy of the system is defined by:

$$\Pi^{\mathrm{K}} = \frac{1}{2}\int_{\Omega} \{\dot{u}\}^{\mathrm{T}} [\mathcal{J}] \{\dot{u}\} \,\mathrm{d}\Omega \tag{3.43}$$

where $\{\dot{u}\}$ is the velocity field of the k-th layer:

$$\{\dot{u}\} = [\mathcal{N}]_k \left\{\dot{d}\right\} \tag{3.44}$$

The total kinetic energy of a system with n-layers is calculated with the kinetic energy contribution of each layer:

$$\Pi^{\mathrm{K}} = \sum_{k=1}^{n} \Pi_k^{\mathrm{K}} \tag{3.45}$$

Replacing by Equation 3.43:

$$\Pi_k^{\mathrm{K}} = \sum_{k=1}^{n} \frac{1}{2}\int_{\Omega_k} \{\dot{u}\}_k^{\mathrm{T}} [\mathcal{J}]_k \{\dot{u}\}_k \,\mathrm{d}\Omega_k \tag{3.46}$$

where $[\mathcal{J}]$ is the inertia matrix of the k-th layer and consists in a diagonal matrix where each component is the layer material's density, ρ_k:

$$[\mathcal{J}]_k = \begin{bmatrix} \rho_k & 0 & 0 \\ 0 & \rho_k & 0 \\ 0 & 0 & \rho_k \end{bmatrix} \tag{3.47}$$

Like in strain energy, the integral of the Equation 3.43 can also be split in a double integral over the area and the thickness:

$$\Pi_k^{\mathrm{K}} = \frac{1}{2}\int_A \int_{z_k} \left\{\dot{d}\right\}^{\mathrm{T}} [\mathcal{N}]_k^{\mathrm{T}} [\mathcal{J}]_k [\mathcal{N}]_k \left\{\dot{d}\right\} \mathrm{d}z_k \mathrm{d}A \tag{3.48}$$

$$\therefore \Pi^{\mathrm{K}} = \frac{1}{2}\int_A \int_{z_k} \left\{\dot{d}\right\}^{T} [J]_k \left\{\dot{d}\right\} \mathrm{d}z_k \mathrm{d}A \tag{3.49}$$

where

$$[J]_k = [\mathcal{N}]_k^{\mathrm{T}} [\mathcal{J}]_k [\mathcal{N}]_k \tag{3.50}$$

After calculating the integral over the thickness, it will be possible to write the final pretended result:

$$\Pi^{\mathrm{K}} = \sum_{k=1}^{n} \frac{1}{2}\int_A \left\{\dot{d}\right\}_k^{\mathrm{T}} [\widehat{\mathcal{J}}]_k \left\{\dot{d}\right\}_k \mathrm{d}A \tag{3.51}$$

Here, it is expressed a modified inertia matrix, $[\widehat{\mathcal{J}}]_k$ that already includes the result of analytical integration [Moreira, 2004]:

$$[\widehat{\mathcal{J}}]_k = \rho_k h_k \begin{bmatrix} 1 & 0 & 0 & \frac{h_1}{2} & 0 & \cdots & h_j & 0 & \cdots & \frac{h_k}{2} & 0 & \vdots \\ & 1 & 0 & 0 & \frac{h_1}{2} & \cdots & 0 & h_j & \cdots & 0 & \frac{h_k}{2} & \vdots \\ & & 1 & 0 & 0 & \cdots & 0 & 0 & \cdots & 0 & 0 & \vdots \\ & & & \frac{h_1^2}{4} & 0 & \cdots & \frac{h_1}{2}h_j & 0 & \cdots & \frac{h_1}{2}\frac{h_k}{2} & 0 & \vdots \\ & & & & \frac{h_1^2}{4} & \cdots & 0 & \frac{h_1}{2}h_j & \cdots & 0 & \frac{h_1}{2}\frac{h_k}{2} & \vdots \\ & & & & & \cdots & & & & & & \vdots \\ & & & & & & h_j^2 & 0 & \cdots & h_j\frac{h_k}{2} & 0 & \vdots \\ & & & & & & & h_j^2 & \cdots & 0 & h_j\frac{h_k}{2} & \vdots \\ & & & & & & & & \cdots & & & \vdots \\ & & & & & & & & & \frac{h_k^2}{3} & 0 & \vdots \\ & & & & & & & & & & \frac{h_k^2}{3} & \vdots \\ \multicolumn{12}{l}{sym.} & \vdots \\ \multicolumn{12}{c}{[0]} & \vdots \end{bmatrix} \tag{3.52}$$

3.4 Finite Element Formulation

Figure 3.3 presents a four-node isoparametric element. Each node has, at least, five degrees of freedom, that corresponds to those of the reference layer. Besides that, each element may have more degrees of freedom, if a damping treatment affects the area of the plate that element is characterizing.

The shape functions of the element are presented in a natural coordinate system (ξ,η), in 2D [Okereke and Keates, 2018].

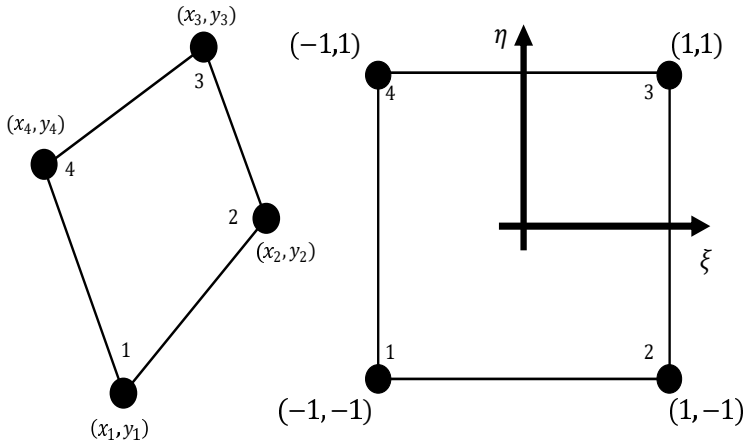


Figure 3.3: Four-node quadrilateral element in natural coordinate system.

The transformation from the local coordinate system to the cartesian coordinate system consists, for each point, in the sum of the multiplication of the shape function N_i, by its cartesian coordinates (x_i,y_i):

$$x(\xi, \eta) = \sum_{i=1}^{4} N_i(\xi, \eta) x_i \tag{3.53}$$

$$y(\xi, \eta) = \sum_{i=1}^{4} N_i(\xi, \eta) y_i \tag{3.54}$$

The shape functions that are about to be used are derived from Equation 3.55:

$$N_i = \frac{1}{4}(1 + \xi_i \xi)(1 + \eta_i \eta) \tag{3.55}$$

with i=1,2,3,4 [Xu et al., 2016].

The shape functions N_1,N_2, N_3 and N_4 are written in Table 3.1:

Table 3.1: Four node quadrilateral element's shape functions.

Node i	ξ_i	η_i	N_i
1	-1	-1	$\frac{1}{4}(1-\xi)(1-\eta)$
2	1	-1	$\frac{1}{4}(1+\xi)(1-\eta)$
3	1	1	$\frac{1}{4}(1+\xi)(1+\eta)$
4	-1	1	$\frac{1}{4}(1-\xi)(1+\eta)$

3.4.1 Discretization

The interpolation of the shape functions can be done separately to each degree of freedom, as they are independent variables. For a four-node element, the approximation functions of the generalized displacements are:

$$\{d\}^e = \sum_{i=1}^{4} N_i(\xi,\eta)\,\{d_i\}^e \tag{3.56}$$

It is possible to define $\{d_i\}^e$ as a matrix of four different vectors. Each vector contains the displacements that correspond to the active degrees of freedom of the nodes of the element. The number of degrees of freedom attached to each node depends on how many treatments an element characterizes. Thus, a shared node can have degrees of freedom that only belongs to one of its elements.

The generalized displacement field is calculated with the nodal displacement field:

$$\{d\} = [N]\,\{d_e\} \tag{3.57}$$

where $[N]$ is the shape function matrix. In the case of four node elements, this matrix is composed by four submatrices $[N]_i$, one per node:

$$[N]_i = \begin{bmatrix} N_i & 0 & 0 \\ & \ddots & 0 \\ sym. & & N_i \end{bmatrix} \tag{3.58}$$

$$[N] = [[N_1]\ [N_2]\ [N_3]\ [N_4]] \tag{3.59}$$

The discretization of the strain field and the stress field is possible due to Equation 3.57:

$$\{\varepsilon\}_k^e = [\mathcal{B}]_k\,\{d\}^e \tag{3.60}$$

that is equal to:

$$\{\varepsilon\}_k^e = [\mathcal{B}]_k[N]\,\{d_i\}^e \tag{3.61}$$

This result can be used in Equation 3.20, in order to discretize the stress field:

$$\{\sigma\}_k^e = [\mathcal{D}]_k\,[\mathcal{B}]_k[N]\,\{d_i\}^e \tag{3.62}$$

3.4.2 Variational Formulation

The weak form is obtained with the sum of the integral forms of each element. Thus, if the mesh contains n_e finite elements, the global form is given by:

$$\sum_{e=1}^{n_t}\sum_{k=1}^{n}\int_{A^e}\{\delta d^e\}^{\mathrm{T}}\left[\widehat{J}\right]_k\left\{\ddot{d}^e\right\}\mathrm{d}A^e+\sum_{e=1}^{n_t}\sum_{k=1}^{n}\int_{A^e}\{\delta d^e\}^{\mathrm{T}}\left[\widehat{\mathcal{B}}\right]_k^T\left[\widehat{\mathcal{D}}\right]_k\left[\widehat{\mathcal{B}}\right]_k\{d^e\}\,\mathrm{d}A^e \quad (3.63)$$
$$-\sum_{e=1}^{n_t}\int_{A^e}\{\delta d^e\}^{\mathrm{T}}\{f^e\}\,\mathrm{d}A^e=0$$

The generalized accelerations are obtained from the derivation of the generalized displacements in order to time:

$$\left\{\ddot{d}^e\right\}=[N]_t\left\{\ddot{d}_i^e\right\} \quad (3.64)$$

Equations 3.57 and 3.64 allow the calculus of stiffness matrix and mass matrix of the element:

$$\sum_{e=1}^{n_t}\left(\{\delta d^e\}^{\mathrm{T}}[M^e]\left\{\ddot{d}\right\}+\{\delta d^e\}^{\mathrm{T}}[K^e]\{d\}-\{\delta d^e\}^{\mathrm{T}}\{f^e\}\right)=0 \quad (3.65)$$

In Equation 3.65, $[M^e]$ is the elementary mass matrix, $[K^e]$ is the elementary stiffness matrix and $[f^e]$ is the elementary generalized load vector.

3.4.3 Stiffness and Mass Matrices

The global stiffness matrix can be established by assembling elementary matrices in one matrix. Each layer presents a proper subelementary stiffness matrix, n per element:

$$[K]^e=\sum_{k=1}^{n}[K]_k^e \quad (3.66)$$

From Equation 3.42, it is easy to identify the elementary stiffness matrix:

$$[K]_k^e=\int_{A^e}\int_{h_k}[N]^{\mathrm{T}}[\mathcal{B}]_k^{e\mathrm{T}}[\mathcal{D}]_k[\mathcal{B}]_k^e[N]\mathrm{d}h_k\mathrm{d}A^e \quad (3.67)$$

In the same way, it is possible to calculate the integral over the thickness:

$$[K]_k^e=\int_{A^e}[N]^{\mathrm{T}}[\widehat{\mathcal{B}}]_k^{e\mathrm{T}}[\widehat{D}]_k[\widehat{\mathcal{B}}]_k^e[N]\mathrm{d}A^e \quad (3.68)$$

Therefore, for a generic k-th layer, the elementary stiffness matrix can be written as established in Equation 3.69:

$$[K]_k^e=\int_{A^e}[B]_k^{e\mathrm{T}}[\widehat{D}]_k[B]_k^e\mathrm{d}A^e \quad (3.69)$$

where $[B]_k=[\widehat{\mathcal{B}}]_k[N]$.

In an identical way, the global mass matrix is an assemble of elementary mass matrices, obtained through discretization of kinetic energy formulation:

$$[M]_k^e=\int_{A^e}[N]^{\mathrm{T}}[\widehat{J}]_k[N]_k^e\mathrm{d}A^e \quad (3.70)$$

3.4.4 Coordinate Transformation

Numerical integration is carried out as follows:

$$\int_{-1}^{1}\int_{-1}^{1} f(\xi,\eta)\mathrm{d}\xi\mathrm{d}\eta = \sum_{i=1}^{p1}\sum_{j=1}^{p2} w_i w_j f(\xi_i,\eta_j) \tag{3.71}$$

which is an approximation of a double integration by a double sum of function values at discretized points within the interval of integration, using weights. Here, the weights vary according with the Gauss points that are used.

All the previous generic equations need a coordinate transformation since the element is represented in a natural coordinate system. For such a transformation, it is used a Jacobian matrix. The following equations represent the stiffness matrix and the mass matrix, being [**J**] the Jacobian matrix:

$$[K]_k^e = \int_{-1}^{1}\int_{-1}^{1} [B]_k^{e\mathrm{T}}[\widehat{D}]_k[B]_k^e \ \det[\mathbf{J}]\mathrm{d}\xi\mathrm{d}\eta \tag{3.72}$$

$$[M]_k^e = \int_{-1}^{1}\int_{-1}^{1} [N]^{\mathrm{T}}[\widehat{J}]_k[N]\det[\mathbf{J}]\mathrm{d}\xi\mathrm{d}\eta \tag{3.73}$$

with

$$[\mathbf{J}] = \begin{bmatrix} \dfrac{\partial x}{\partial \xi} & \dfrac{\partial y}{\partial \xi} \\ \dfrac{\partial x}{\partial \eta} & \dfrac{\partial y}{\partial \eta} \end{bmatrix} \tag{3.74}$$

The derivatives of the global coordinate system can be calculated through the following equation:

$$\frac{\partial}{\partial x} = [\mathbf{J}]^{-1}\frac{\partial}{\partial \xi} \tag{3.75}$$

$$\frac{\partial}{\partial y} = [\mathbf{J}]^{-1}\frac{\partial}{\partial \eta} \tag{3.76}$$

3.4.5 Assembling with Partial Damping Treatments

In finite element mesh, the application of partial damping treatments has direct implications. In the case of total viscoelastic treatments, the layer of such case is present in the entire structure, so, all the elements of the mesh present the degrees of freedom provided by that layer and their presence is noted in the elementary stiffness and mass matrices. For partial damping treatments, the layer is not applied to the entire structure, thereby, the degrees of freedom of this layer are present only in some of the elements of the mesh.

In the assembling algorithm process, the length and the width of the viscoelastic layer are used, as well as the coordinates of the lower-left point of that layer, which positions the layer in the plate. Thus, only the elements that characterize the area affected by the treatment, contain information about the degrees of freedom provided by the damping layer.

The algorithm ensures that in nodes shared by different elements (where some of the elements characterize areas with damping treatments, while the others do not), the degrees of freedom that are added by the damping layer, are not used to build the elementary matrices in elements that are out of the damped area. This is explained and exemplified in Appendix A.

3.4.6 Shear Locking

Some theories (like Reissner-Mindlin, for instance) enunciate the presence of a phenomenon called "shear locking" occurs in plates. In these cases, one option is to apply the reduced integration method.

On thin plates, shear transverse deformations are not taken into account and the stiffness matrix of the element contains some high coefficients, leading to wrong values in the calculus of the generalized displacements field. That is when shear locking occurs. It is an expressive artificial increase of stiffness, especially in coefficients related to shear.

The reduced integration is a simple way to overcome the shear locking effects. This proceeding begins at the integration of the shear terms at the stiffness matrix, with $(m-1)^2$ Gauss points (being m the number of nodes that one element has on its side). In this case, a four-node element has two nodes on each side, so, $m = 2$. The reduced integration does not calculate shear terms of the stiffness matrix with precision, however, shear locking will not be a problem anymore [Oñate, 2013; Reddy, 2005].

3.5 Equations of Motion

In systems where viscoelastic materials provide damping capacity, the stiffness matrix depends on frequency and temperature, being $[\bar{K}(\omega, T)]$. Therefore, the system of equations of motion is written as:

$$[M]\{\ddot{x}(t)\} + [\bar{K}(\omega, T)]\{x(t)\} = \{f(t)\} \tag{3.77}$$

with $\{x(t)\}$ and $\{f(t)\}$ representing the response function and the load vector, respectively. This load vector is assumed as harmonic, being characterized with the phase vector $\{F(\omega)\}\, e^{j\omega t}$ with frequency ω:

$$\{f(t)\} = \{F(\omega)\}\, e^{j\omega t} \tag{3.78}$$

Considering that the system has a steady-state harmonic response, the amplitudes are characterized by $\{X(\omega)\}$ (frequency-dependent), with a relative lag δ_l, as a consequence of viscoelastic damping. The response presents a complex vector component, with frequency ω:

$$\{x(t)\} = \{X(\omega)\}\, e^{(j\omega - \delta_l)t} = \left\{\bar{X}(\omega)\right\} e^{j\omega t} \tag{3.79}$$

Both expressions 3.78 and 3.79, as well as derivative of 3.79 can now be introduced in the system of Equations 3.77:

$$\left[[\bar{K}(\omega, T)] - \omega^2[M]\right]\left\{\bar{X}(\omega)\right\} = \{F(\omega)\} \tag{3.80}$$

However, if the process occurs in isothermal conditions, the stiffness matrix will not depend on temperature:

$$\left[[\bar{K}(\omega)] - \omega^2[M]\right]\left\{\bar{X}(\omega)\right\} = \{F(\omega)\} \tag{3.81}$$

In Equation 3.81, $\left[[\bar{K}(\omega)] - \omega^2[M]\right]$ represents the dynamic stiffness matrix of the system. This matrix can also be represented by a shorter nomenclature, $[\mathcal{Z}(\omega)]$:

$$[\mathcal{Z}(\omega)]\left\{\bar{X}(\omega)\right\} = \{F(\omega)\} \tag{3.82}$$

3.6 Modes of Vibration

The characteristic equation allows obtaining the modes of vibration (even though the modes of vibration presented in this work are obtained with the eigs() function from MATLAB®). They are defined as synchronous harmonic motions since the harmonic motion is identical for all degrees of freedom. They are characterized by a natural frequency, ω_r and the corresponding mode shape.

These mode shapes represent the system's spatial configuration through its n degrees of freedom. In the modal matrix, each column represents each mode shape of vibration and each line corresponds to a different degree of freedom.

In dynamical analysis, it is usual to present a criterion of normalization for the modal vectors: normalization to unit modal mass, represented here by $\{\phi\}$. The criterion is the following:

$$\{\phi\}_i^{\mathrm{T}} [M] \{\phi\}_i = 1 \tag{3.83}$$

with $i = 1, ..., n$.

Modal vectors present orthogonality properties concerning mass matrix and stiffness matrix. Normalized modal vectors also present those properties, although they are called orthonormal properties:

$$\{\phi\}_i^{\mathrm{T}} [M] \{\phi\}_i = [I] \tag{3.84a}$$

$$\{\phi\}_i^{\mathrm{T}} [K] \{\phi\}_i = [\Omega^2] \tag{3.84b}$$

There, $[I]$ is the identity matrix and $[\Omega^2]$ is a diagonal matrix with the square values of natural frequencies [Rodrigues, 2019].

3.7 Frequency Response Functions

It is possible to define a Frequency Response Function (FRF) by Direct Frequency Analysis or Partial Fraction Expansion.

3.7.1 Direct Frequency Analysis

In the case of Direct Frequency Analysis, the FRF in the form of receptance, mobility or acceleration are defined as the ratio between a phasor of displacement, velocity or acceleration, respectively, and the amplitude of the load vector:

Receptance

$$\alpha_{jk}(\omega) = \frac{\bar{X}_j(\omega)}{F_k} \tag{3.85}$$

Mobility

$$Y_{jk}(\omega) = \frac{\bar{V}_j(\omega)}{F_k} = j\omega\alpha_{jk}(\omega) \tag{3.86}$$

Accelerance

$$A_{jk}(\omega) = \frac{\bar{A}_j(\omega)}{F_k} = -\omega^2\alpha_{jk}(\omega) \tag{3.87}$$

In each column k, for $i = 1, ..., n$, if $k \neq i$, then $F_i = 0$, since the excitation is applied only in one degree of freedom.

The frequency response functions in the form of receptance offer information about not only the amplitude of the motion, but also the lag between the response and the excitation, indicated by the argument [Moreira, 2004]. About the notation, for instance, in the FRF in the form of receptance, $\alpha_{jk}(\omega)$, $\bar{X}_{\mathrm{j}}(\omega)$ represents the amplitude and the lag of the response (in the degree of freedom j) of the system when is applied an excitation $F_{\mathrm{k}}(\omega)$ in the degree of freedom k

3.7.2 Partial Fraction Expansion

The matrix $[\alpha(\omega)]$ corresponds to the inverse of the dynamic stiffness matrix. Using an algebraic manipulation:

$$[\alpha(\omega)] = [\mathcal{Z}(\omega)]^{-1} \therefore [\alpha(\omega)]^{-1} = [\mathcal{Z}(\omega)] \tag{3.88}$$

Now, pre-multiplying by $[\phi]^{\mathrm{T}}$ and post-multiplying by $[\phi]$ the inverse of the FRF matrix:

$$[\phi]^{\mathrm{T}}[\alpha(\omega)][\phi] = [\phi]^{\mathrm{T}}[\mathcal{Z}(\omega)][\phi] = [\omega_r^2 - \omega^2] \tag{3.89}$$

Applying orthonormality properties of modal vectors concerning both mass and stiffness matrices it is created a diagonal matrix, whose coefficients are the difference between the square values of natural frequencies, ω_r^2 and frequencies ω^2:

$$[\alpha(\omega)] = [\phi][\omega_r^2 - \omega^2]^{-1}[\phi]^{\mathrm{T}} \tag{3.90}$$

So, the FRF matrix is the product of the modal matrix, the inverse of $\omega_r^2 - \omega^2$ and the transpose of $[\phi]$. Next, that result is multiplied by the transposed matrix (where each line is the same mode shape used before). The result is the FRF, given by the sum of n terms, where each one of them is a fraction with denominator $\omega_r^2 - \omega^2$ and in the numerator is the product between the components of the mode shapes of vibration. The first fraction corresponds to the first mode of vibration, the second fraction to the second mode, and so on:

$$\alpha_{jk}(\omega) = \sum_{r=1}^{n} \frac{\phi_{jr}\phi_{kr}}{(\omega_r^2 - \omega^2)} \tag{3.91}$$

Each fraction is the contribution of each mode to the frequency response function. This way of representing those functions is called the Partial Fraction Expansion [Rodrigues, 2019].

3.8 Numerical Validation

Now that the finite element is presented, it is time to check if all the results are correct. Thus, it is proposed the validation of this model, which was implemented in MATLAB ®. This validation consists of a modal analysis, where it is checked the consonance between theoretical and numerical values.

One easy way to validate the results is by comparing the results between nondimensionalized frequencies, since they are only dependent on ratios between properties of the material and geometry, as expressed in Equation 3.92:

$$\bar{\omega} = \omega \left(\frac{a^2}{h}\right)\sqrt{\frac{\rho}{E_2}} \tag{3.92}$$

The following results consider a simply supported square plate. Table 3.2 details all the properties and conditions that were considered for these two tests.

Table 3.2: Properties of the plate.

l=b /m	h /m	E_1 /Pa	G_{12} /Pa	G_{13} /Pa	G_{23} /Pa	ν_{12}	ρ /kg.m^{-3}
0.3	$0.1a$	25×10^6	$0.6E_2$	$0.6E_2$	$0.5E_2$	0.25	1800

This plate is a four-layer symmetric cross-ply square plate ($a = 0.3$ m) with fiber orientation (0/90/90/0) and it is simply supported at all edges:

$$u = 0,\ \theta_x = 0,\ x = 0, a \tag{3.93a}$$

$$v = 0,\ \theta_y = 0,\ y = 0, b \tag{3.93b}$$

Table 3.3 presents the theoretical values from Reddy [2003], used to check if the obtained values in MATLAB ® are close so that the accuracy of the results can be verified.

Table 3.3: Theoretical nondimensionalized frequencies $\bar{\omega}$ of four layer cross-ply laminates [Reddy, 2003].

$\frac{E_1}{E_2}$	$\frac{l}{h}$	$\bar{\omega}$
3	5	6.570
	10	7.243
10	5	8.298
	10	9.841
20	5	9.567
	10	12.218
40	5	10.854
	10	15.107

3.8.1 Influence of the Mesh Size

Since the theoretical nondimensionalized frequencies were already presented, it is possible to analyze several nondimensionalized frequencies obtained for each fundamental natural frequency, with different meshes. It is predictable that the error of such values decreases as mesh size increases.

This validation allows to check which mesh size is acceptable to use in the analysis of any case since high refined meshes need more computing time, which is a disadvantage. Thus, in Table 3.4, it is possible to compare nondimensionalized frequencies for different mesh sizes with the theoretical first natural frequency.

Table 3.4: Nondimensionalized frequencies $\bar{\omega}$ of four layer cross-ply laminates.

			Mesh				
$\frac{E_1}{E_2}$	$\frac{l}{h}$	$\bar{\omega}$	5×5	10×10	20×20	40×40	60×60
3	5	**6.570**	6.695	6.526	6.484	6.474	6.472
	10	**7.243**	7.521	7.287	7.231	7.216	7.214
10	5	**8.298**	8.295	8.125	8.082	8.071	8.069
	10	**9.841**	10.146	9.846	9.773	9.754	9.752
20	5	**9.567**	9.399	9.246	9.207	9.197	9.196
	10	**12.218**	12.467	12.137	12.054	12.034	12.030
40	5	**10.854**	10.449	10.323	10.291	10.283	10.281
	10	**15.107**	15.182	14.846	14.762	14.704	14.702

According to Table 3.4, as expected, the refinement of the mesh led the values to converge. All the nondimensionalized frequencies converge to values that are lower than the theoretical ones. It is possible to say that, for a 20×20 mesh, the nondimensionalized frequencies are already close to the theoretical values obtained with a FSDT theory, thus, that mesh can represent the plate.

3.8.2 Number of Layers

The values from Reddy [2003] are calculated with FSDT theories, whose reference plane is at the middle of the laminate. In Layerwise Theory, this reference plane is the middle plane of the lower layer. It provides numerical flexibility to the model. To verify this, the four-layer laminate is now an eight-layer laminate (0/0/90/90/90/90/0/0) with the same thickness. In Table 3.5, it is possible to compare nondimensionalized frequencies for the first natural frequency, for different mesh sizes.

Table 3.5: Nondimensionalized frequencies $\bar{\omega}$ of eight layer cross-ply laminates.

			Mesh		
$\frac{E_1}{E_2}$	$\frac{l}{h}$	$\bar{\omega}$	5×5	10×10	20×20
3	5	**6.570**	6.666	6.499	6.458
	10	**7.243**	7.510	7.278	7.221
10	5	**8.298**	8.230	8.063	8.021
	10	**9.841**	10.114	9.817	9.744
20	5	**9.567**	9.294	9.145	9.108
	10	**12.218**	12.402	12.075	11.994
40	5	**10.854**	10.294	10.173	10.142
	10	**15.107**	15.053	14.724	14.642

Comparing both Tables 3.4 and 3.5, it is possible to see that the increase in the number of layers get the nondimensionalized frequencies' values down. Thereby, the increase in the number of layers causes the decrease of $\bar{\omega}$.

Chapter 4

Dynamical Analysis of Viscoelastic Damping Treatments

4.1 Introduction

Following the previous discussion about viscoelastic damping treatments, the Frequency Response Functions (FRF) provide, for instance, information about the number of modes in the bandwidth of interest, natural frequencies, damping efficiency, or the influence of the structure's geometry, as well as of its properties.

In the ongoing chapter, it is presented the dynamical analysis on seven specimen plates. Firstly, seven 254×198 mm are presented, however, they are cut in halves and this analysis focuses its attention in seven 198×126 mm plates. Some of the aims of this dynamical analysis are the study of the effects that the relation between length and thickness has in the final results, as well as to understand the effectiveness of partial damping treatments.

4.2 Viscoelastic Materials

The composite plate specimens manufactured for this experimental campaign used Hexcel 8552 IM7 Unidirectional Prepreg plies, manually stacked at INEGI by the co-advisor of the present work as part of his ongoing doctoral thesis work. The main subject of his work is, contrary to the classical damping treatments where viscoelastic layers take part in a stacking sequence of composite laminae to increase damping, to study partially distributed viscoelastic material within specific layers - integrated damping patches.

The main concern about such configurations is their feasibility. Traditional viscoelastic materials do not support autoclave temperatures. To overcome this issue, SMAC-Group Montblanc Technologies developed a patented product called SMACWRAP ST® that withstands composite curing, including autoclave process, so might be embedded into composite structures. Other viscoelastic materials require co-curing, and contrary to the SMACWRAP ST®, which withstands autoclave curing but does not undergo a chemical reaction, KRAIBON® rubber must vulcanize at 150 °C. Plate specimens used in the present work were manufactured using samples of both viscoelastic materials, whose properties were obtained in the context of the referred work at 24°C. Table 4.1 presents the constitutive model parameters for SMACWRAP ST ®

Table 4.1: SMACWRAP ST ® constitutive model parameters at 24°C.

E_0 /Pa	E_∞ /Pa	τ /s	α	ν	ρ /kg.m^{-3}
$1{,}5408 \times 10^6$	$1{,}3907 \times 10^9$	$5{,}0933 \times 10^{-8}$	0,4827	0,49	1300

Figure 4.1 shows the Young Modulus and the loss factor variation with frequency for SMACWRAP ST ®.

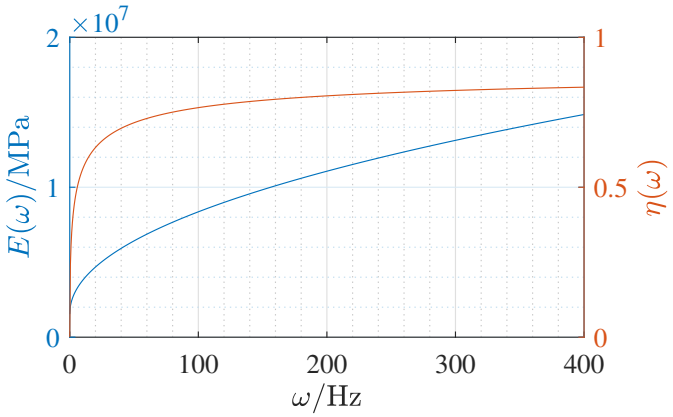


Figure 4.1: Storage modulus and loss factor of SMACWRAP ST ®.

In addition to SMACWRAP ST ®, KRAIBON ® is also used. Its properties are shown in Table 4.2.

Table 4.2: KRAIBON ® constitutive model properties at 24°C.

E_0 /Pa	E_∞ /Pa	τ /s	α	ν	ρ /kg.m^{-3}
4,8542×10^6	8,0067×10^9	2,3725×10^{-8}	0,3316	0,49	1740

Figure 4.2 presents the relationship between Young modulus and loss factor with frequency of storage modulus and loss factor for KRAIBON ®.

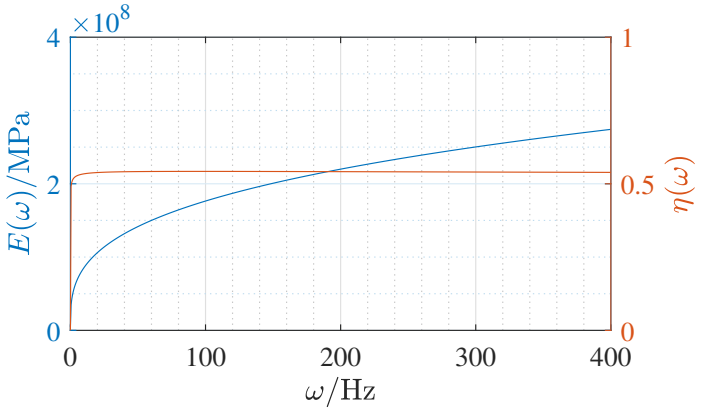


Figure 4.2: Storage modulus and loss factor of KRAIBON ®.

4.3 Specimens Characterization

Previously, seven CFRP specimens in this analysis were manufactured by a curing process. At first, those specimens were 254×198 mm. That seven plates were cut in halves, resulting in fourteen plates. Figure 4.3 presents the nodes of interest in this analysis, as well as all the main dimensions.

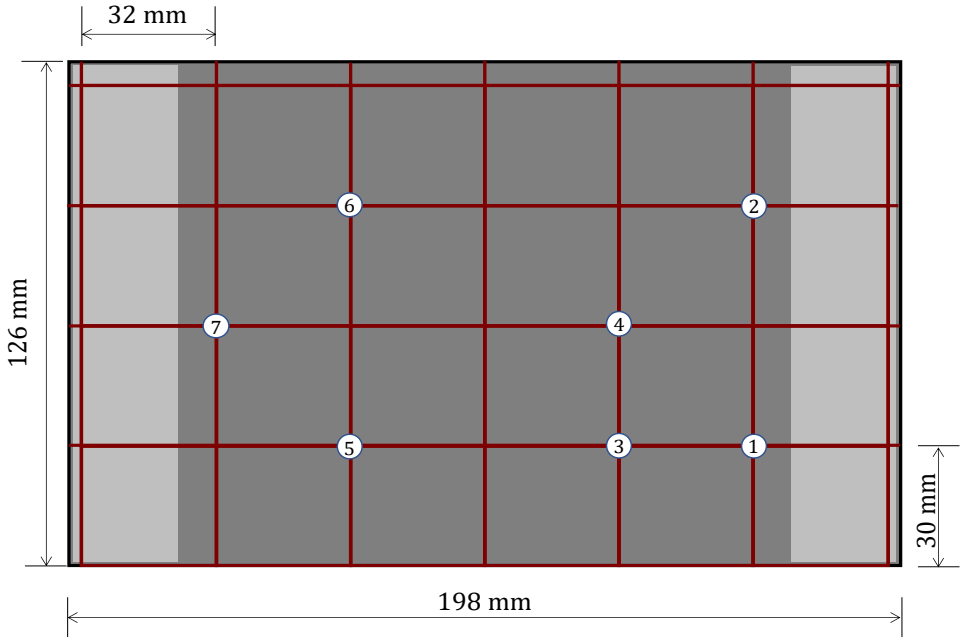
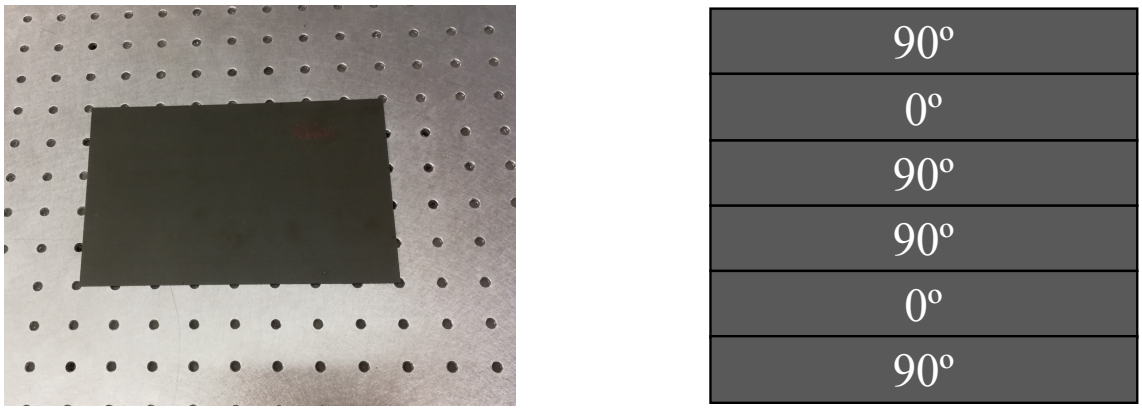


Figure 4.3: Mesh (the lighter area represents the location of the viscoelastic strips).

Figure 4.4a shows one of the plates. One considers a reference specimen for comparison purposes, with no damping treatment applied. It is a symmetric laminate composite plate with stacking sequence $(90/0/90/90/0/90)_S$ - Figure 4.4b. The thickness of each layer is 0.125 mm.



(a) Specimen.

(b) Stacking sequence.

Figure 4.4: Laminate composite plate.

The composite material used to manufacture this plates was Hexcel 8552 IM7®, whose properties are listed in Table 4.3.

Table 4.3: Properties of Hexcel 8552 IM7®.

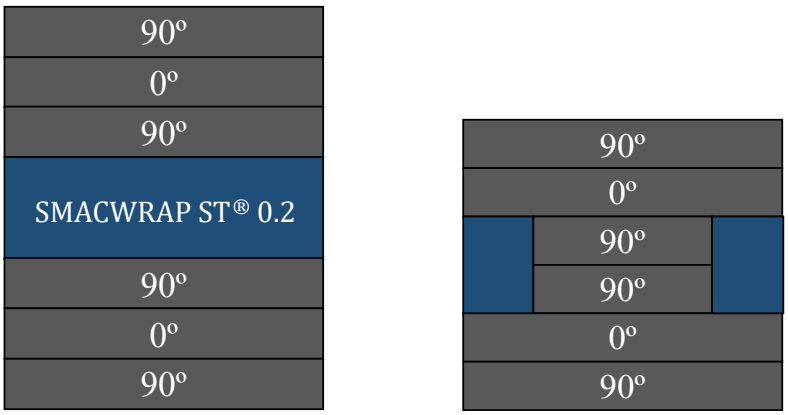
E_1 /Pa	E_2 /Pa	ν_{12}	ν_{13}	ν_{23}	G_{12} /Pa	G_{13} /Pa	G_{23} /Pa	ρ /kg.m^{-3}
161×10^9	11.38×10^9	0.32	0.32	0.45	5.2×10^9	5.2×10^9	3.9×10^9	1570

The other six plates have different damping treatment configurations: SMACWRAP

ST ® 0.2 mm - Figures 4.5a (total treamtent) and 4.5b (partial treatment) -, SMACWRAP ST 0.1 mm® - Figures 4.6a (total treatment) and 4.6b (partial treatment) - and KRAIBON ® - Figures 4.7a (total treatment) and 4.7b (partial treatment).

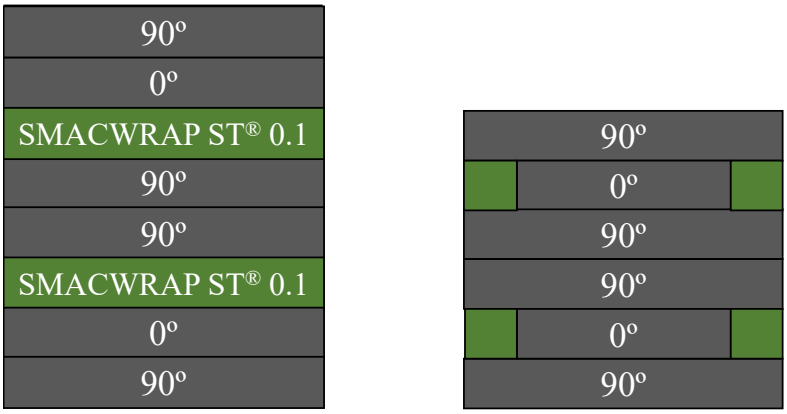
The arrangements with SMACWRAP ST ® present different configurations, as they use viscoelastic layers with 0.1 mm or 0.2 mm of thickness. The purpose is to realize the importance of the viscoelastic core in the stacking sequence, using the same amount of material in both scenarios. KRAIBON ® plates have a viscoelastic layer with 0.5 mm of thickness, in which two extra layers of orthotropic material were added to the structure.

The plates with SMACWRAP ST ® present a viscoelastic core with 0.1 mm or 0.2 mm of thickness, instead of 0.125 mm or 0.25 mm, which are the design thicknesses of one or two orthotropic layers, respectively. However, these layers were not included in the curing process: they were glued and the remaining space was filled with glue. The validation tests confirmed that using 0.1 mm or 0.2 mm for numerical tests does not interfere with the accuracy of the final numerical results.



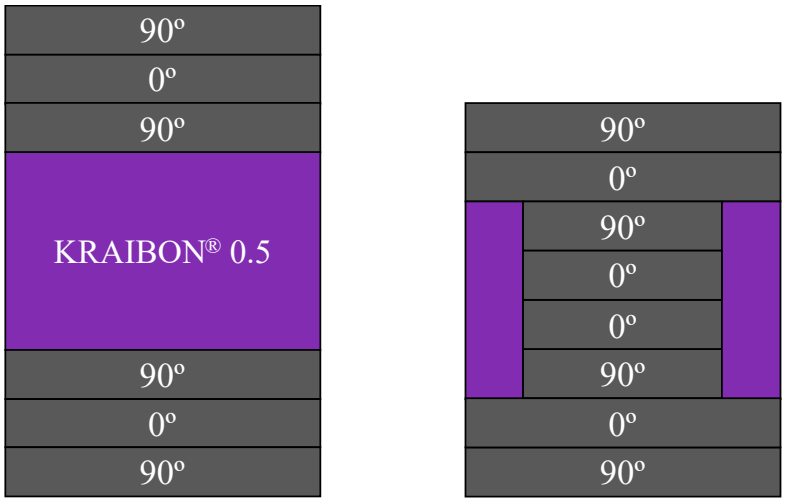
(a) Total damping treatment. (b) Partial damping treatment.

Figure 4.5: SMACWRAP ST ® 0.2 mm configurations.



(a) Total damping treatment. (b) Partial damping treatment.

Figure 4.6: SMACWRAP ST ® 0.1 mm configurations.



(a) Total damping treatment. (b) Partial damping treatment.

Figure 4.7: KRAIBON ® 0.5 mm configurations.

4.4 Experimental Setup and Procedure

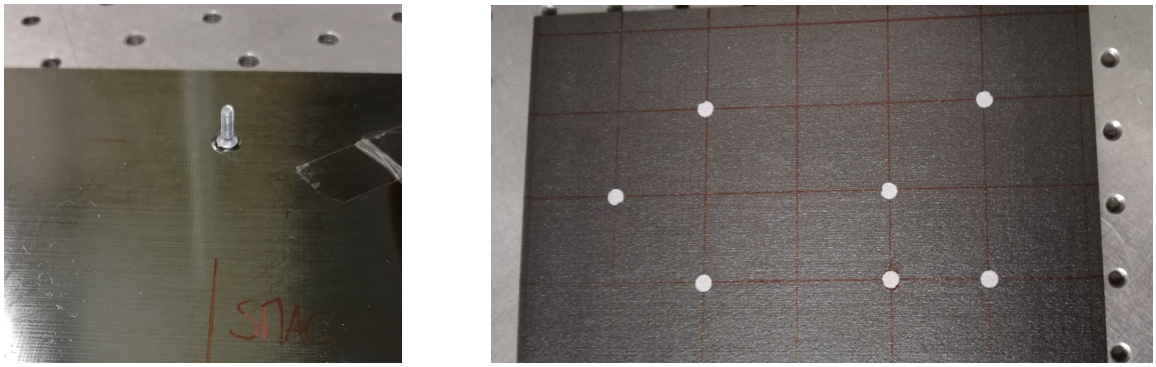
The experimental setup simulates a system where a free edge plate vibrates when it is submitted to a random excitation in a specific point. Some adjustments were carried out, since it is too difficult to have a free edge system. The plate is suspended in the air, in a rigid frame, using two nylon wires, that are bonded to the plate by an adhesive, 43 mm away from the plate corners - see Figure 4.8.



Figure 4.8: Suspended Plate.

The connection between the plate and the force transducer is made through the bolt

of Figure 4.9a, that is in node 3 in every plate. On the other side of the plate, there is reflective paper on each of the previous numbered nodes, as Figure 4.9b shows.

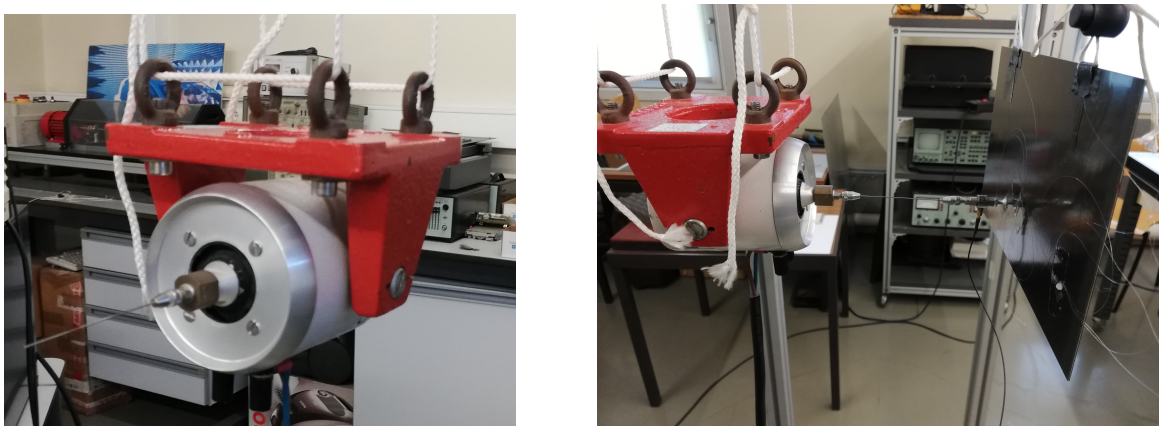


(a) Bolt.

(b) Reflective paper.

Figure 4.9: Instrumented plate.

The electromagnetic shaker of Figure 4.10a receives the signal generated in the analyzer and converts it into a mechanical excitation. The bolt that is on the surface of the plate will have a force transducer, depicted Figure 4.10b, that will connect to the shaker by a connecting rod.



(a) Electromagnetic Shaker.

(b) Force transducer attached to the plate.

Figure 4.10: Excitation of the system.

A contactless laser doppler vibrometer measures the velocity of the plate surface. The main advantage of this contactless measuring method is to establish an experimental procedure avoiding possible mass and stiffness disturbances which may lead to erroneous results, particularly in light structures. The sensor head sends and receives a helium laser from the plate and the controller decodes the signal from the laser.

The response in node 3 provides a point FRF. These two devices are represented in Figure 4.11.



(a) Laser head.



(b) Vibrometer controller.

Figure 4.11: Laser Doppler Vibrometer System.

The force transducer and the laser vibrometer provide information to the FFT spectral analyzer of figure 4.12, that are used to generate the frequency response functions.



Figure 4.12: FFT spectral analyser.

The sensitivities of the force transducer and the laser vibrometer are listed in Table 4.4.

Table 4.4: Sensitivity of the transducers.

Device	Force Transducer /pC $N^{-}1$	Laser Vibrometer /mm $s^{-}1$ $V^{-}1$
Sensitivity	3.3	25

The diagram of Figure 4.13 represents the experimental setup for this work.

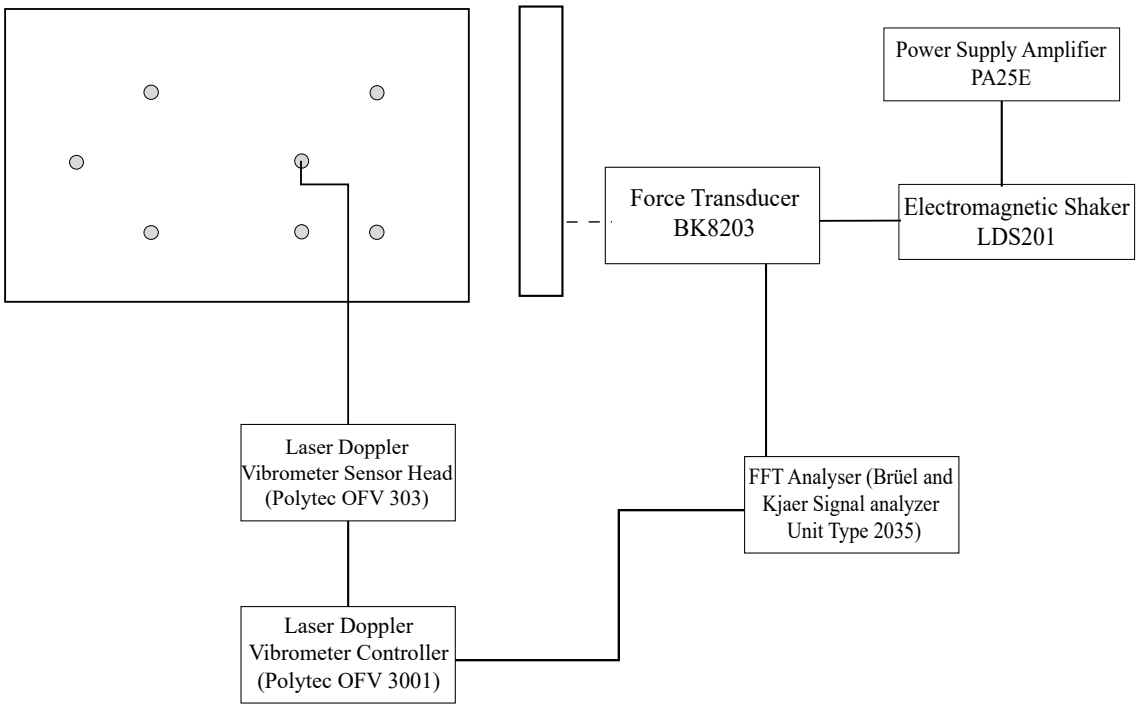


Figure 4.13: Diagram of the experimental setup.

4.5 Frequency Domain Based Approaches

The following methods allow to calculate the loss factor by different ways, based on frequency domains. The first one is the Modal Strain Energy approach, a complex modulus approach that predicts the loss factor in structures with viscoelastic damping treatments from the ratio between the dissipated modal strain energy of the viscoelastic part and the storage modal strain energy of the structure. The MSE approach establishes that the undamped modes of vibration represent the damped modal model with a frequency-independent stiffness matrix. However, MSE methods provide poor viscoelastic damping estimations in structures with high damping capacity, which leaded to new iterative approaches.

The Iterative Modal Strain Energy is an upgrade of MSE and also assumes frequency-independent stiffness matrices. However, in the current work, it is necessary a method that does not assume that the modes of the undamped system represent the damped system, as IMSE does.

The Iterative Complex Eigensolution (ICE) method does that. Its approach does not estimate the modal loss factor as MSE, for instance. ICE uses the complex eigenvalue to calculate an exact modal loss factor value, although its high computational cost is a disadvantage. This method successively updates the complex stiffness matrix by an iterative process. The complex eigensolution provides complex eigenvalues, according to a convergence criterion.

By ICE, the numerical accuracy is significantly better than the one provided by IMSE. The modal density or the bandwidth of interest can control the computational costs since each mode requires several complex eigensolutions before the convergence [Vasques, 2008].

As said before, ICE and IMSE approaches have similar algorithms. The only difference is on eigensolution pairs, which may consider complex quantities. The following algorithm summarizes the essence of the ICE approach that was used.

Step 1: Eigensolution with $\omega = \omega^0$:

$$\mathrm{Re}\left[\mathbf{K}_{uu}(j\omega^0)\right]\phi_r = (\omega_r^0)^2\mathbf{M}_{uu}\phi_r$$

Step 2: Loop for each eigenpair $(\omega_r^0, \{u_r\})$ with r=1,...,p:

1. Initial Value

$$\omega_r^i = \omega_r^0$$

2. Iterative loop for each natural frequency and mode shape:

- Eigensolution $(\omega_s^0, \{\phi_s\})$ with s=1,...,r

$$\mathbf{K}_{uu}(j\omega_r^i)\phi_s = (\omega_s^{i+1})^2\mathbf{M}_{uu}\phi_s$$

- Iterated damped natural frequency

$$\begin{cases} \omega_s^{i+1} : \text{rejected} & ,\text{for s} < \text{r} \\ \omega_r^{i+1} = \sqrt{\mathrm{Re}(\omega_s^{i+1})} & ,\text{for s} = \text{r} \end{cases}$$

- Convergence condition test

$$\Delta_\omega = \frac{|\omega_r^{i+1} - \omega_r^i|}{\omega_r^{i+1}} \leq \Delta_{max}$$

Step 3: Determination of modal loss factor:

$$\eta_r = \frac{\mathrm{Im}(\omega_r^{i+1})}{\mathrm{Re}(\omega_r^{i+1})}$$

4.6 Correlation Indicator

As expected, numerical and experimental results differ one from another. One way to compare both of them is by correlation indicators, such as the Local Amplitude Criterion (LAC). This criterion determines how close the two FRF's are and shows in a clear-sighted way the regions of good and poor correlation between them:

$$\mathrm{LAC}_{jk}(\omega) = \frac{2|\left\{H_{jk}^{num}(\omega)\right\}^{\mathrm{H}}\left\{H_{jk}^{exp}(\omega)\right\}|}{\left\{H_{jk}^{num}(\omega)\right\}^{\mathrm{H}}\left\{H_{jk}^{num}(\omega)\right\} + \left\{H_{jk}^{exp}(\omega)\right\}^{\mathrm{H}}\left\{H_{jk}^{exp}(\omega)\right\}} \tag{4.1}$$

where $\left\{H_{jk}^{num}\right\}$ and $\left\{H_{jk}^{exp}\right\}$ denote the FRF's obtained by numerical and experimental procedures, respectively. The index H represents the conjugate of the vector.

The LAC correlation provides enough information to check which frequency ranges have a poor correlation between experimental and numerical FRF's for the degrees of freedom in analysis. This indicator consists of a value between 0 (no correlation verified) and 1 (perfect correlation) [Moreira, 2004].

4.7 Reference Plate Results: 254×198 mm

The evaluation of the frequency response functions starts with an analysis, in this subchapter, of the results with FRF in the form of mobility for base 254 × 198 mm plates, accompanied by quantitative comparisons of both FRF using LAC. The following figures present only point FRF.

4.7.1 Reference Plate

Figure 4.14 shows the numerically generated FRF and the experimental FRF for the reference plate. Figure 4.15 depicts the evaluation of correlation with LAC.

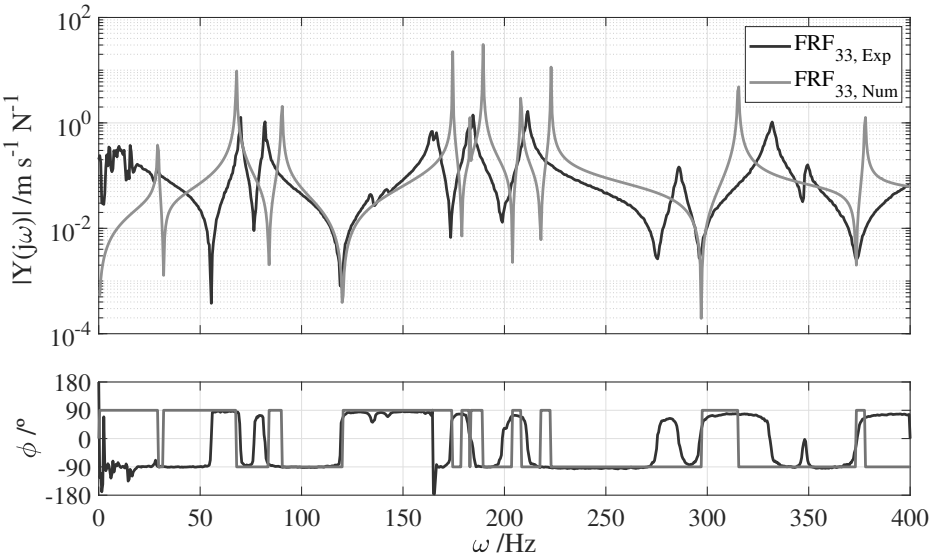


Figure 4.14: Numerical and experimental FRF_{33} for the reference base plate.

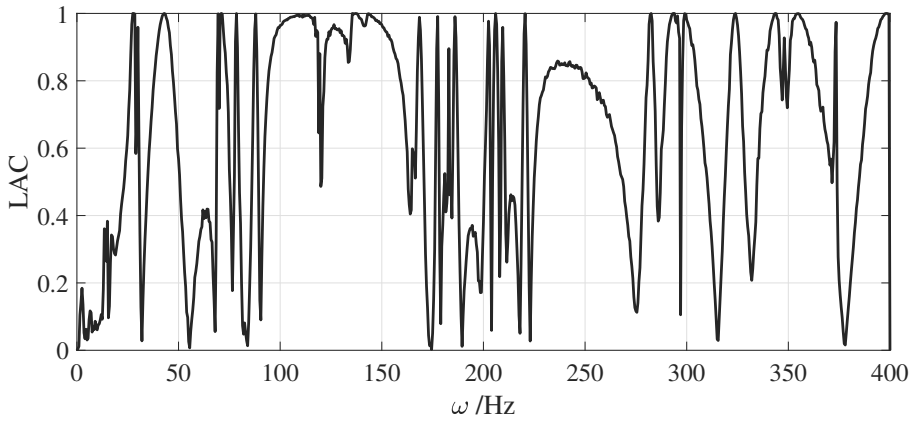


Figure 4.15: LAC for the FRF_{33} of the reference base plate.

For the reference plate, the evaluation by LAC exposes the difficulties of predicting the behavior of the plate in the experimental situation by the numerical model. One of the explanations resorts in the plate's thickness. It is more difficult to predict the response of a thin structure since geometric imperfections that appear due to the manufacture of a composite structure (variability of the mechanical properties due to storage conditions or

assuring the predicted stacking sequence, among others) may be more evident in thinner plates, where this manufacturing restrictions can promote warping, for instance.

4.7.2 SMACWRAP ® 0.2 mm Damping Treatment

Figure 4.16 illustrates the representation of the numerical and experimental FRF's, using the configuration from Figure 4.5a. LAC comparison is shown in Figure 4.17.

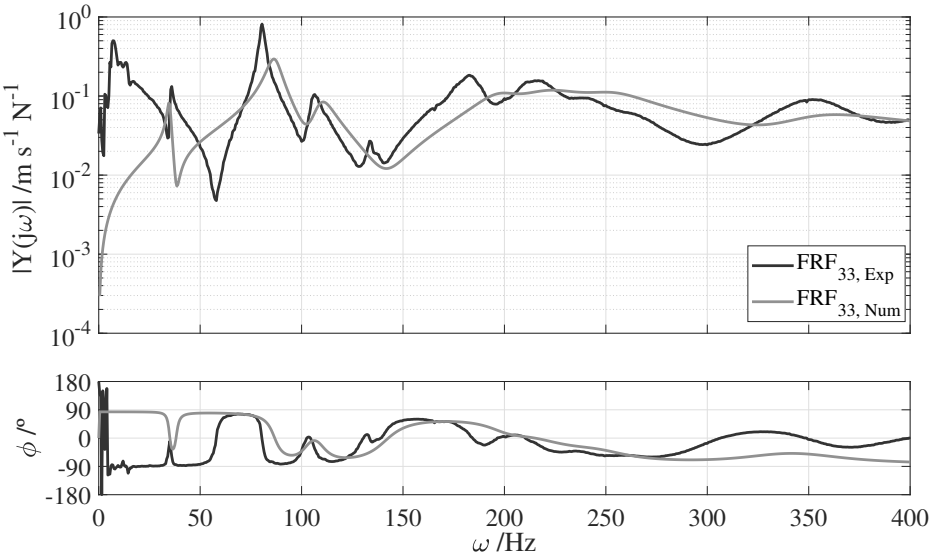


Figure 4.16: Numerical and experimental FRF_{33} for the base plate with SMACWRAP ® 0.2 mm total damping treatment.

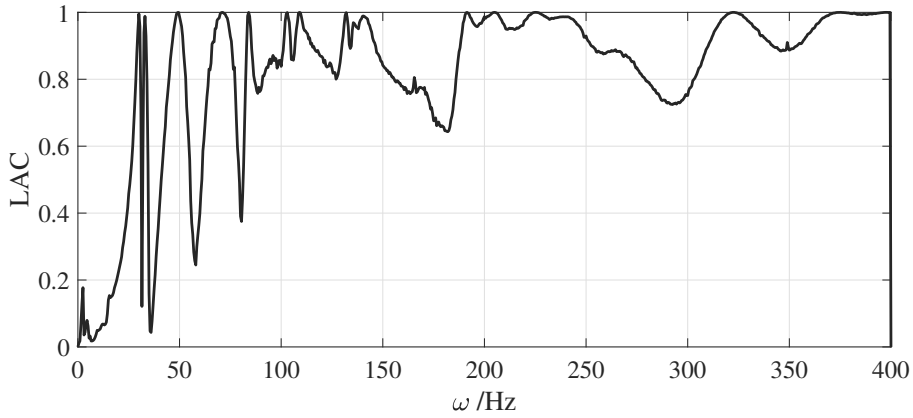


Figure 4.17: LAC for the FRF_{33} for the base plate with SMACWRAP ® 0.2 mm total damping treatment.

Bearing in mind that the thickness of these plates is higher than the thickness of the reference plate, when ω=100 Hz, there is an attenuation of the curve, since resonance frequencies are no longer easily detectable, which evidences the damping capacity of the structure. Besides that, the curve acquires a plateau shape. LAC shows a good approximation between the numerical FRF and the experimental FRF for that range of frequencies. It is possible due to the plateau shape caused by damping in modes with higher frequencies. Another important cause is the increase in thickness.

Figures 4.18 and 4.19 present the information for treatments with the SMACWRAP ® 0.2 mm partial damping treatment. This plate has the same total thickness as the reference base plate, which will help to understand the effects of adding viscoelastic material by removing CFRP material.

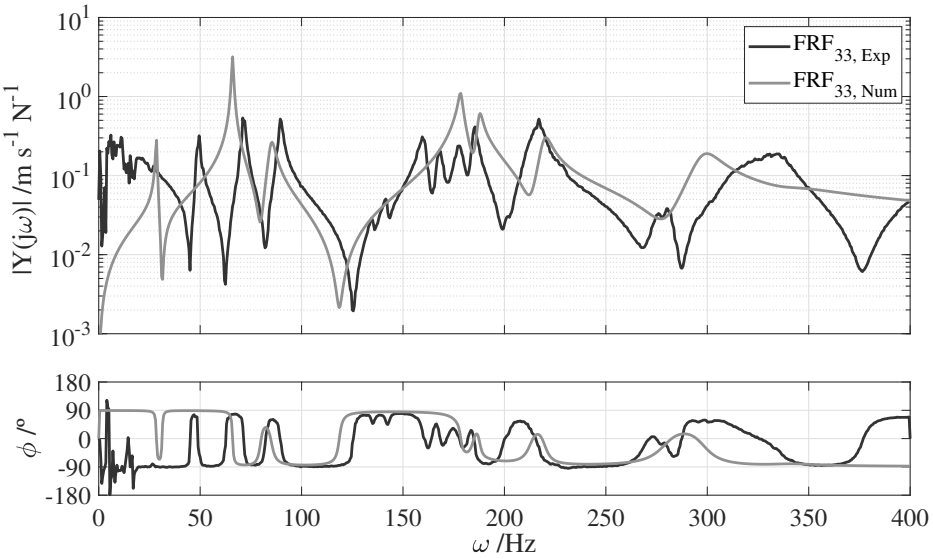


Figure 4.18: Numerical and experimental FRF_{33} for the base plate with SMACWRAP ® 0.2 mm partial damping treatment.

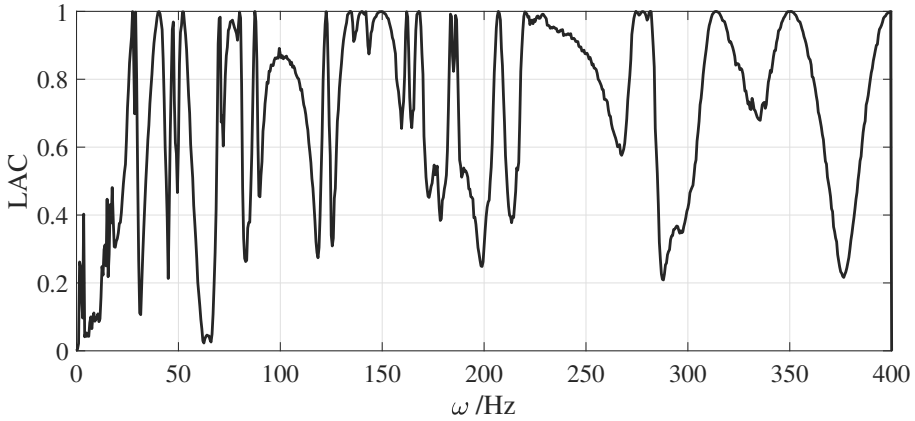


Figure 4.19: LAC for the FRF_{33} for the base plate with SMACWRAP ® 0.2 mm partial damping treatment.

Comparing Figure 4.19 with Figure 4.15, the results show a better correlation in the partial damped plate, which is only provided by the treatment, despite the experimental FRF presents a higher number of peaks. The FRF's regarding the partial damping treatment, which present a lower thickness, do not show clearly the provided damping capacity as the total treatment does.

4.7.3 SMACWRAP ® 0.1 mm Damping Treatment

This configuration has, approximately, the same amount of VEM (it is not guaranteed since the manufacture of a layer with a constant thickness of 0.2 mm is easier than a layer

with 0.1 mm, however, the strips have half of the thickness and they are not at the middle plane of the plate. Figure 4.20 shows the representation of the numerical and experimental FRF's, using the configuration from Figure 4.6a. The evaluation by LAC is in Figure 4.21.

In some configurations, especially the ones with the lowest thicknesses (such as the reference plate or SMACWRAP ® 0.1 mm configuration), the plate presented a curvature that in this last configuration offered to the plate a bistable state, before cutting.

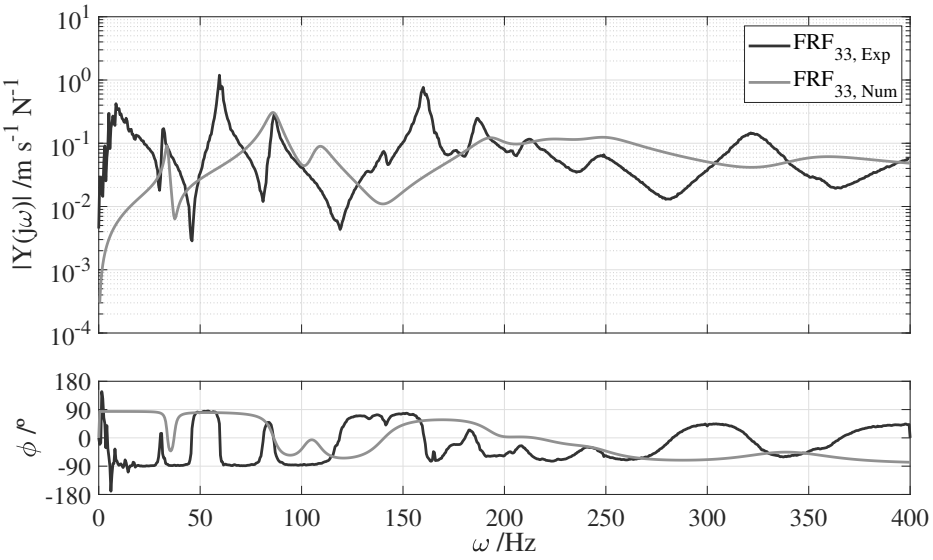


Figure 4.20: Numerical and experimental FRF_{33} for the base plate with SMACWRAP ® 0.1 mm total damping treatment.

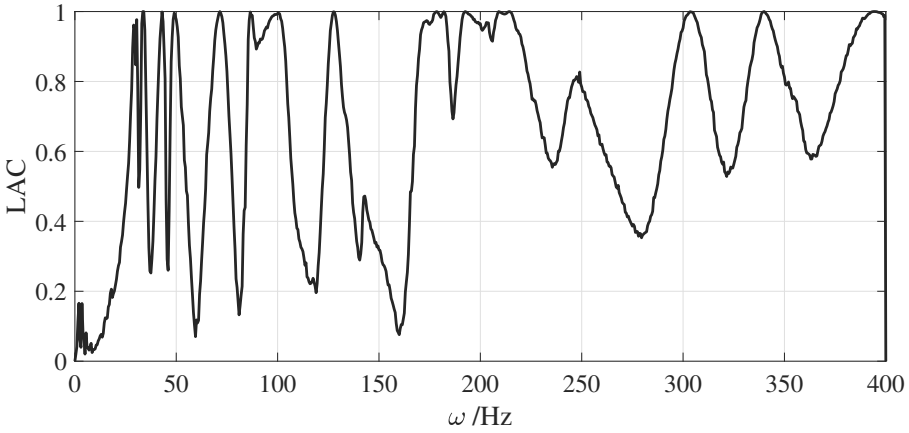


Figure 4.21: LAC for the FRF_{33} for the base plate with SMACWRAP ® 0.1 mm total damping treatment.

Comparing with the equivalent case of SMACWRAP ® 0.2 mm configuration, the results are worse in terms of correlation. The damping capacity is not as good as before and the reason for that is the position of the strips in the stacking sequence: the innermost, the better for damping capacity as it was explained before for integrated damping treatments. Modes of vibration with higher frequencies are more influenced by damping treatments.

An equivalent comparison can be made for partial damping treatments - Figure 4.22 with LAC in Figure 4.23. This plate has the 0.1 mm strips in a partial configuration,

together with the new stacking positioning.

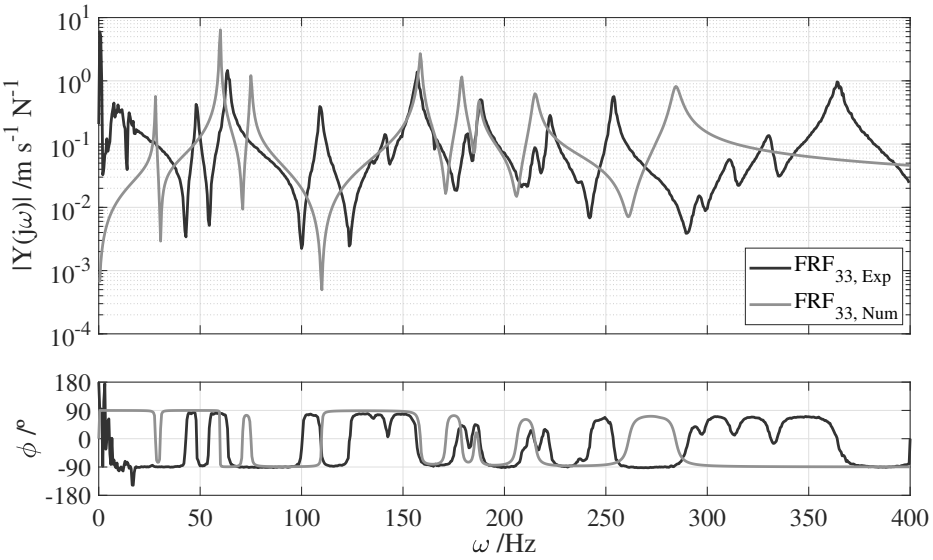


Figure 4.22: Numerical and experimental FRF_{33} for the base plate with SMACWRAP ® 0.1 mm partial damping treatment.

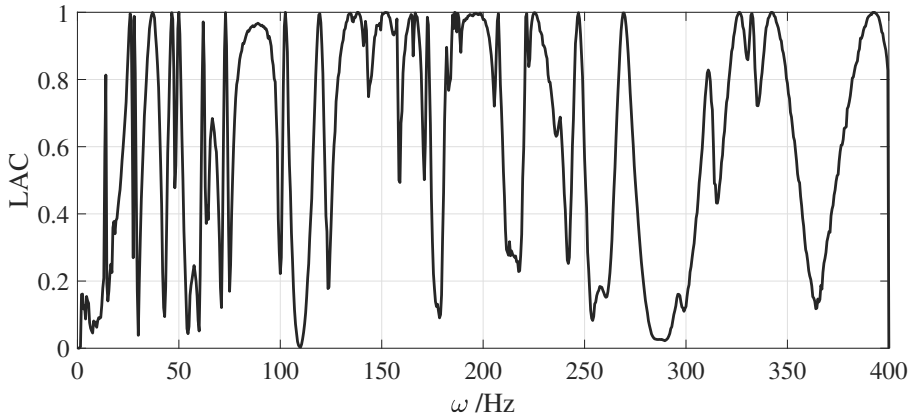


Figure 4.23: LAC for the FRF_{33} for the base plate with SMACWRAP ® 0.1 mm partial damping treatment.

Here, given the conditions, it is almost undetectable the presence of the viscoelastic layer. Comparing with the graphic of the reference plate, the numerical FRF may present some damping at higher frequencies, which is not corroborated by the experimental FRF. This configuration seems to not provide any advantage when compared with the other ones. The correlation between the FRF's is also low, evidencing that a thin plate with thin partial treatments can amplify the effects of the plate's imperfections.

4.7.4 KRAIBON ® 0.5 mm Damping Treatment

Plates with KRAIBON ® 0.5 mm total damping treatment are the thickest ones of the entire analysis, with a viscoelastic core at the middle plane of the plate. Figures 4.24 and 4.25 help in the confirmation of such assumptions.

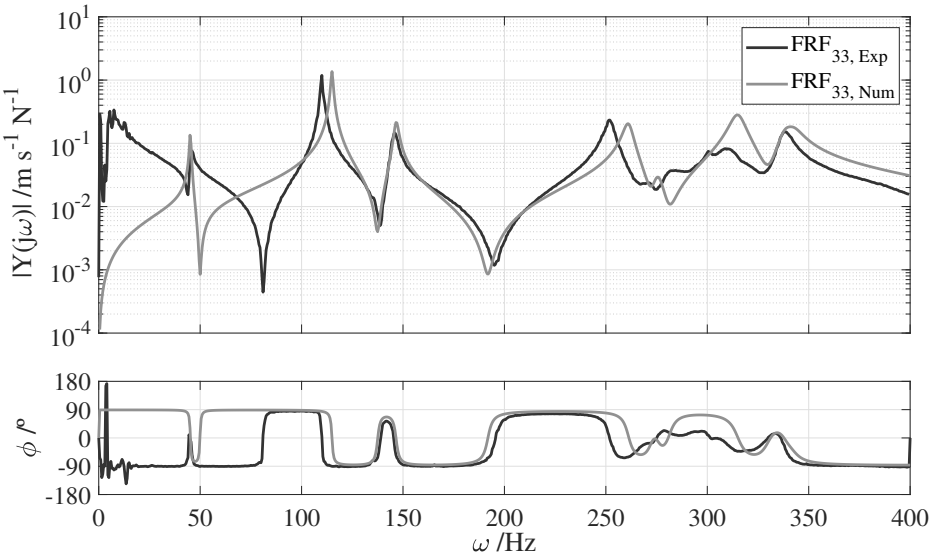


Figure 4.24: Numerical and experimental FRF_{33} for the base plate with KRAIBON® 0.5 mm total damping treatment.

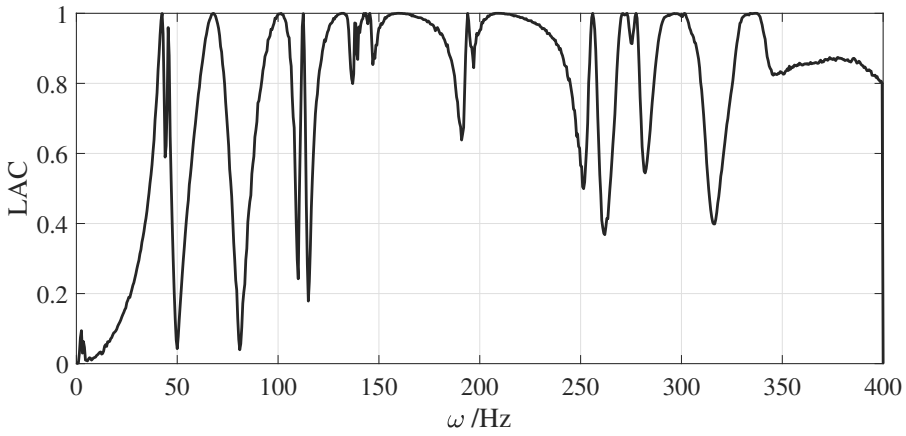


Figure 4.25: LAC for the FRF_{33} for the base plate with KRAIBON® 0.5 mm total damping treatment.

Comparing with the LAC evaluation from Figure 4.17, which is the best configuration so far, the results of Figure 4.25 are not better in general. The materials are different, so, the conditions that each one offers are necessarily different.

The partial damping treatment's results are in Figure 4.26 and 4.27.

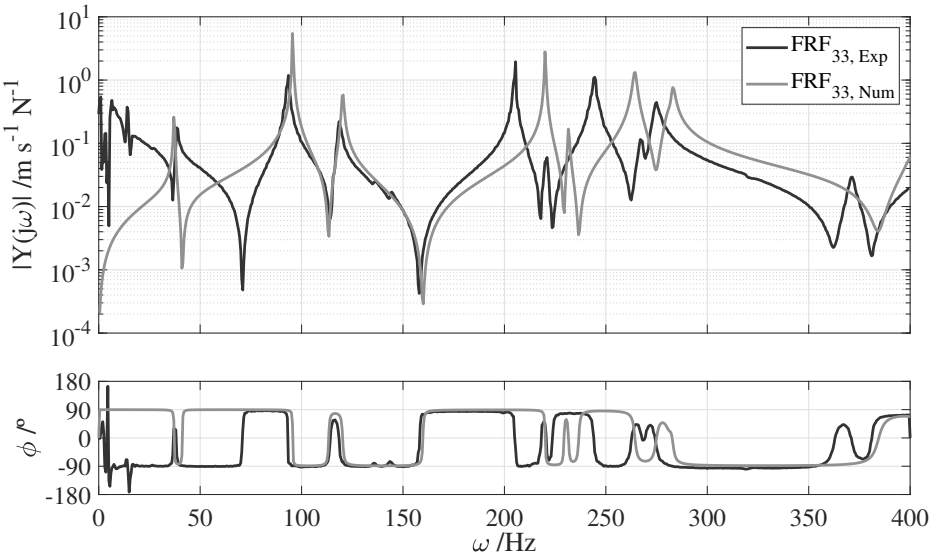


Figure 4.26: Numerical and experimental FRF_{33} for the base plate with KRAIBON® 0.5 mm partial damping treatment.

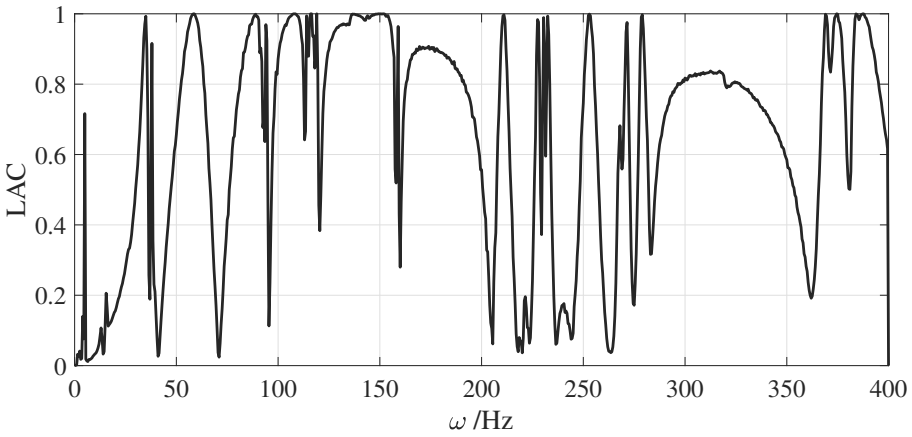


Figure 4.27: LAC for the FRF_{33} for the base plate with KRAIBON® 0.5 mm partial damping treatment.

The behavior of this plate is like the verified with SMACWRAP® 0.2 mm partial damping treatment, which was the best option so far. Once again, there are two materials with different properties, so few conclusions can be taken from these figures. Nevertheless, the correspondence between some modes of vibration is good, specially at lower frequencies.

Despite the difference is small, the plates with total damping treatments may present better correlations since the thickness is higher. LAC evaluation also shows that the second mode of vibration is in the frequency range where the concordance is better.

4.8 Reference Plate Results: 198×126 mm

In the context of this work, the base reference plate of each configuration was cut into two halves. The plates are now 198 × 126 mm.

In relative terms, the relation between length and thickness of these plates is bigger than the base reference one, so, despite being smaller, these plates shall be more stable.

Figure 4.28 shows the numerical and experimental point FRF for the reference plate. The correlation between these two is in Figure 4.29.

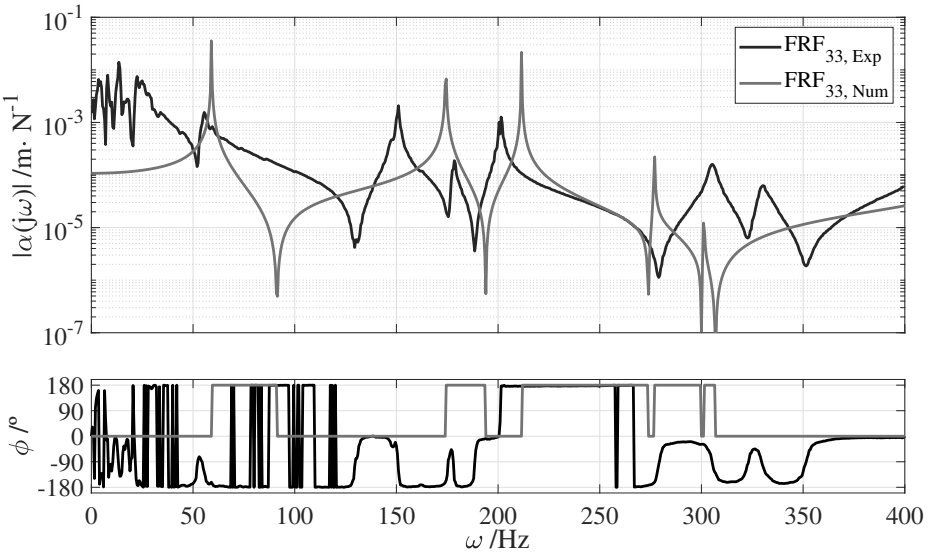


Figure 4.28: Numerical and experimental FRF_{33} for the reference base plate.

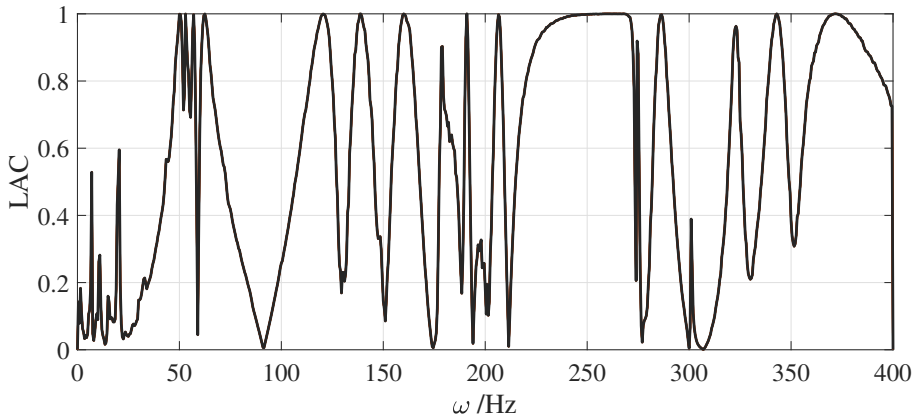


Figure 4.29: LAC for the FRF_{33} of the reference base plate.

The identical analysis that represent the response in node 6 by FRF_{63} is in Figure 4.30 (FRF) and Figure 4.31 (LAC).

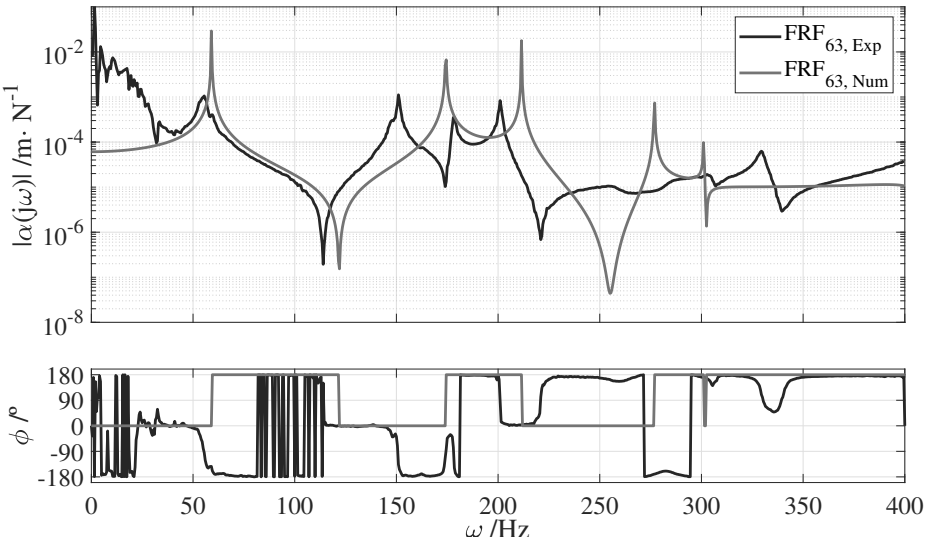


Figure 4.30: Numerical and experimental FRF_{63} for the reference base plate.

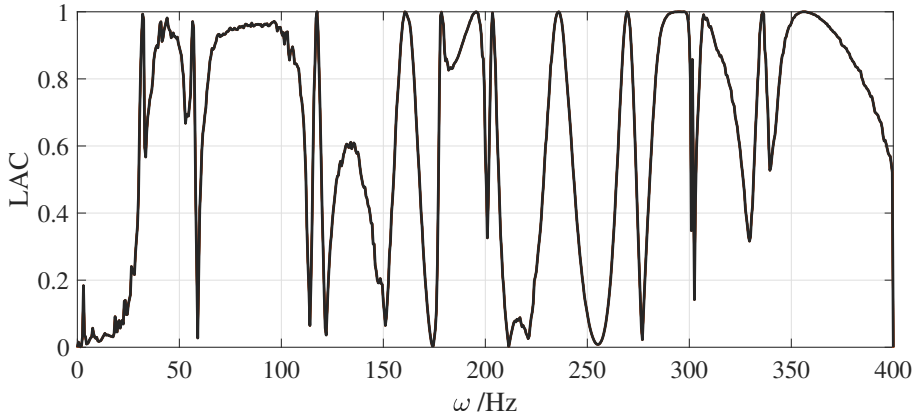


Figure 4.31: LAC for the FRF_{63} of the reference base plate.

LAC shows some instability concerning the correlation between experimental and numerical results in both FRF comparisons. The experimental results show one peak missing in the numerical model. In general, the lower natural frequencies are lower than the predicted numerically and the higher natural frequencies are higher than numerical ones. There is a lag in the phase for some ranges of frequency.

Thickness plays an important role in LAC's results. The base plate results show that the increment of thickness helps the FRF to get closer to the numerical prediction. The half plates are relatively thicker than the base ones because the relationship between their length and thickness is higher, but in this case, it was not enough to get better correspondence between both FRF's, albeit there is an improvement that shows the need of work on the quality of the specimens, in order to improve the results.

The initial noise is caused by the nylon wires that suspend the plate in the air.

4.9 Influence of Thickness and Damping Materials

Another aspect concerning SMACWRAP ® 0.1 mm configuration is that this is a harder configuration to achieve since layers with 0.1 mm are extremely thin and that value may vary in the plate, due to some conditions of the manufacturing process.

Starting with point FRF, Figure 4.32 brings a perspective about the experimental FRF's of three configurations: the reference plate, total damping treatment with KRAIBON ® 0.5 mm and total damping treatment with SMACWRAP ® 0.2 mm.

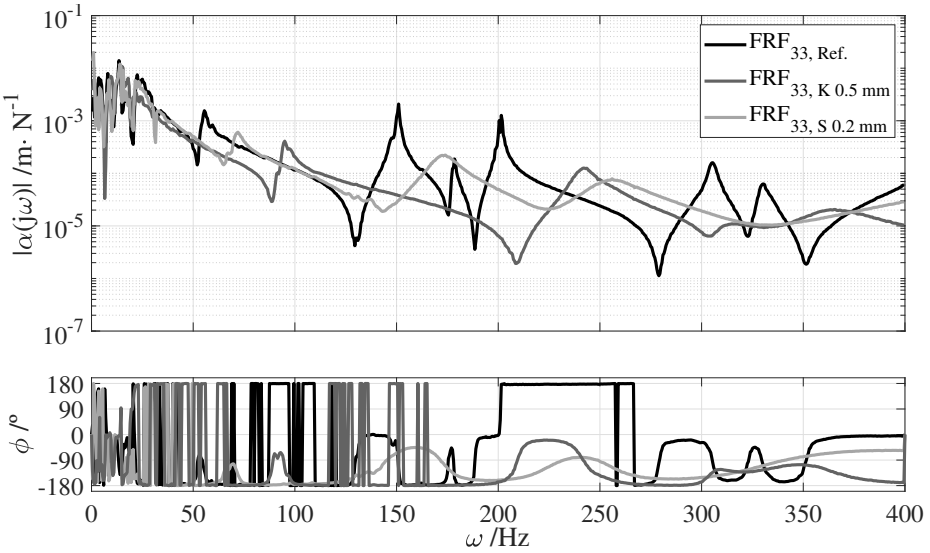


Figure 4.32: Experimental point FRF's of the reference plate, KRAIBON ® 0.5 mm configuration and SMACWRAP ® 0.2 mm configuration.

It is possible to observe the effects of damping, as the resonance peaks are less evident in damped plates. The damped plates are also thicker, which can be a plus, however, the manufacture of the same reference plate, but with thicker layers would help to understand the real influence of thickness, in comparison with the present reference plate.

Concerning the damped plates, KRAIBON ® 0.5 mm seems to provide a better damping capacity, as the graphic tends to reduce its magnitude and reach a plateau shape.

Regarding transfer FRF, Figure 4.33 shows the experimental FRF_{63} obtained with the same three configurations presented before.

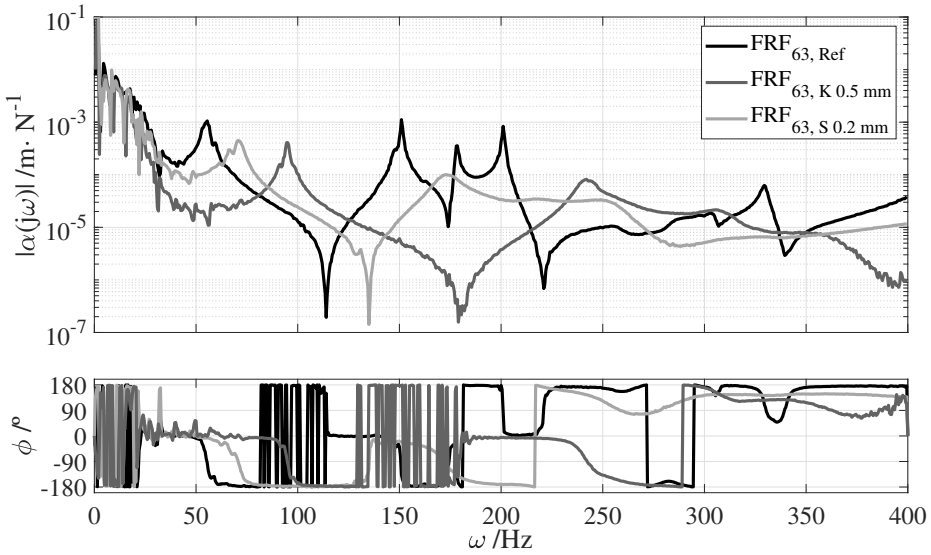


Figure 4.33: Experimental transfer FRF's of the reference plate, KRAIBON ® 0.5 mm configuration and SMACWRAP ® 0.2 mm configuration.

Here, in the range [50,150] Hz, both configurations show different behaviors: the higher the thickness, the stiffer the place. It happens because the resonance frequencies are higher at this range.

4.10 Total and Partial Damping Treatments

Partial damping treatments are an alternative to total damping treatments, and they can be an interesting approach. Some modes of vibration strongly evidence the presence of damping capacity, as well as reinforce the differences between the two treatments and the absence of treatments.

4.10.1 SMACWRAP ® 0.2 mm

FRF_{33}

Concerning SMACWRAP ® 0.2 mm configuration, Figure 4.34 presents the numerical and experimental FRF_{33}, with LAC evaluation in Figure 4.35, for a total damping treatment.

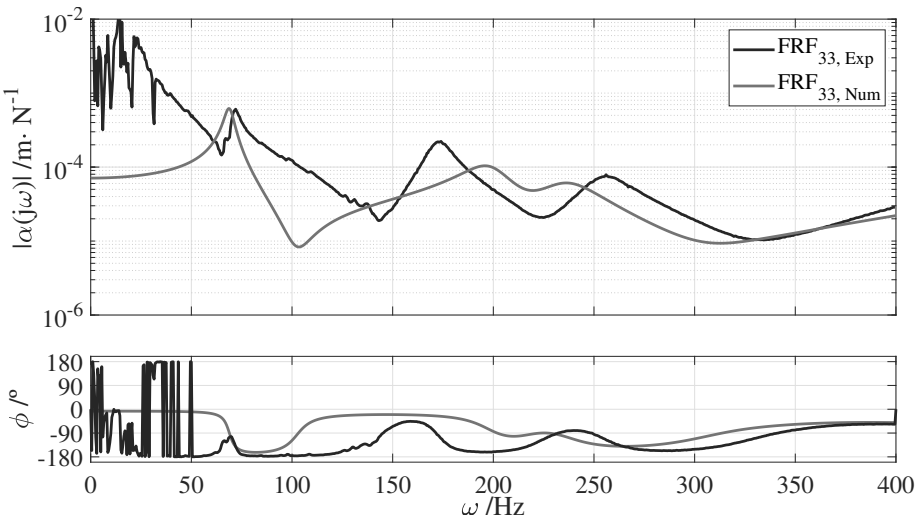


Figure 4.34: Numerical and experimental FRF_{33} for SMACWRAP ® 0.2 mm total damping treatment configuration.

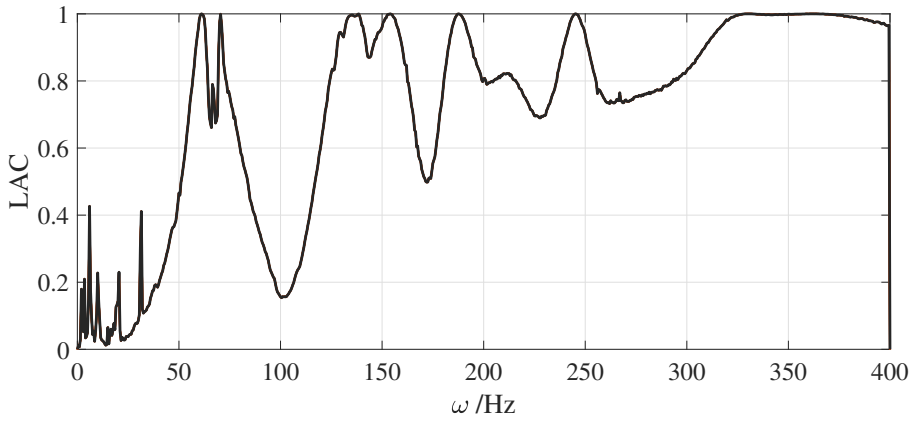


Figure 4.35: LAC for the FRF_{33} with SMACWRAP ® 0.2 mm total damping treatment configuration.

The values of LAC show a good correlation between both numerical and experimental results. Damping becomes clear as frequency rises and the observed peaks registered close values to the numerical ones. The influence of the excitation is less evident than in the previous configurations. The results for the partial treatment are presented in 4.36 (FRF) and 4.37 (LAC).

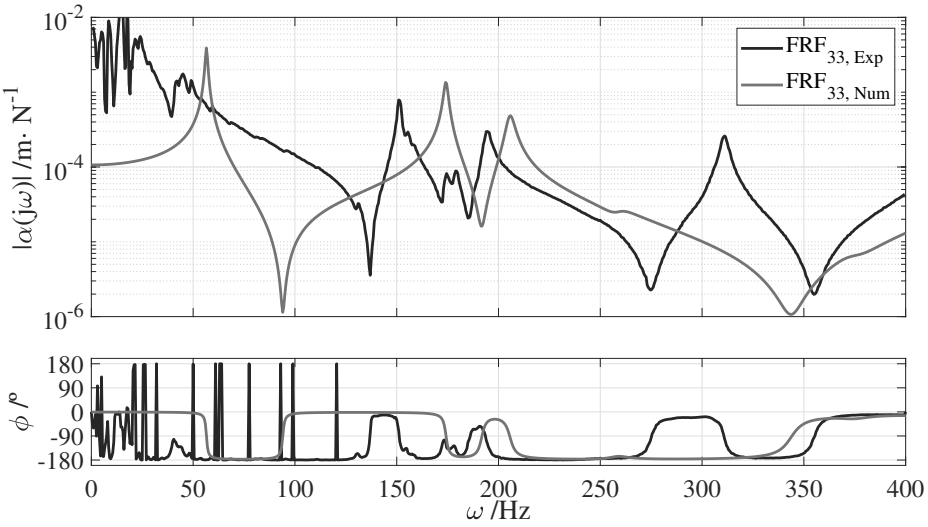


Figure 4.36: Numerical and experimental FRF_{33} for SMACWRAP ® 0.2 mm partial damping treatment configuration.

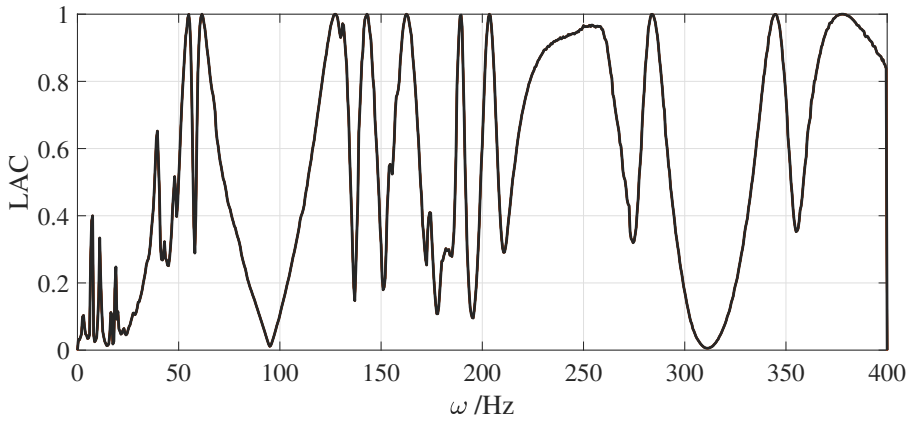


Figure 4.37: LAC for the FRF_{33} with SMACWRAP ® 0.2 mm partial damping treatment configuration.

Unexpected experimental peaks appear in the FRF. This partial treatment has the same pattern as the previous ones: the plate has the same thickness as the reference plate, but the presence of a 0.2mm partial strip at the middle plane of the plate enables a better correspondence between both curves than the one of the reference plate.

FRF_{63}

The following frequency response function (either numerical or experimental) - Figure 4.38 - represents the transfer FRF which measures the response at node 6. LAC is in Figure

4.39.

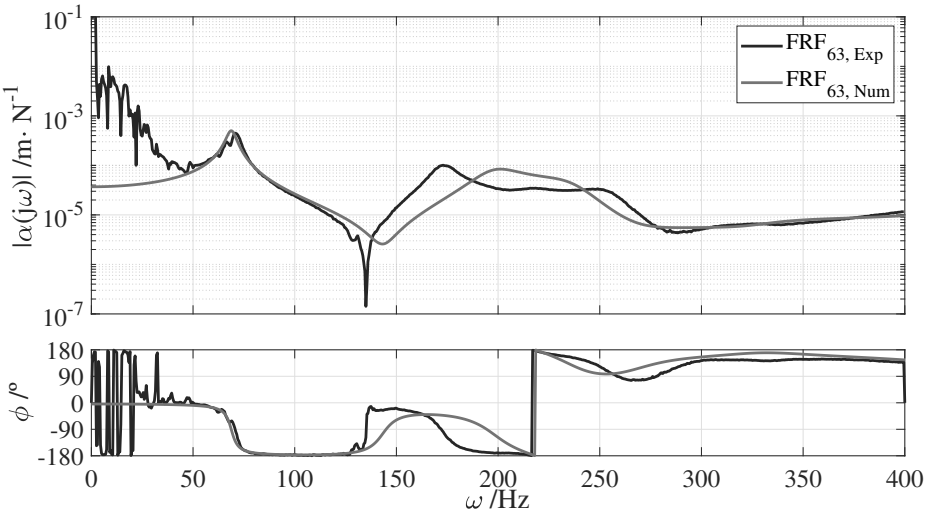


Figure 4.38: Numerical and experimental FRF_{63} for SMACWRAP ® 0.2 mm total damping treatment configuration.

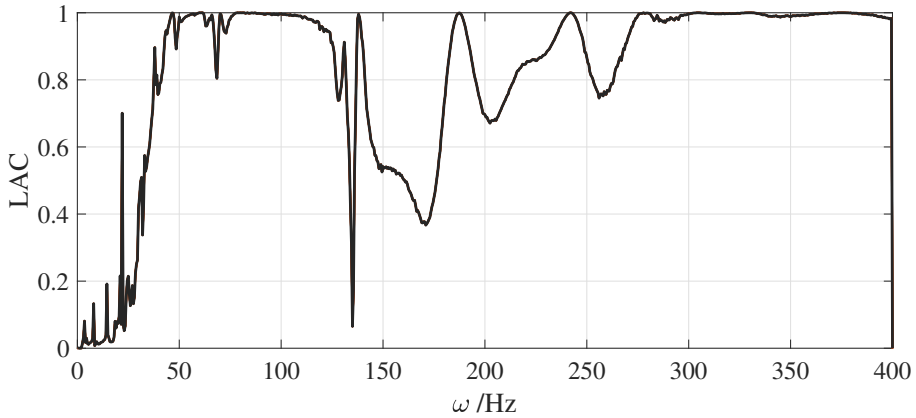


Figure 4.39: LAC for the FRF_{63} with SMACWRAP ® 0.2 mm total damping treatment configuration.

In terms of correlation, both FRF's of the partial damping treatment have an excellent correlation at higher frequencies. The presence of a viscoelastic layer is evident and the increase of thickness by adding a 0.2 mm layer to the entire plate promotes the accuracy of the results. Figure 4.40 and 4.41 present the same analysis for partial treatments.

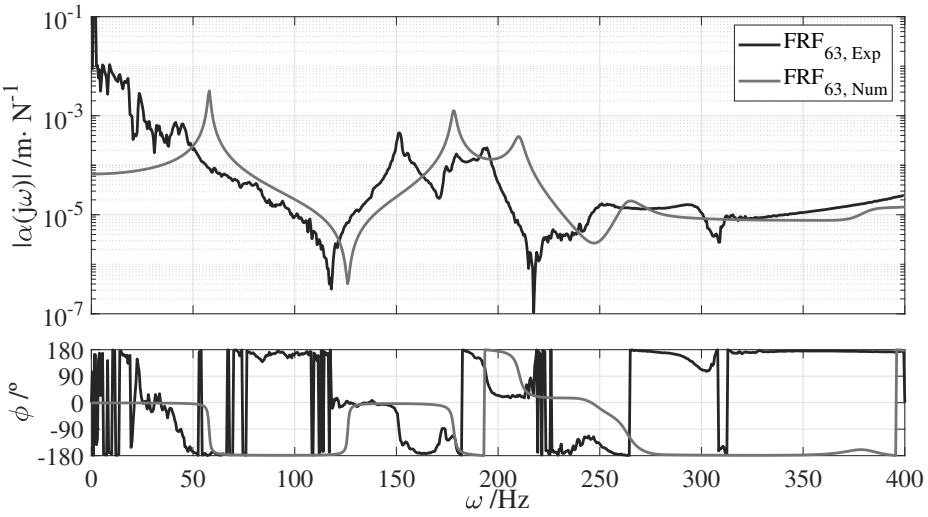


Figure 4.40: Numerical and experimental FRF_{63} for SMACWRAP ® 0.2 mm partial damping treatment configuration.

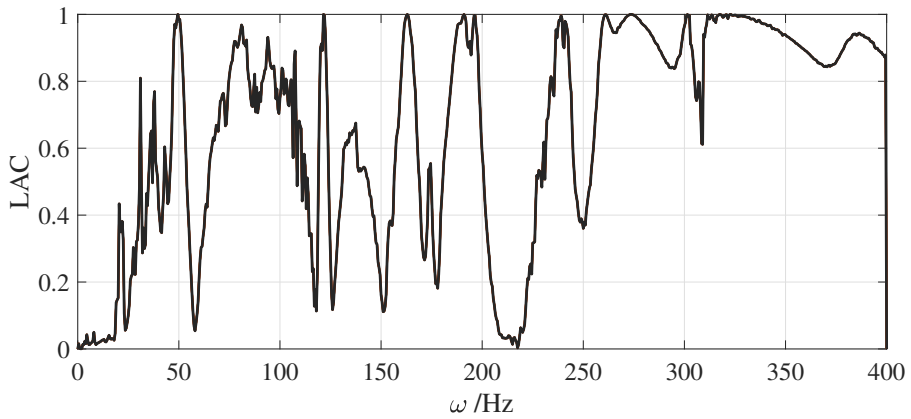


Figure 4.41: LAC for the FRF_{63} with SMACWRAP ® 0.2 mm partial damping treatment configuration.

The experimental FRF presents some noise in several frequency ranges. This noise was observed mostly in FRF's that are more distant from the excitation point, however, there is not a strong reason that justifies this phenomenon. That noise is also visible in Figure 4.41, but it does not compromise the results. As expected, this treatment's behavior is similar to the previous FRF, with an improved correlation for the higher frequencies of the bandwidth.

4.10.2 SMACWRAP ® 0.1 mm

For these plates, the aim is to observe the influence of the positioning of the viscoelastic layers, together with the reduction of the thickness of each individual strip.

FRF_{33}

In Figure 4.42, the numerical and experimental FRF's are put together. Their analysis is made with the help of LAC evaluation in Figure 4.43.

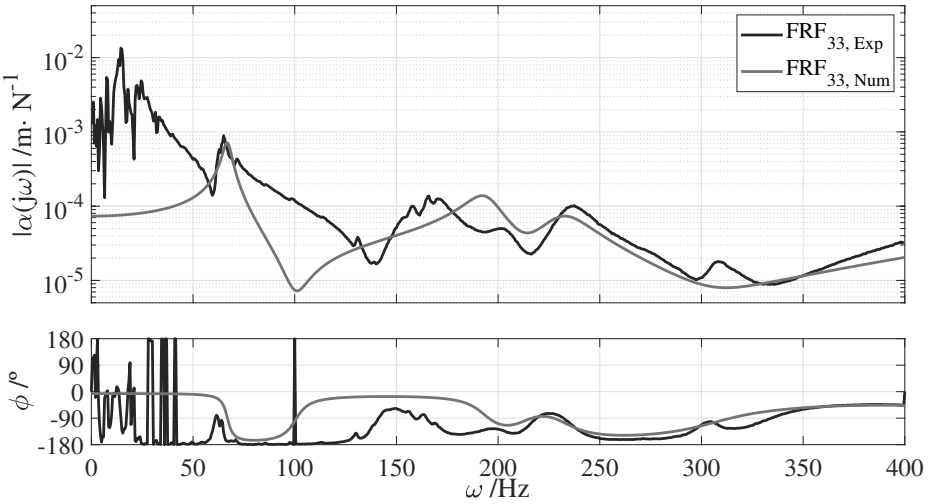


Figure 4.42: Numerical and experimental FRF_{33} for SMACWRAP ® 0.1 mm total damping treatment configuration.

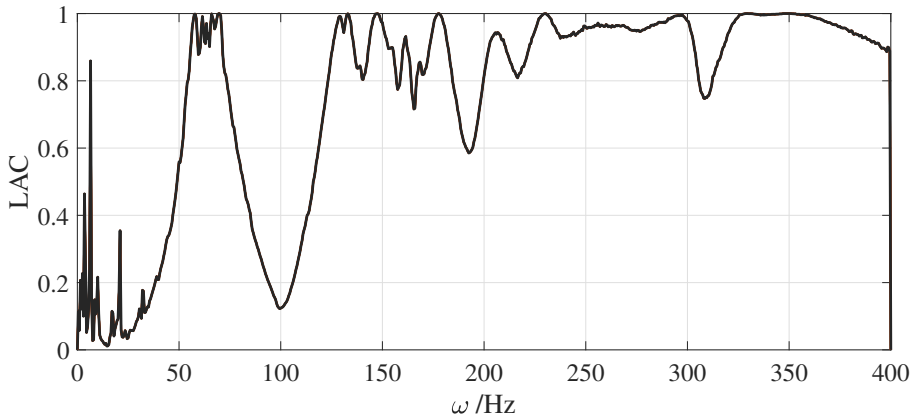


Figure 4.43: LAC for the FRF_{33} with SMACWRAP ® 0.1 mm total damping treatment configuration.

Despite the reduction of the thickness of each layer, this configuration still presents some good values of LAC when compared with the same situation for SMACWRAP ® 0.2 mm total damping treatment configuration. The experimental FRF evidences the presence of the mode shapes, with no extra relevant peaks. However, the magnitudes are higher as expected, due to the location of the strips in the stacking sequence.

The following analysis - in Figure 4.44 and 4.45 - related with partial damping treatment, shows something different.

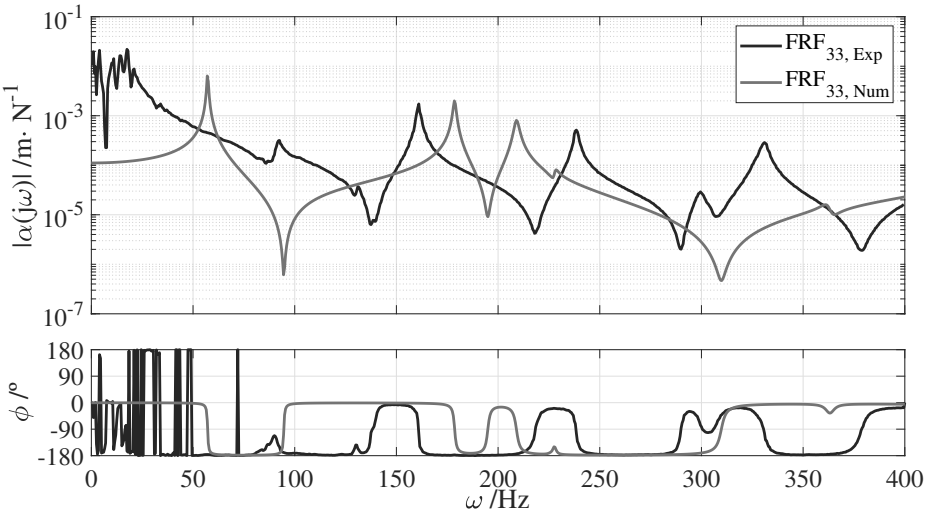


Figure 4.44: Numerical and experimental FRF_{33} for SMACWRAP ® 0.1 mm partial damping treatment configuration.

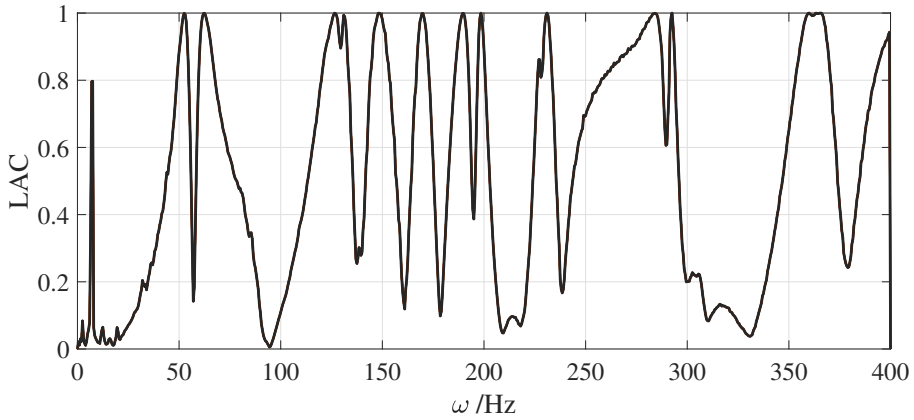


Figure 4.45: LAC for the FRF_{33} with SMACWRAP ® 0.1 mm partial damping treatment configuration.

This plate has the same thickness as the reference plate, with a partial damping treatment applied with the viscoelastic strips in different stacking positions. In partial damping treatments, there are more relevant peaks in the experimental frequency response function, with the LAC showing a constant variation of correlation in the bandwidth of interest, as before. The presence of the viscoelastic layer is not clear, which shows the disadvantage of this damping configuration.

FRF_{63}

Concerning the transfer FRF of interest in this configuration, Figure 4.46 and Figure 4.47 provide the information for the evaluation.

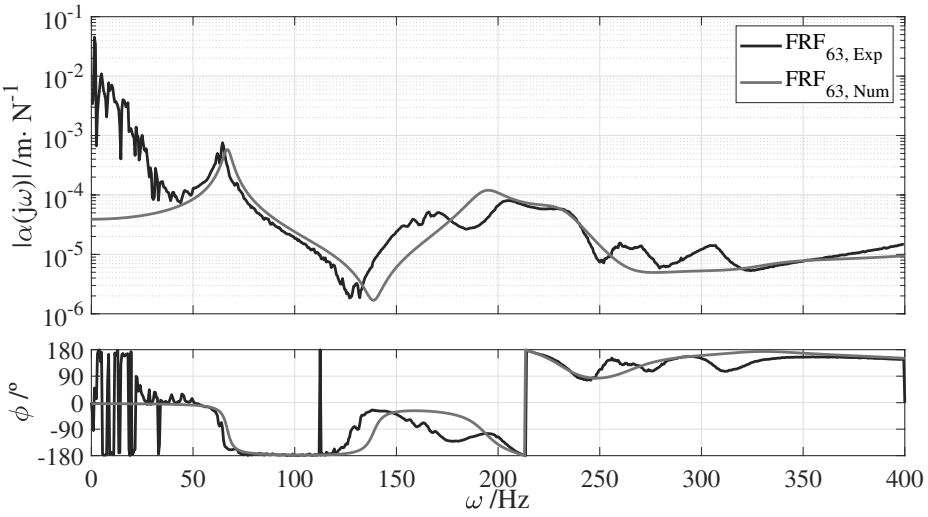


Figure 4.46: Numerical and experimental FRF_{63} for SMACWRAP ® 0.1 mm total damping treatment configuration.

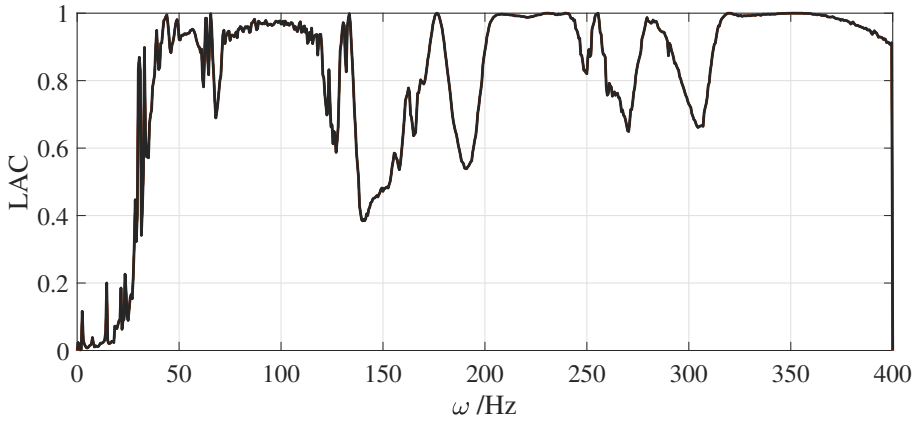


Figure 4.47: LAC for the FRF_{63} with SMACWRAP ® 0.1 mm total damping treatment configuration.

The total damping treatment ensures again a close correlation between both FRF's. The numerical model is a quite soft approach, with smooth peaks. After 200 Hz, there is a shift on the phase that represents a turn of 360° and occurs approximately at the same frequency in both curves, which is a good foreword of the accuracy of the results. Comparing with SMACWRAP ® 0.2 mm total damping treatment configuration, the stacking position influences the results of LAC and the plateau shape that denotes the presence of damping is not as obvious as before.

The analysis of partial damping treatments with the response at point 6 is exposed in Figure 4.48 , with LAC in Figure 4.49.

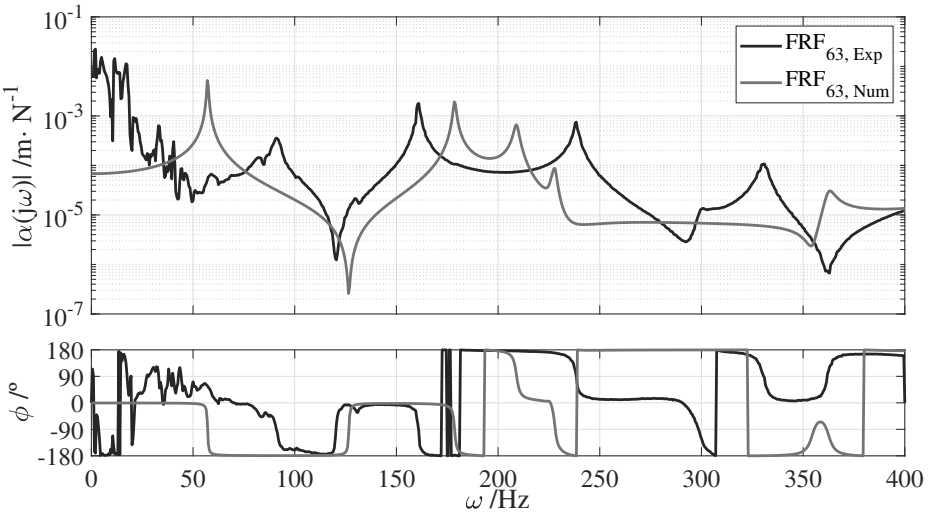


Figure 4.48: Numerical and experimental FRF_{63} for SMACWRAP ® 0.1 mm partial damping treatment configuration.

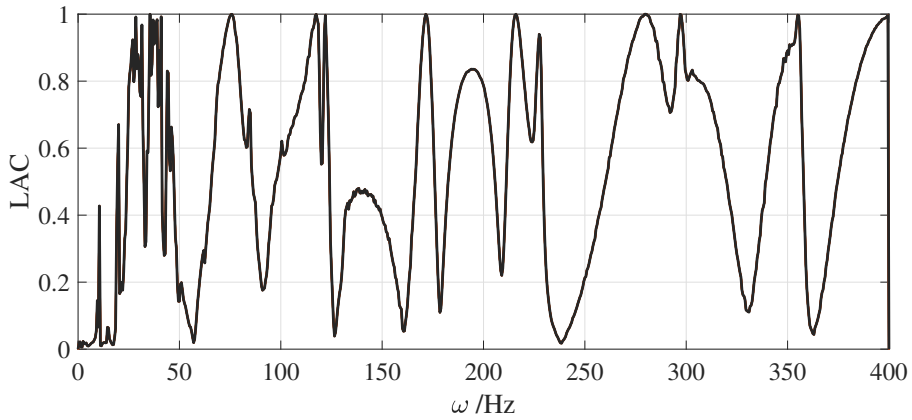


Figure 4.49: LAC for the FRF_{63} with SMACWRAP ® 0.1 mm partial damping treatment configuration.

The numerical and experimental FRF_{63} also prove a lower efficiency of this treatment configuration, sustained by the average correspondence with LAC. The numerical model shows only a few peaks of resonance and anti-resonance, for instance, between 250 and 300 Hz, where an anti-resonance is present. Concerning the damping capacity of the plate, it is not so clear as it is in previous partial FRF, which is interesting and reinforces the positioning of the viscoelastic layer, as close as possible to the middle plane of the plate, together with higher thicknesses.

In conclusion, the stacking sequence is one of the parameters that play an important role in the design of the plates. The innermost viscoelastic strips provide more damping capacity since the deformation energy is higher at that region.

4.10.3 KRAIBON ® 0.5 mm

In comparison with SMACWRAP ® configurations, this one presents a thicker viscoelastic core. The material is not the same, which provides a comparison that helps to understand the one that was already done with the 254 × 198 mm plates, using this viscoelastic

material.

FRF$_{33}$

Figure 4.50 illustrates the numerical and experimental FRF$_{33}$, followed by its LAC evaluation in Figure 4.51, when a total damping treatment is applied on the plate.

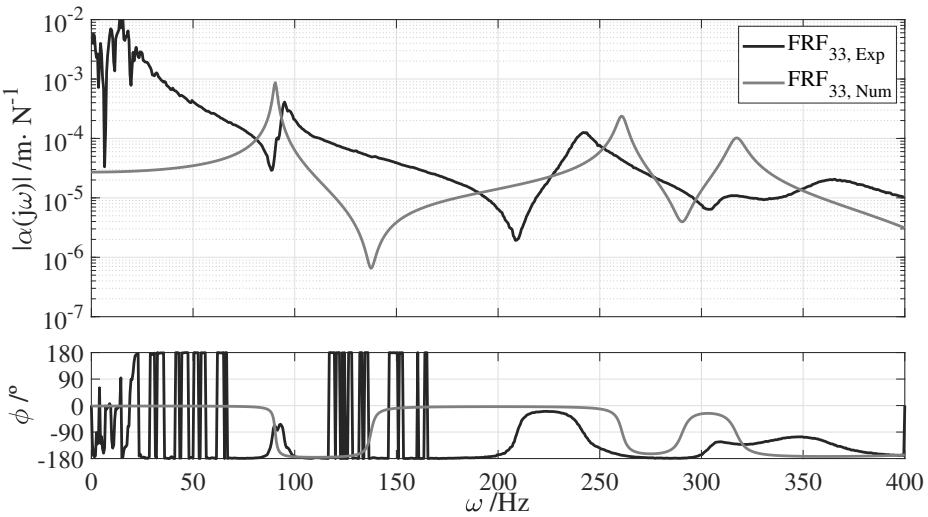


Figure 4.50: Numerical and experimental FRF$_{33}$ for KRAIBON® 0.5 mm total damping treatment configuration.

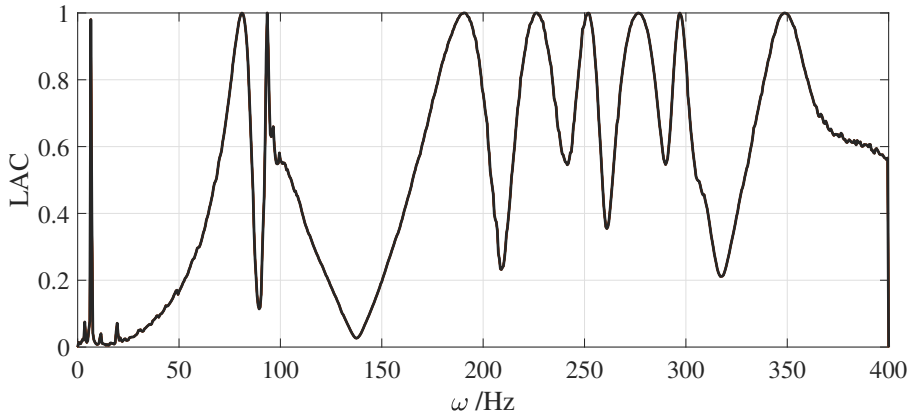


Figure 4.51: LAC for the FRF$_{33}$ with KRAIBON® 0.5 mm total damping treatment configuration.

The numerical and experimental results do not have a perfect correlation. At high frequencies, the FRF shows a better damping capacity than the one that was predicted by the numerical model. As usual, the wires of the experimental setup create some noise in the range [0,50] Hz. Comparing with SMACWRAP® 0.2 mm, the correspondence was better with similar magnitudes, which is an interesting point.

Figure 4.52 shows the comparison between the numerical and experimental FRF$_{33}$ with the LAC evaluation in Figure 4.53.

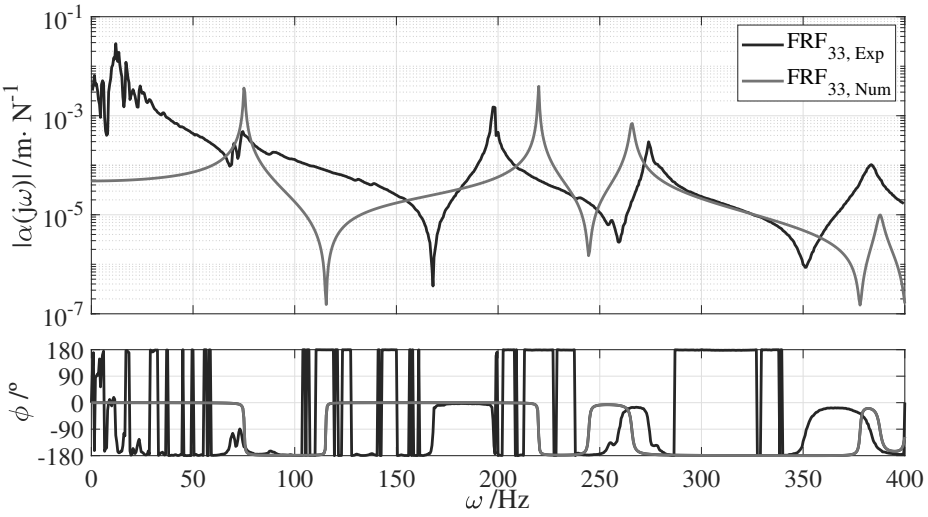


Figure 4.52: Numerical and experimental FRF_{33} for KRAIBON ® 0.5 mm partial damping treatment configuration.

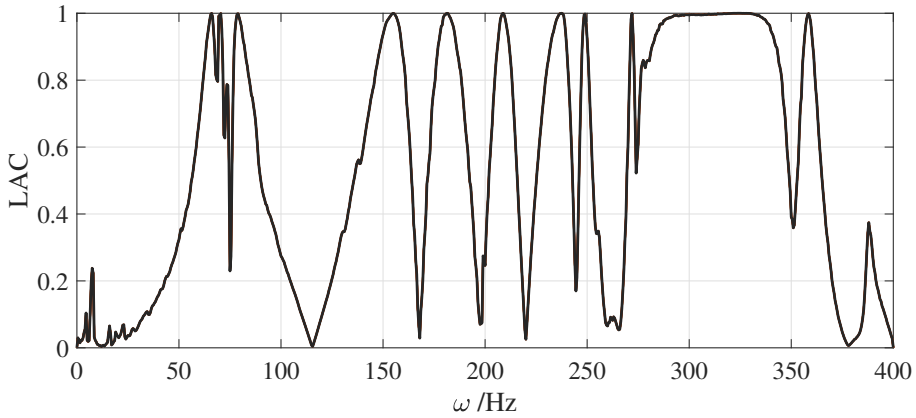


Figure 4.53: LAC for the FRF_{33} with KRAIBON ® 0.5 mm partial damping treatment configuration.

The results are coincident in terms of the number of modes of vibration. Except for the fourth mode of vibration, all the other modes present frequencies that are lower than the numerical frequencies. LAC comparison shows that the correlation is not strong, despite there is a zone where LAC is equal to 1. Comparing with previous equivalent partial damping treatment configurations, the results are similar. The correspondence reaches its best performance around 300 Hz.

$\mathbf{FRF}_{63}$

Figure 4.54 shows the numerical and experimental FRF_{63} and evaluation by LAC can be observed in Figure 4.55, in order to observe the response in another region of the plate considering the total damping treatment,

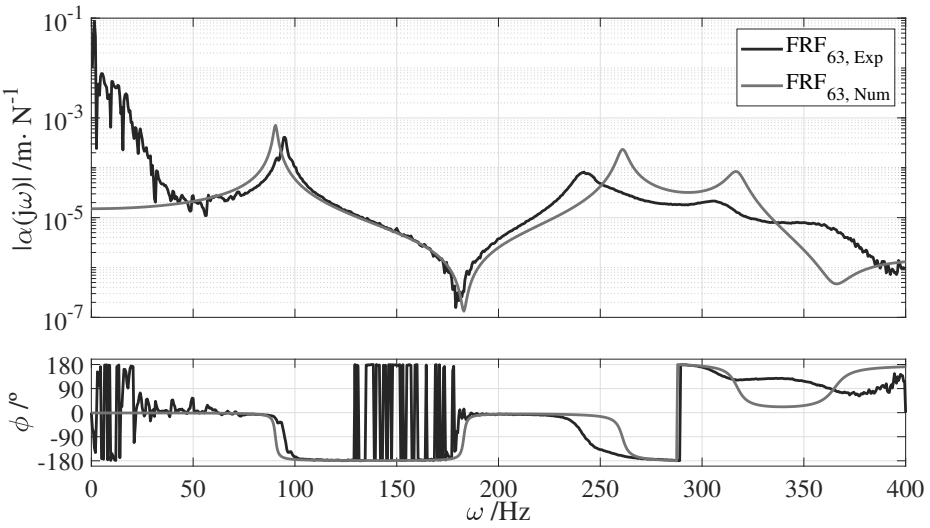


Figure 4.54: Numerical and experimental FRF_{63} for KRAIBON® 0.5 mm total damping treatment configuration.

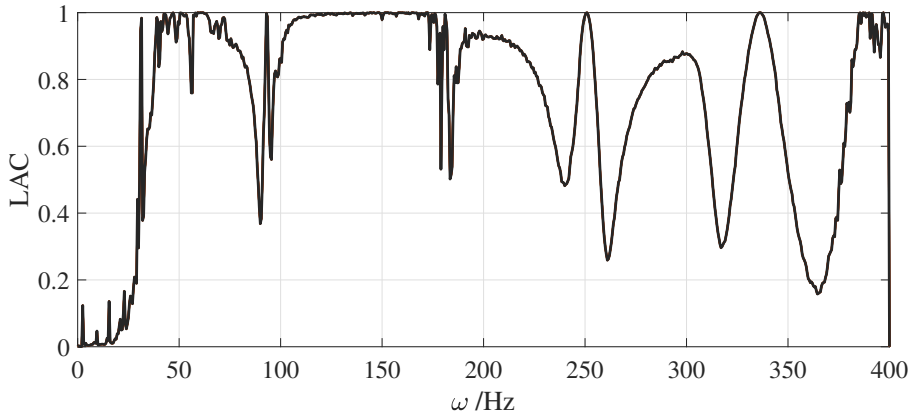


Figure 4.55: LAC for the FRF_{63} with KRAIBON® 0.5 mm total damping treatment configuration.

The values of LAC express a good correlation between numerical and experimental FRF_{63}, even with the presence of noise, albeit this correlation was better for the initial plates (before cutting).

In general, the numerical results are conservative in relation to the experimental results. The reached magnitudes are similar to the ones of previous treatments. Thereby, the plates with KRAIBON® 0.5 mm total damping configuration present a relationship between length and thickness that is not so beneficial as the one concerning SMACWRAP® 0.2 mm total damping configuration, for instance.

Figure 4.56 presents the equivalent FRF for the partial damping treatment, with LAC in Figure 4.57.

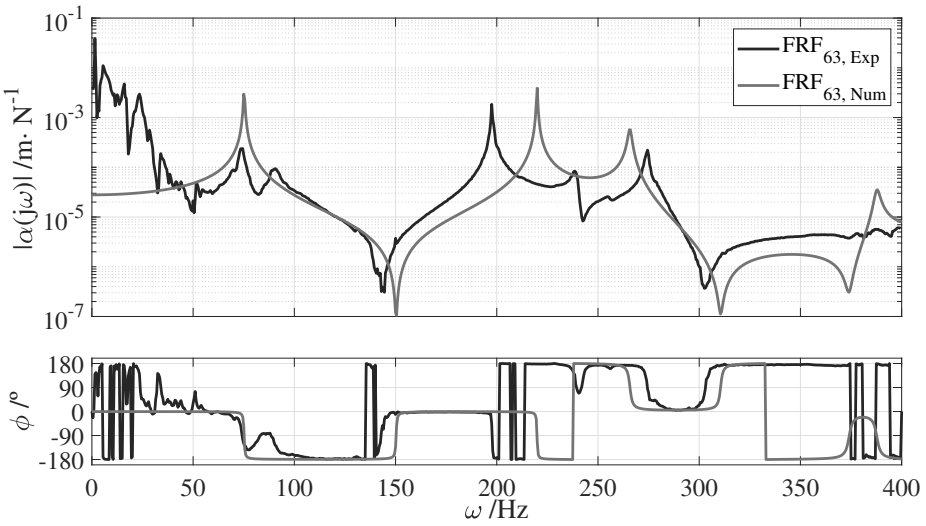


Figure 4.56: Numerical and experimental FRF_{63} for KRAIBON ® 0.5 mm partial damping treatment configuration.

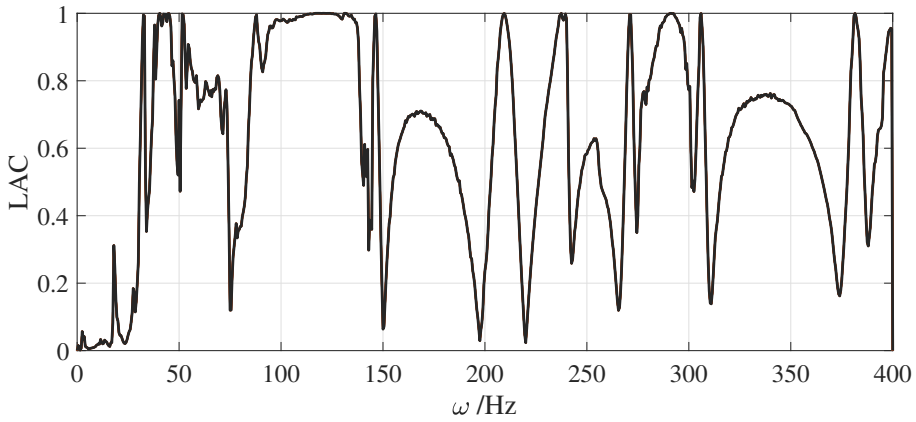


Figure 4.57: LAC for the FRF_{63} with KRAIBON ® 0.5 mm partial damping treatment configuration.

Once again, the correlation is worse in partial damping treatment - worse damping capacity. There are several peaks that the numerical model does not predict. One interesting aspect is that, even though damping capacity is worse, the peaks predicted by the numerical FRF present higher magnitude than the observed in the experimental model and some of them present lower frequencies in reality.

Therefore, the partial damping treatments provide some damping, since some resonance frequencies reach lower magnitudes, in comparison with the reference plates.

Chapter 5

Parametric Study on the Efficiency of Partial Damping Tratments

5.1 Introduction

The efficiency of viscoelastic damping treatments relies not only on the properties of the viscoelastic layers, but also on the properties of the structure. The manufacturing of structures without any previous parametric study may compromise the efficiency of the damping layers.

As said before, an equilibrium between the stiffness of the structure and the damping capacity of the material is necessary. Thereby, a parametric analysis concerning the application of partial damping treatments enlightens the main adavntagens and concerns that the design of such treatments brings to the engineer.

In this chapter, the configurations presented in Chapter 5 are changed and several parameters are analyzed: width, thickness and position of the viscoelastic strips, as well as the stacking sequence of the composite plate. The aim is to, on the one hand, know the influence of the mode shapes on the damping capacity of the treatments inserted in the plates and, on the other hand, discuss the effects of the evaluated parameters between them.

5.2 Configurations and Mesh Parameters

The following analysis is based on the fact that the orthotropic plate is a six-layered symmetric laminate composite plate. Besides that, the mesh will be equal for all the cases. The first group of cases presents an analysis of the variation of width in viscoelastic strips, according to their location on the plate. Thus, there are two types of configurations, based on the location of the viscoelastic strips:

- Configuration E-C: the strips are placed next to the edges of the plate. In this configuration, one considers the width increase from edges to center - see Figure 5.1.
- Configuration C-E: here, the strips are at the center of the plate and the evolution of the process is from the center to the edges of the plate - see Figure 5.2.

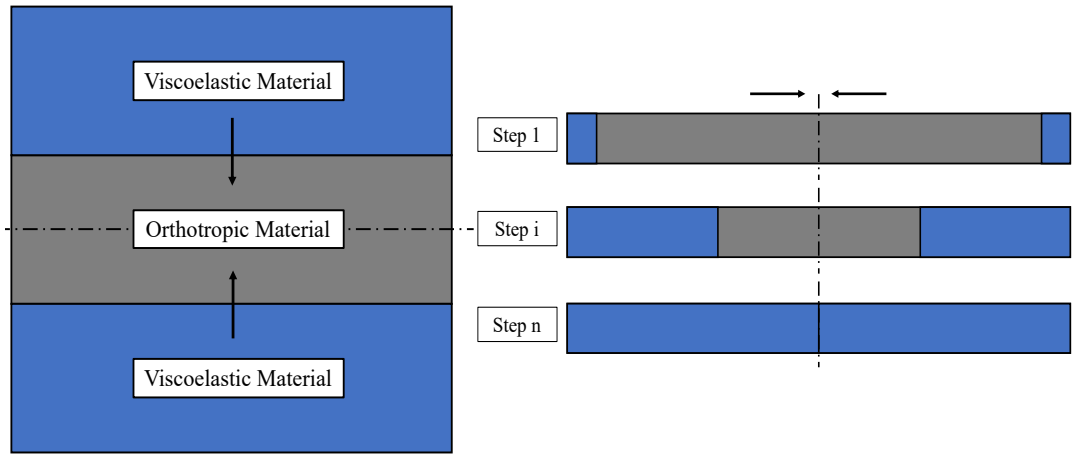


Figure 5.1: Configuration E-C: direction of width increase, with the upper view of the plate on the left and the generic representation of width from Step 1 to Step N on the right.

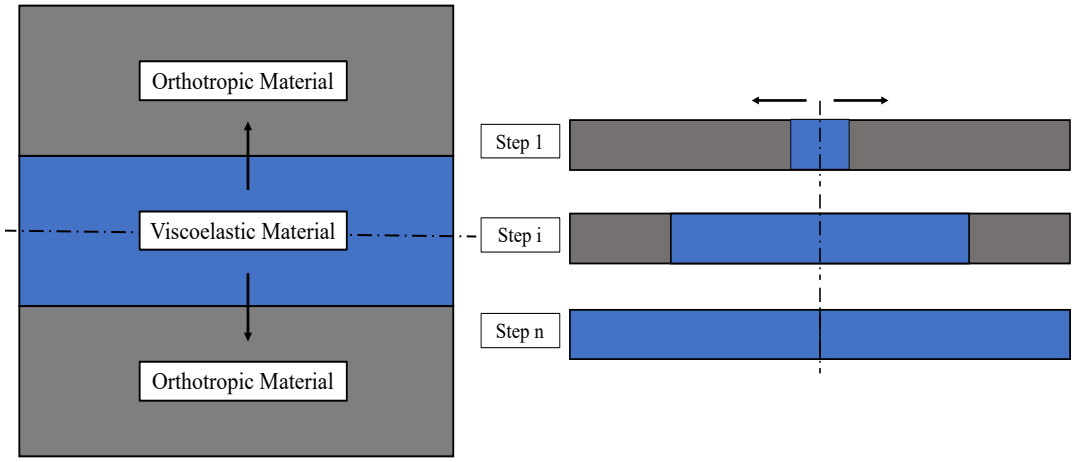


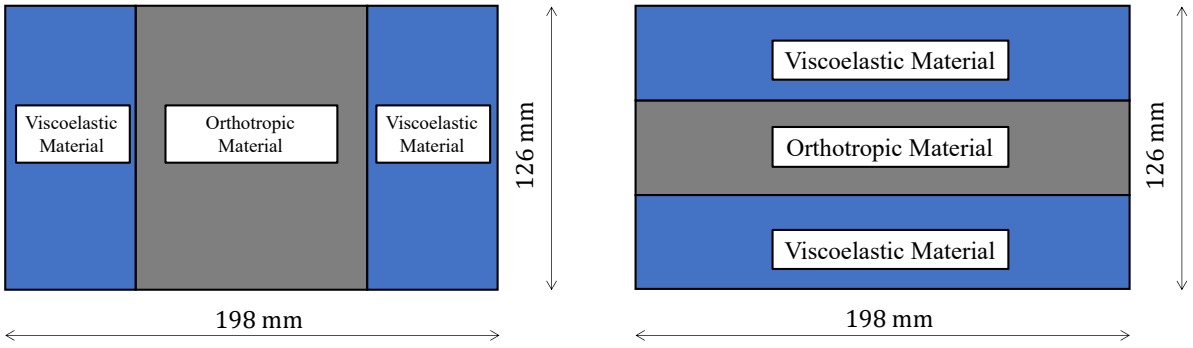
Figure 5.2: Configuration C-E: direction of width increase, with the upper view of the plate on the left and the generic representation of width from Step 1 to Step N on the right.

The mesh has 384 elements (24×16). The number of nodes and the number of degrees of freedom vary according to each damping treatment. The position of the viscoelastic strips (alongside length or width) determines the existence of two types of new configurations:

- Configuration 1, where the viscoelastic strips are parallel to the smaller edges of the plate
- Configuration 2, where the viscoelastic strips are parallel to the bigger edges of the plate.

The arrangements E-C and C-E exist in both Configurations 1 and 2. Figure 5.3 represents both Configurations. Each step corresponds to a discrete value that represents the percentage of the covered area by viscoelastic strips. The first ones are related with the growth direction of the strip, as the second ones represent the position of the strip. Table 5.1 shows those values and the corresponding step, for each configuration. It is important to mention that Configuration 1 has 12 steps, while Configuration 2 has eight

steps, depending on the location of viscoelastic strips on the plate, since the mesh is 24×16, based on the accuracy from the results of the validation tests.



(a) Configuration 1.

(b) Configuration 2.

Figure 5.3: Location of the viscoelastic strips at the plate.

Table 5.1: Covered area on each step for each configuration.

Step	1	2	3	4	5	6	7	8	9	10	11	12
Config.1 /%	8.3	16.7	25.0	33.3	41.7	50.0	58.3	66.7	75.0	83.3	91.7	100.0
Config.2 /%	12.5	25	37.5	50	62.5	75	87.5	100				

5.3 Width and Location - SMACWRAP ® 0.2 mm Configurations

In chapter 4, it was considered a fixed width for the viscoelastic strips, without considering if its value was the optimal one. Furthermore, the strips are at the edges of the plate, but its application at a different area could benefit the treatment. The aim of the study is to check the influence of the position of viscoelastic strips in the plate. That position influences the values of the loss factor, one of the parameters that permit the control of the parametric study.

5.3.1 Width Increase from the Edges to the Center - Configuration 1, E-C

The first scenario presents an increase in the viscoelastic strips' width. In this case, the strips are at the smaller edges of the plate, as Figure 5.4 shows.

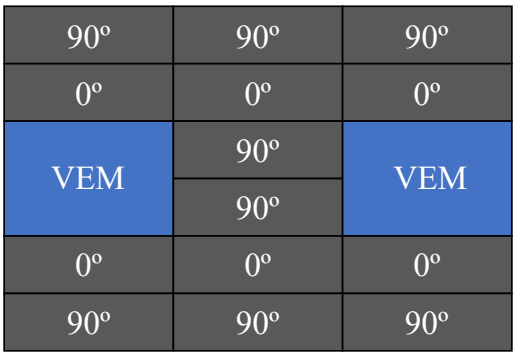
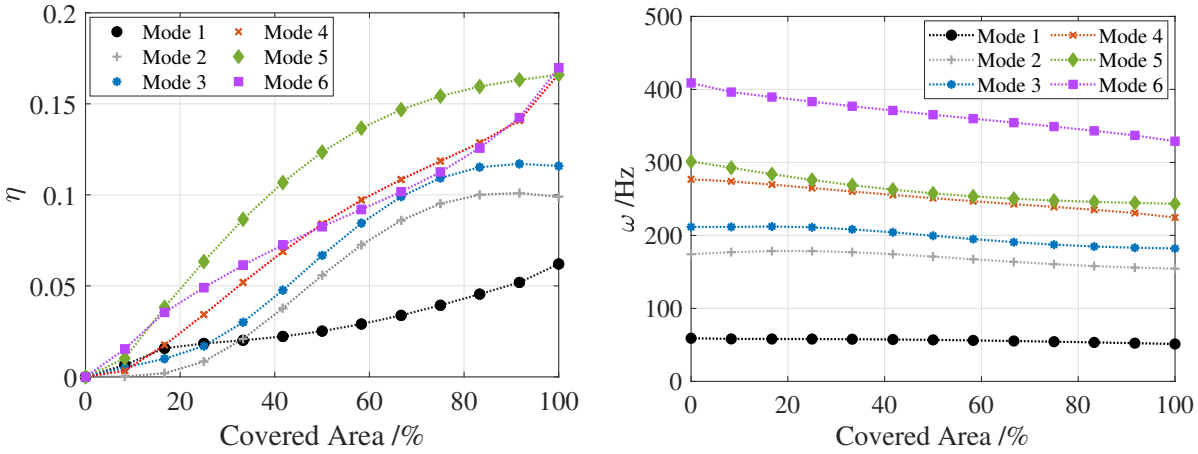


Figure 5.4: Stacking sequence and position with SMACWRAP ® 0.2 mm strips and Configuration 1, E-C.

Both loss factor and natural frequency are prime targets in this analysis. Their representation as a function of the covered area is on Figure 5.5a and 5.5b, respectively.



(a) Loss Factor, η.

(b) Natural Frequency, ω.

Figure 5.5: Influence of the width increase from the edges to the center.

Starting the width increase at the center of the plate, the stiffness of the plate reduces and natural frequencies vary, decreasing as the percentage of covered area increases. Nevertheless, the decrease occurs at different rates for different modes.

It is also possible to see that the maximum values of loss factor occur when the plate has a total damping treatment (or close to that, since Modes 2 and 3 have a slightly higher value of loss factor when the percentage of the covered area is 90%, approximately) Furthermore, some modes of vibration present a tendency to some value of loss factor.

5.3.2 Width Increase from Center to the Edges - Configuration 1, C-E

The second case is very similar to the last one, however, here the strips are applied at the center - as Figure 5.6 shows - of the plate and extend until the edges of the plate.

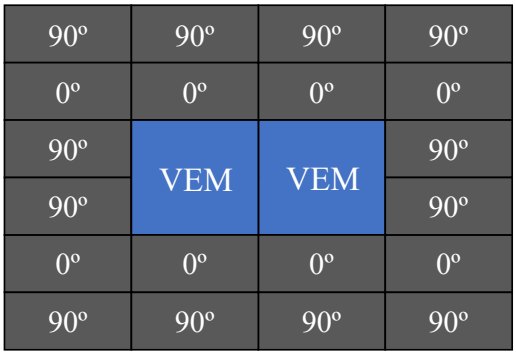
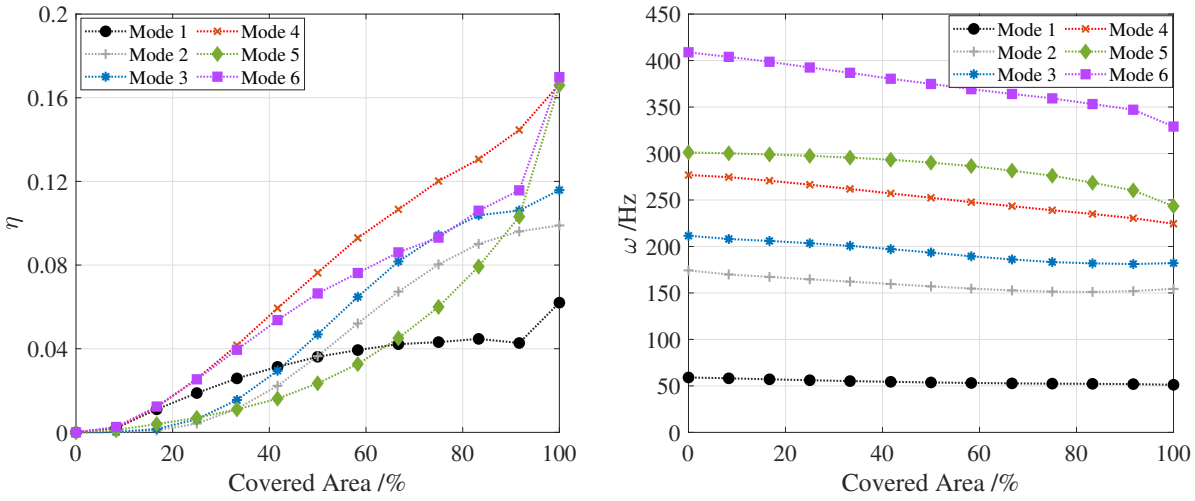


Figure 5.6: Stacking sequence and position with SMACWRAP ® 0.2 mm strips and Configuration 1, C-E.

Figures 5.7a and 5.7b summarize the behavior of the plate with the present configuration in terms of loss factors and natural frequencies, respectively.



(a) Loss Factor, η.

(b) Natural Frequency, ω.

Figure 5.7: Influence of the width increase from center to the edges.

Figure 5.7a shows that the application of viscoelastic strips at different locations influences the behavior of the plate in many ways, as some modes benefit more from one width than others. Figure 5.7b shows a reduction of natural frequency in every mode. Apparently, a viscoelastic core reduces the natural frequency of a mode as its width increases, but further studies should be carried on this subject.

5.3.3 Discussion and Comparison of Configurations 1, C-E and E-C

For every mode, the evolution of either the loss factor or natural frequency with the covered area in both configurations enables one to realize which (or if any) of them is favourable. Figure 5.8 guides the following discussion.

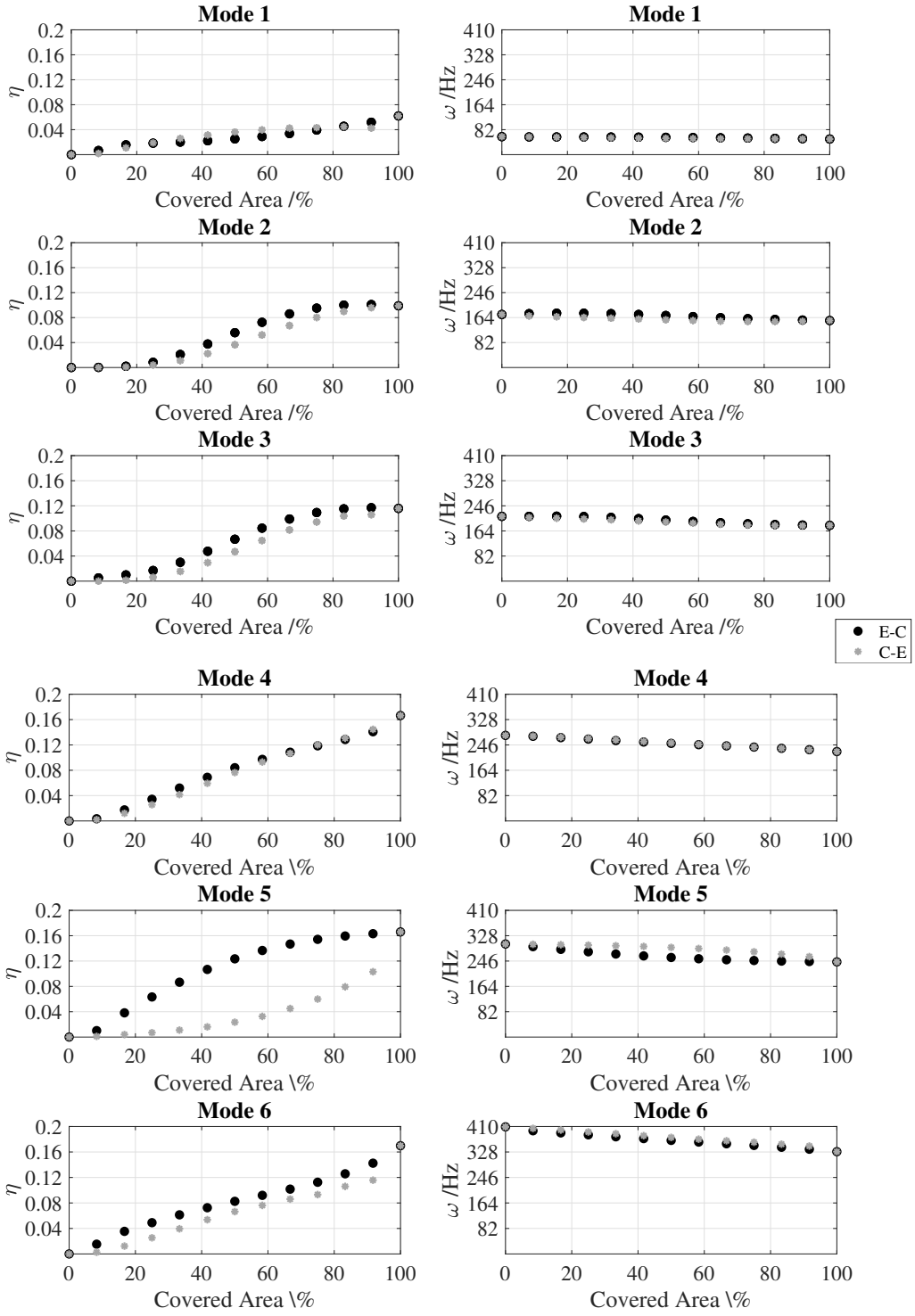


Figure 5.8: Comparison of loss factor and natural frequency between configurations E-C C-E with SMACWRAP ® 0.2 mm strips for the first six modes of vibration.

According to Figure 5.8, the registered differences between natural frequencies are insignificant in the majority of the modes.

Concerning the loss factor, the analysis of the correspondent curves shows that the configuration C-E (from the center to the edges) presents, in general, lower values in many modes. In the first mode of vibrations, this is not the case, although differences between discrete values for the same percentage of covered area are higher in the remaining modes.

As the covered area value rises, the value of the loss factor also rises. Its maximum is reached close to the maximum covered area or even in that situation - total damping treatment.

Comparing natural frequency and the loss factor, the increase of the natural frequency promotes the increase of the limits of a range, where the maximum loss factor is present. Figure 5.9 helps to understand if frequency and loss factor are related somehow.

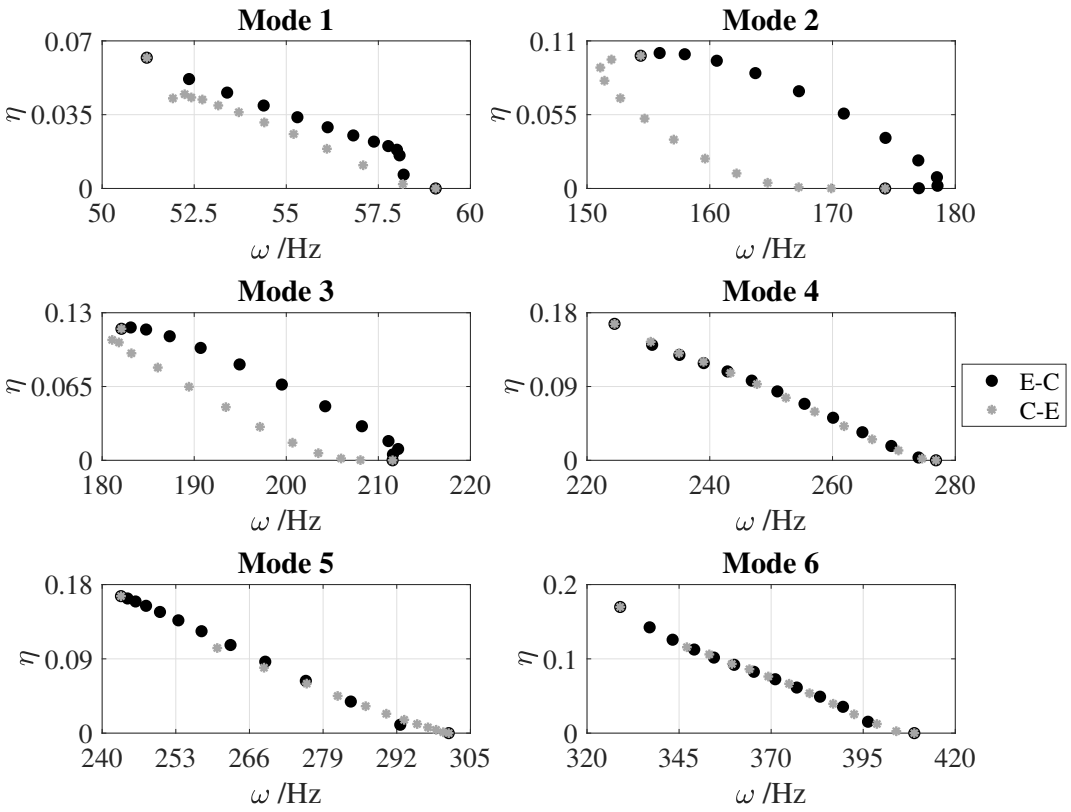


Figure 5.9: Comparison between natural frequency and loss factor.

It is not clear what kind of relationship exists between frequency and loss factor. For lower modes, there is not a pattern in the evolution of that relationship, being dependent on the location of the viscoelastic core layers. But for higher modes, that relationship seems to be linear, no matter what type of configuration. Nevertheless, in Mode 5 there is a concentration of values in opposite sides of the plot for the two configurations.

5.4 Width and Location - SMACWRAP ® 0.1 mm Configurations

An equivalent study is presented for configurations with SMACWRAP ® 0.1 mm strips. The two studies are then compared, aiming to understand the differences and the advantages of each one and which one provides a better damping capacity.

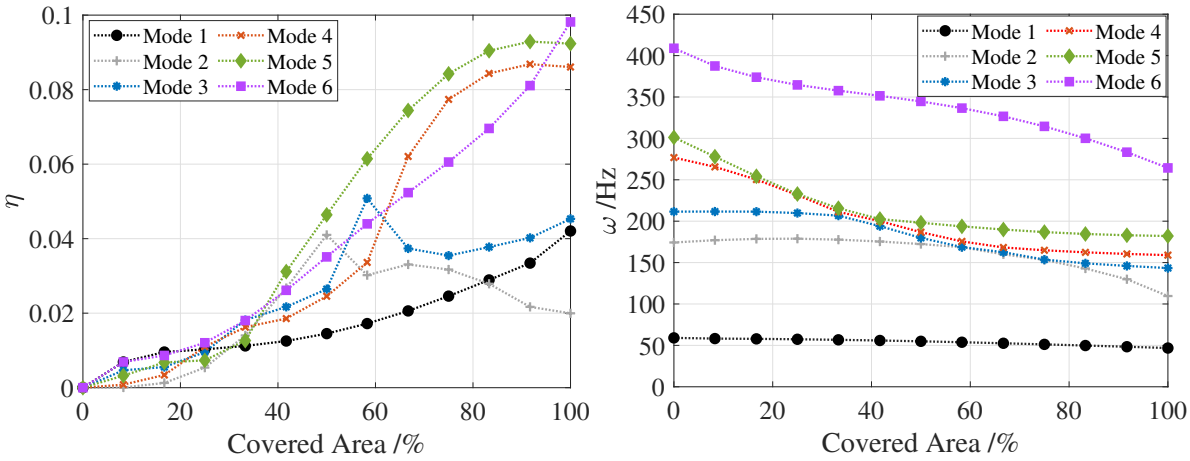
5.4.1 Width Increase from Edges to the Center - Configuration 1, E-C

Once again, the first scenario is the one concerning the viscoelastic strips at the edges of the plate, but now with two separate layers on each edge, as it is represented in Figure 5.10.

90º	90º	90º
VEM	0º	VEM
90º	90º	90º
90º	90º	90º
VEM	0º	VEM
90º	90º	90º

Figure 5.10: Stacking sequence and position with SMACWRAP® 0.1 mm strips and Configuration 1, E-C.

The comparison on loss factor and frequency for all the modes is shown in Figures 5.11a and 5.11b, respectively.

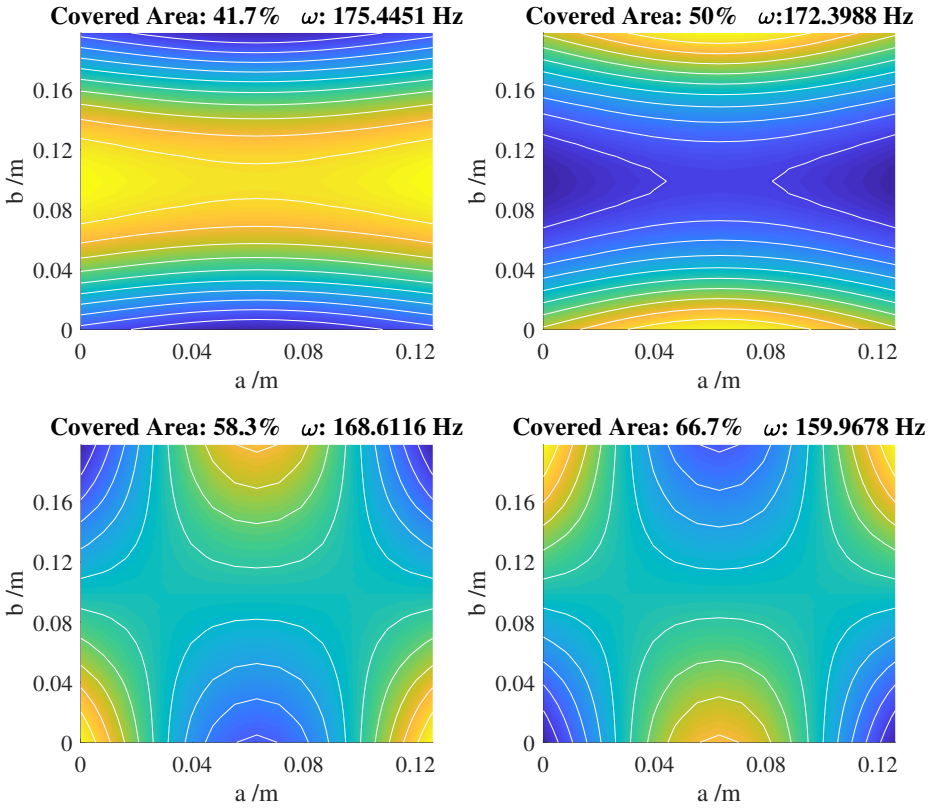


(a) Loss Factor, η.

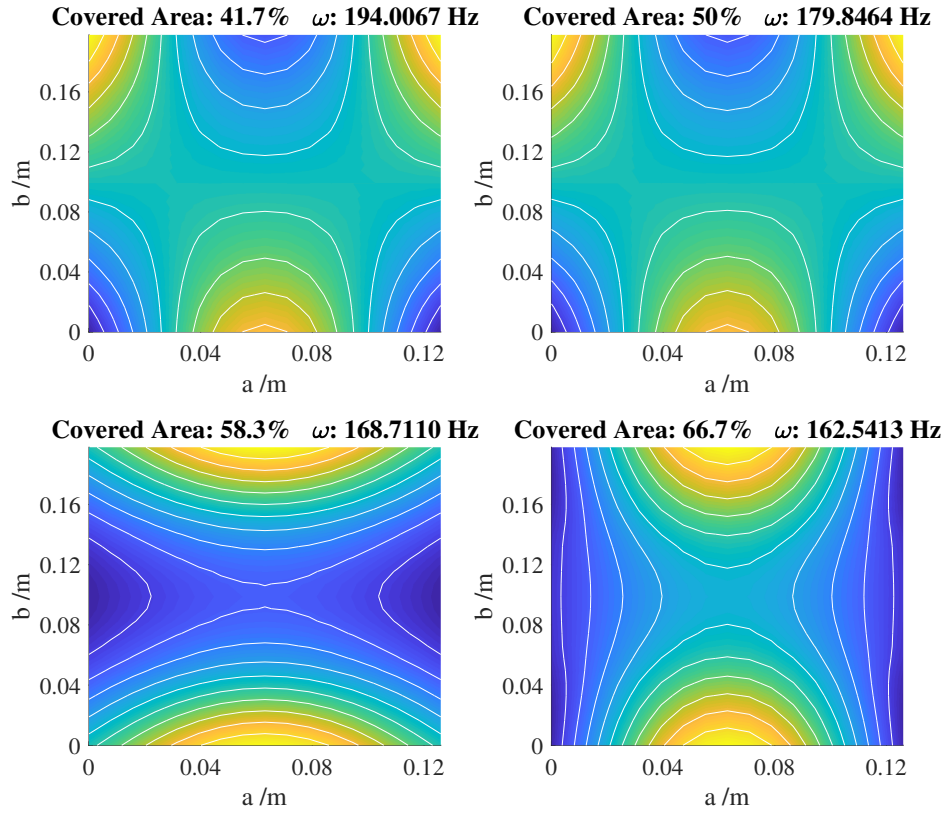
(b) Natural Frequency, ω.

Figure 5.11: Influence of the width increase from the edges to the center.

Figure 5.11b shows that, for 50% of covered area, several modes have close natural frequencies. Sometimes, when two modes present identical natural frequencies, switches between them occur: mode shapes switch order between two modes of vibration. For SMACWRAP® 0.2 mm configurations, this was not so evident for this SMACWRAP® 0.1 mm E-C configuration. Figure 5.12 presents the evolution of mode shapes between 41.7% and 66.7% covered area, exemplifying the switches.



(a) Second mode of vibration.



(b) Third mode of vibration.

Figure 5.12: Mode shapes between 41.7% and 66.7% covered area (switches between 50% and 58.3%).

In Figure 5.11b, this switch occurs when both modes of vibration have close natural frequencies and the tendency of natural frequency variation along with the covered area exchanges between them. In Figure 5.11b, this situation is observed when the same tendency of variation switch between modes, creating a maximum loss factor at 41.7% for Mode 2 and at 58.3% for Mode 3.

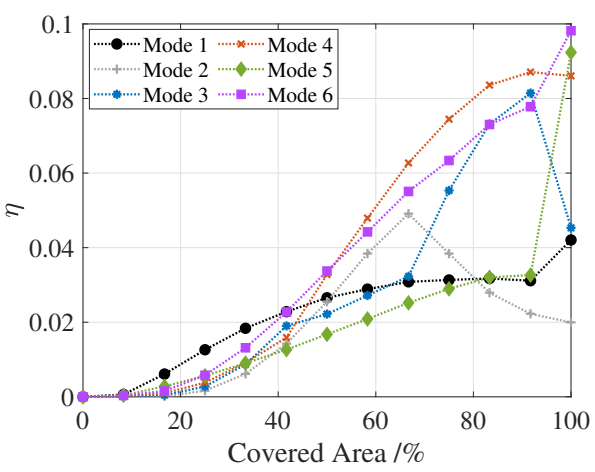
5.4.2 Width Increase from Center to the Edges - Configuration 1, C-E

Similarly to Section 5.3.2, on the following discussion the strips are at the center of the plate, with the stacking sequence of Figure 5.13.

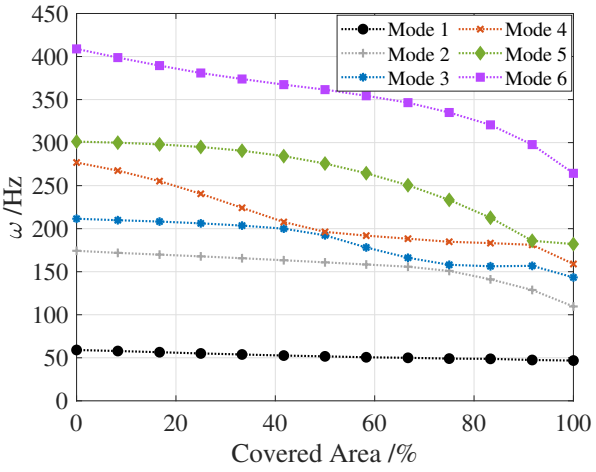
90º	90º	90º	90º
0º	VEM	VEM	0º
90º	90º	90º	90º
90º	90º	90º	90º
0º	VEM	VEM	0º
90º	90º	90º	90º

Figure 5.13: Stacking sequence and position with SMACWRAP® 0.1 mm strips and Configuration 1, C-E.

Once more, Figures 5.13a and 5.13b help to analyze another switch.



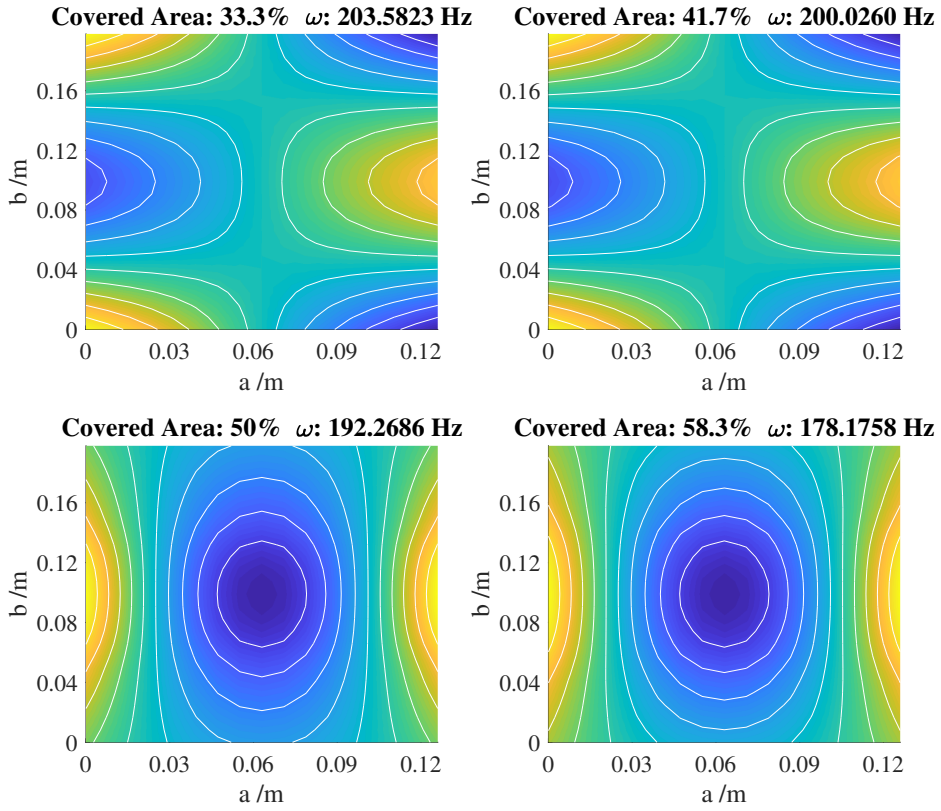
(a) Loss Factor, η.



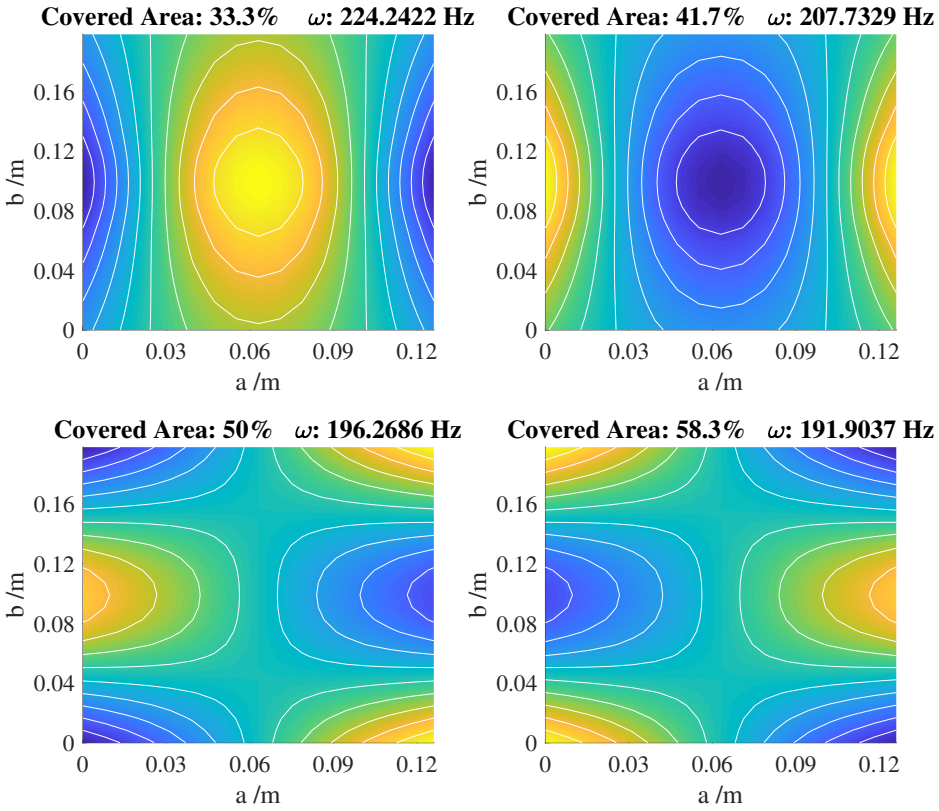
(b) Natural Frequency, ω_r.

Figure 5.13: Influence of the increase of width from the edges to the center.

Comparing both images, it is possible to conclude that, for covered areas between 33.3% and 58.3%, modes 3 and 4 present variations in the evolution of both loss factor and natural frequencies. Since the values of ω are close for those covered area ratios, it was verified that mode shapes switched between them (Figure 5.14), which affected the course of both parameters in this study. The switch occurs to close natural frequencies and the tendency of natural frequency variation along with the covered area switch. The variation of tendency is also observed in the loss factor evolution with covered area.



(a) Third mode of vibration.



(b) Fourth mode of vibration.

Figure 5.14: Mode shapes between 33.3% and 58.3% covered area (switches between 41.7% and 50%).

5.4.3 Discussion and Comparison of both Configurations

Figure 5.15 illustrates the comparison between the last two presented scenarios in terms of natural frequency and loss factor.

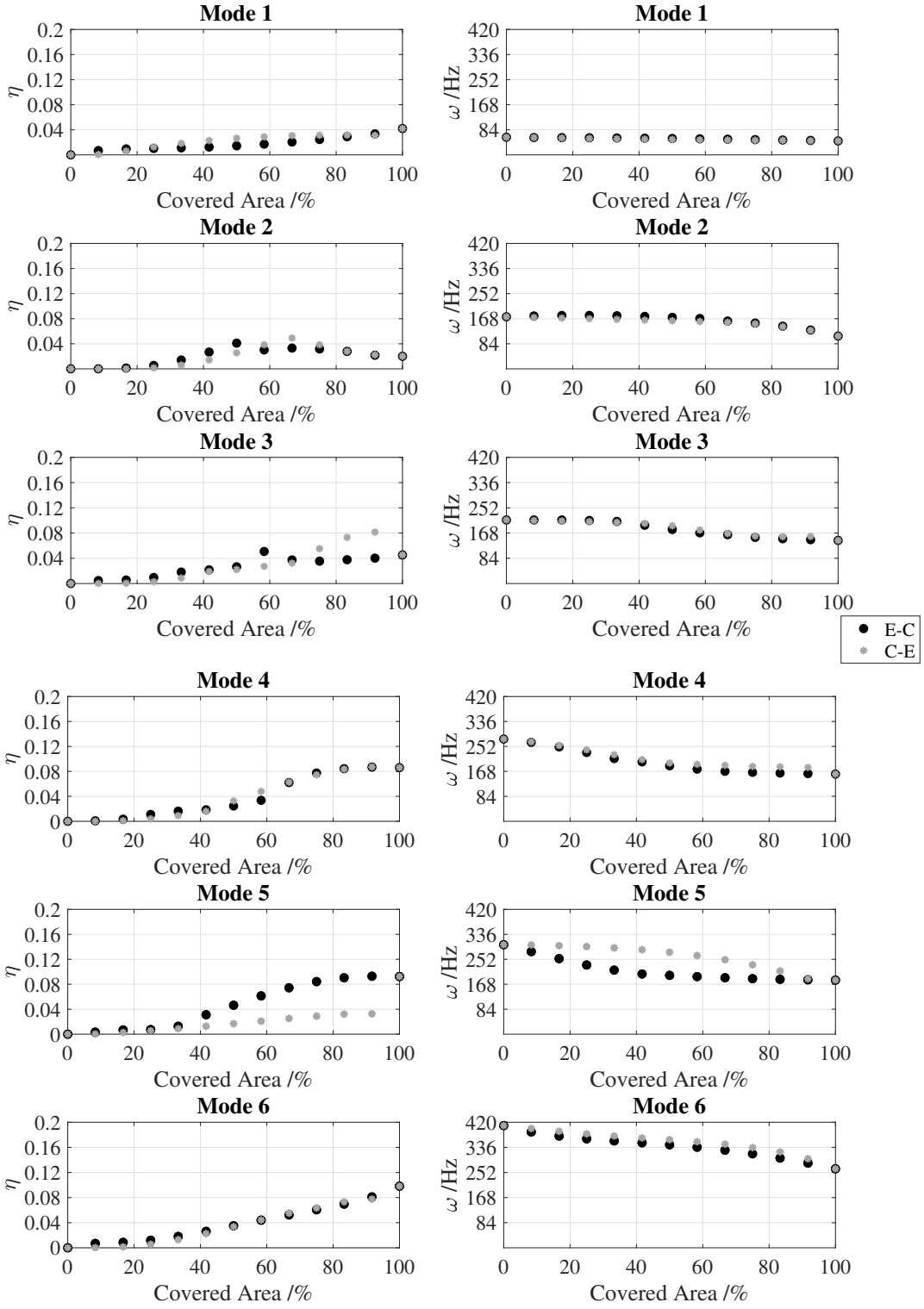


Figure 5.15: Comparison of loss factor and frequency between Configurations E-C and C-E using SMACWRAP ® 0.1 mm for the first six modes of vibration.

Unlike SMACWRAP ® 0.2 mm configurations, where E-C configuration offers better values of loss factor, here, there is not a prevalence of one configuration over the other one, although E-C is still dominant in some modes. The loss factor is not much higher for higher modes, in contrast with SMACWRAP ® 0.2 mm arrangements, on which the loss factor was often three or four times bigger in modes 5 and 6, in comparison with modes 1 or 2, for instance.

5.5 Notes and Remarks about Width and Location

The previous configurations present the same amount of viscoelastic material, but in different locations. The width varies, as well as the thickness, that is 0.2 mm in the first two scenarios, and 0.1 mm in the last two.

The loss factor benefits from the increase of VEM's quantity. It means that the structure has a better damping capacity. Nevertheless, sometimes, some partial damping treatments occasionally present better values of loss factor. Thus, despite a total damping treatment is the preferable situation to achieve the best loss factor values, it is not the best solution in all cases.

The analysis with the same material shows which one of the two configurations, in terms of location, is preferable. This discussion is presented in the sequence of the analysis of Figure 5.16.

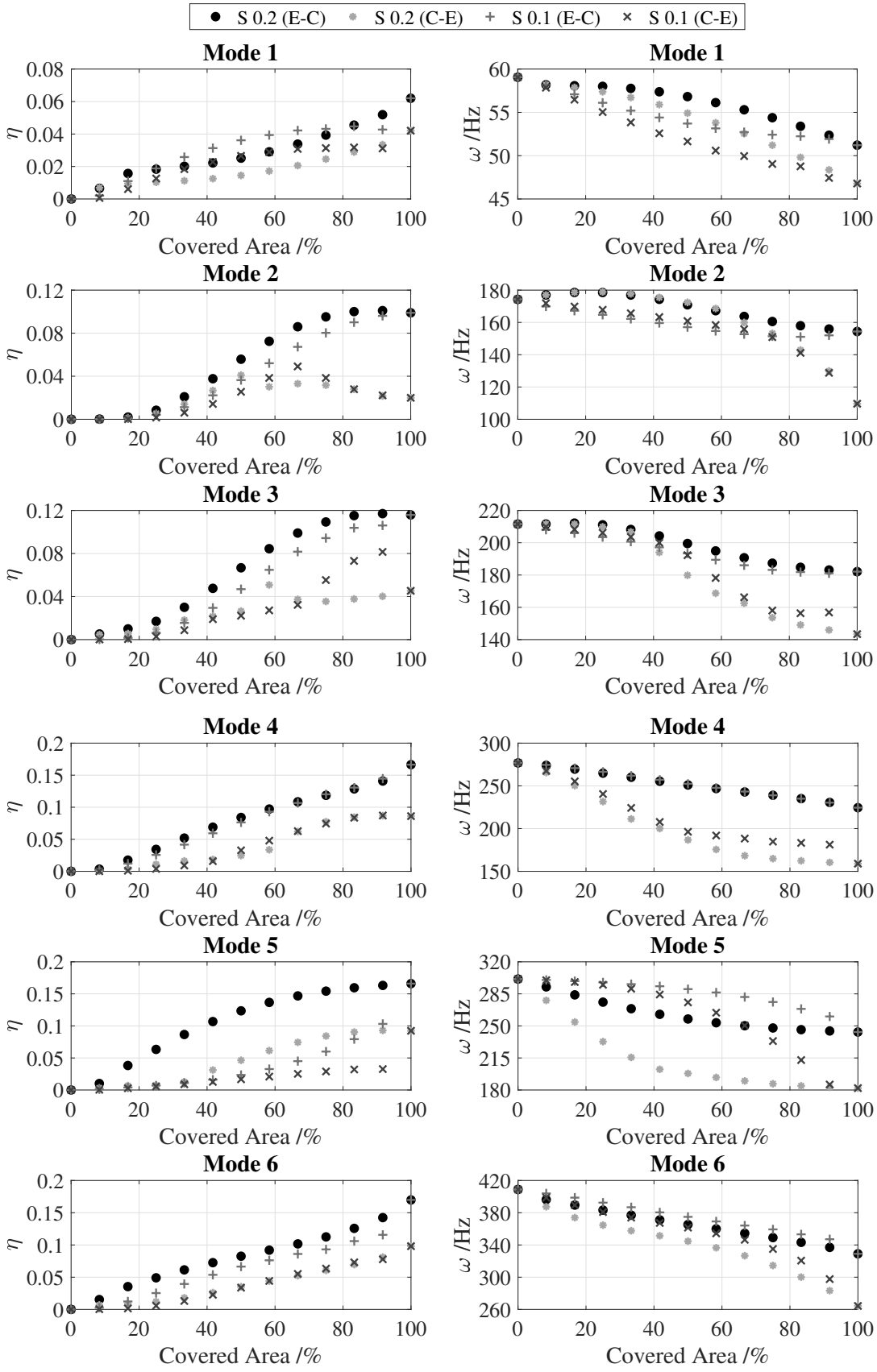


Figure 5.16: Comparison between SMACWRAP ® 0.2 mm (S 0.2) and SMACWRAP ® 0.1 mm (S 0.1) arrangements, in E-C and C-E configurations, in terms of natural frequency and loss factor.

Regarding the location of viscoelastic strips, both configurations with viscoelastic strips at the edges of the plate, E-C, reach higher values regarding the loss factor. For medium values of covered area, a higher quantity of viscoelastic material closer to the edges, promotes higher values of shear deformation energy.

In terms of thickness and position in the stacking sequence, SMACWRAP ® 0.2 mm arrangements proved to be advantageous. Despite some competition from SMACWRAP ® 0.1 mm E-C arrangements, the robustness of that treatment is clear for all modes. In this arrangement, the layer is at the middle plane, surrounded by a higher amount of composite material, which will help to produce quantity of shear deformation energy. So, SMACWRAP ® 0.2 mm with viscoelastic strips applied at the edges of the plate is the best arrangement of the studied ones. Besides that, this configuration does not present the worst stiffness loss, as it is shown in Figure 5.16.

Finally, regarding the width, total damping treatments are not always the best solution. Depending on the combination between the width and other parameters, it is possible to provide higher efficiency with partial damping treatments, saving costs and material. Besides that, mode shapes play a crucial role, as switching mode shapes between different modes of vibration also determine the value of the loss factor.

Table 5.2 enumerates the highest values of loss factor for each one of the six modes, considering the four studied arrangements and the respective covered area.

Table 5.2: Loss factor of the six modes of vibration for each arrangement.

	SMACWRAP ® 0.2 mm				SMACWRAP ® 0.1 mm			
Mode	E-C	Area %	C-E	Area %	E-C	Area %	C-E	Area %
1	0.0620	100	0.0620	100	0.0421	100	0.0420	100
2	0.1010	91.7	0.0989	100	0.0410	50	0.0491	66.7
3	0.1170	91.7	0.1159	100	0.0508	58.3	0.0815	91.7
4	0.1664	100	0.1664	100	0.0868	91.7	0.0871	91.7
5	0.1660	100	0.1660	100	0.0929	91.7	0.0923	100
6	0.1698	100	0.1698	100	0.0982	100	0.0982	100

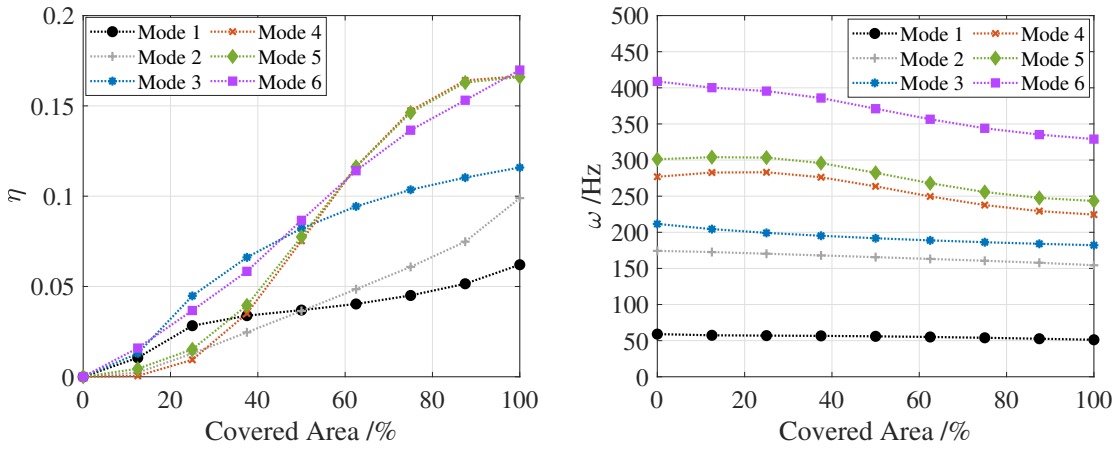
This table shows that configurations with SMACWRAP ® 0.1 mm promote loss factors that are approximately half of those promoted by SMACWRAP ® 0.2 mm configurations.

5.6 Position of the Viscoelastic Strips

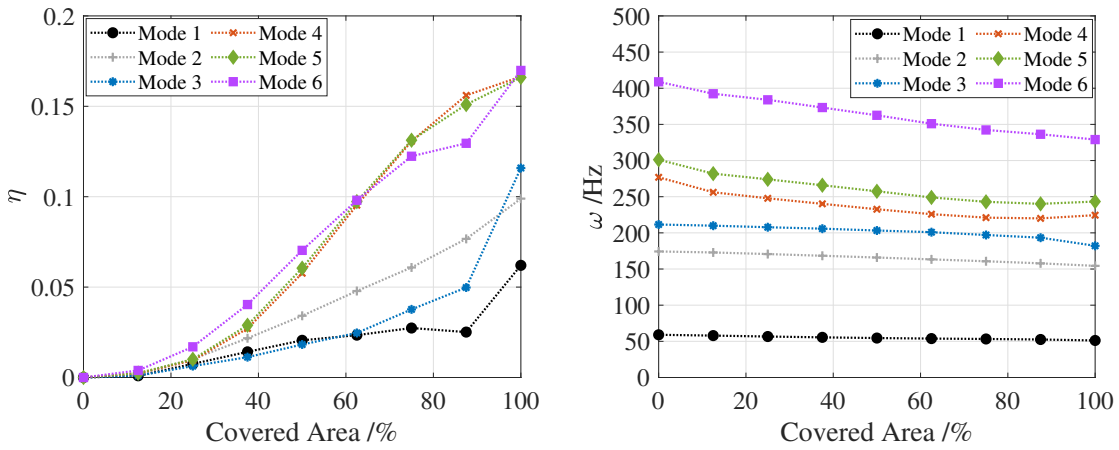
Until now, the application of the viscoelastic strips was at the larger sides of the rectangular plate. The purpose of this section is to study if the application along the smaller edges - as Figure 5.3 exemplifies - would promote any interesting change in the obtained loss factor values.

5.6.1 Width increase

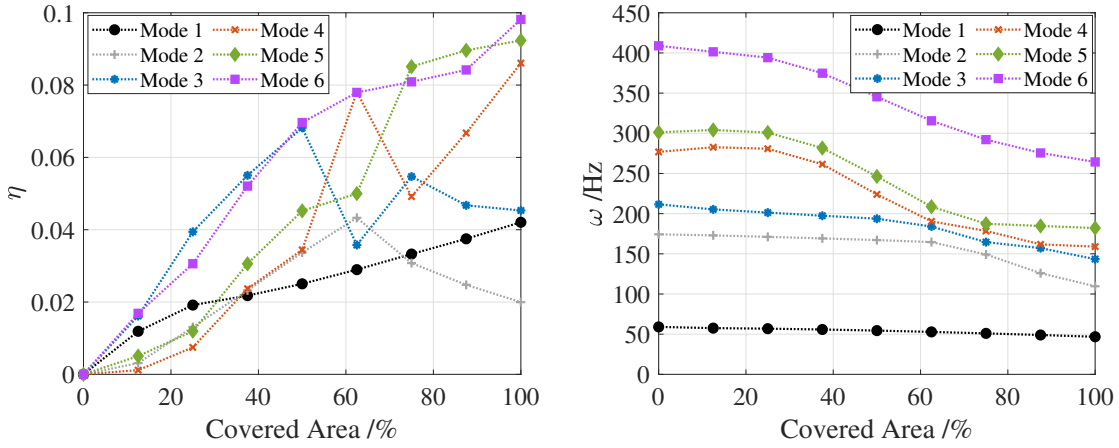
Figures 5.17a , 5.17b , 5.17c and 5.17d present an analysis to the ones from sections 5.3.1, 5.3.2, 5.4.1 and 5.4.2, respectively.



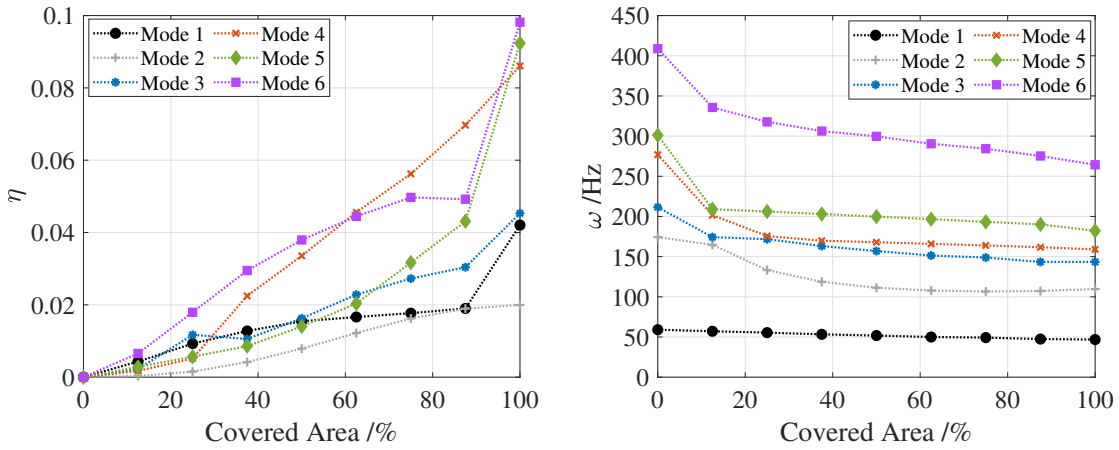
(a) Loss factor and natural frequency variation with width increase from the edges to the center and SMACWRAP ® 0.2 mm arrangement.



(b) Loss factor and natural frequency variation with width increase from center to the edges and SMACWRAP ® 0.2 mm arrangement.



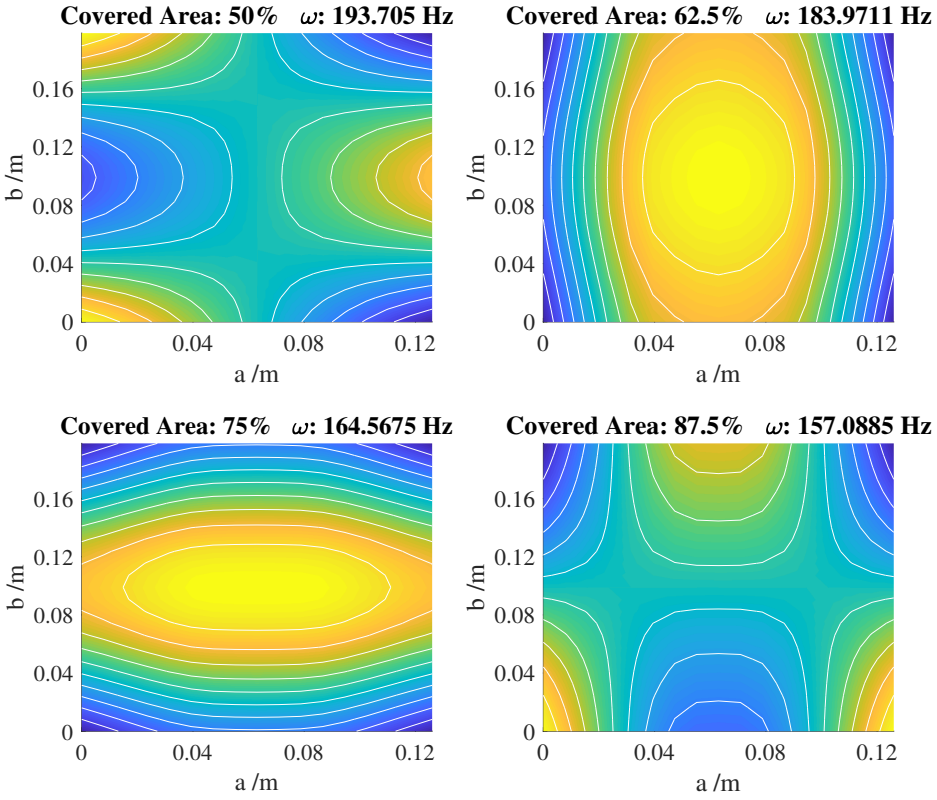
(c) Loss factor and natural frequency variation with width increase from the edges to the center and SMACWRAP ® 0.1 mm arrangement.



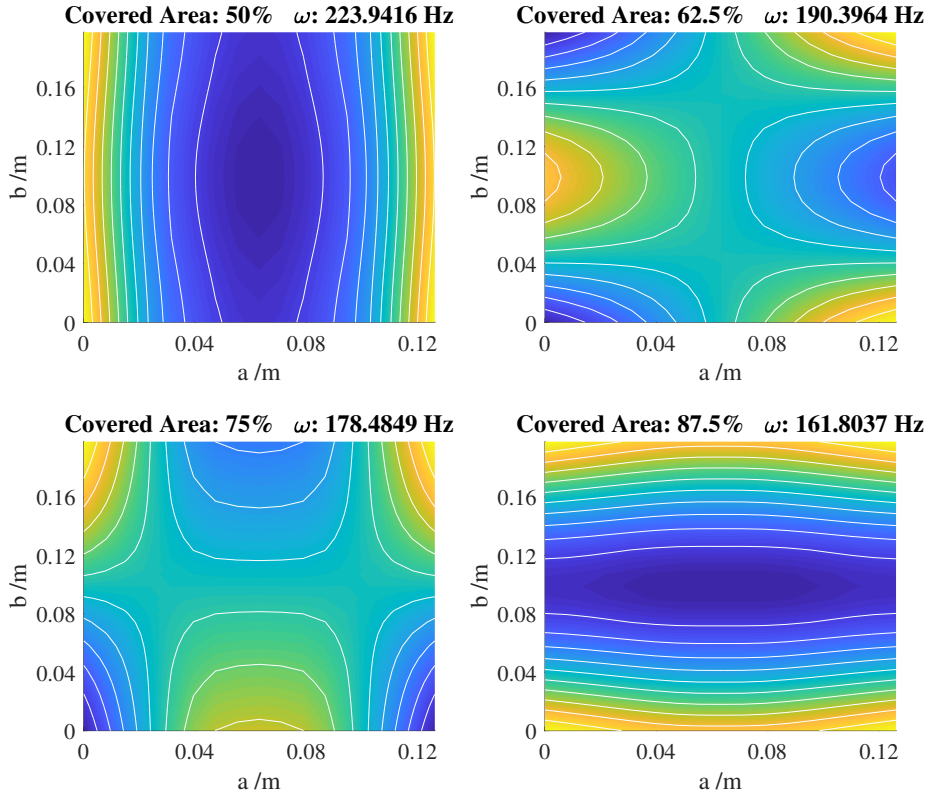
(d) Loss factor and natural frequency variation with width increase from center to the edges and SMACWRAP ® 0.1 mm arrangement.

Figure 5.17: Influence of width increase for viscoelastic strips along the shortest edges.

Once more, a comparison between some regions of the graphs suggests that mode shapes switch between them when the amount of viscoelastic material rises. Figure 5.17c presents that situation when the covered area varies between 50% and 87.5%, for the third and the fourth modes of vibration - as shown in Figure 5.18. Nevertheless, these changes only reinforce the idea that mode shapes influence decisively the value of the loss factor. For different modes, that switch is visible in the natural frequency curves, where it coincides with a continuation of the tendency of one mode's evolution in another mode evolution, and that switch occurs when both modes have similar natural frequencies.



(a) Third mode of vibration.



(b) Fourth mode of vibration.

Figure 5.18: Mode shapes between 50% and 87.5% covered area.

5.6.2 Remarks on the Location of Viscoelastic Strips

Tables 5.3 and 5.2 present the maximum loss factors for each case, when the viscoelastic strips are applied along the shortest or longest edges, respectively.

Table 5.3: Loss factor of the six modes of vibration for each arrangement.

	SMACWRAP ® 0.2 mm				SMACWRAP ® 0.1 mm			
Mode	E-C	Area %	C-E	Area %	E-C	Area %	C-E	Area %
1	0.0620	100	0.0620	100	0.0421	100	0.0420	100
2	0.0989	100	0.0989	100	0.0432	62.5	0.01997	100
3	0.1159	100	0.1159	100	0.0682	50	0.0453	100
4	0.1664	100	0.1664	100	0.0861	100	0.0861	100
5	0.1660	100	0.1660	100	0.0923	100	0.0923	100
6	0.1698	100	0.1698	100	0.0982	100	0.0982	100

In this last table, it is possible to conclude that the majority of the values are from total damping treatments. Even though there are some differences, in general, the only aspect influencing the value of the loss factor, concerning the position of the strips, is its location at the edges or at the center of the plate.

From now on, the stacking sequence is the one that is considered.

5.7 Influence of Viscoelastic Layer's Thickness

In this section, one focuses on the influence of the viscoelastic core's thickness. Table 5.4 presents the thickness, at each step, of viscoelastic core and orthotropic material.

Table 5.4: VEM thickess on each step.

Step	VEM thickness $/\times 10^{-3}$ mm	$\frac{h_{VEM}}{h_{Comp}}$	$\frac{h_{VEM}}{h_{total}}$
1	62.6	0.0909	8%
2	125	0.2	17%
3	187.6	0.3333	25%
4	250	0.5	33%
5	312.6	0.7142	42%
6	375	1	50%
7	437.6	1.4	58%
8	500	2	67%
9	562.6	3	75%
10	625	5	83%
11	687.6	11	92%

Using the SMACWRAP ® 0.2 mm arrangement, the evaluation of the thickness' influence considers viscoelastic strips at the edges of the plate is shown in Figure 5.19. The width of each viscoelastic strip is 49.5 mm.

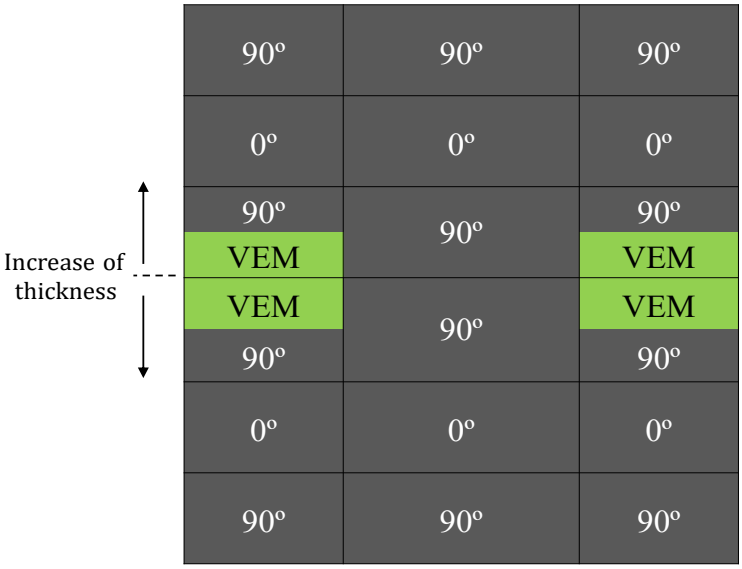


Figure 5.19: Stacking sequence and position of viscoelastic strips.

The analysis of the evolution of thickness through steps is presented in Figure 5.20. Each set of bars represents a ratio between the viscoelastic strip's thickness and the remaining thickness of the plate belonging to the composite material.

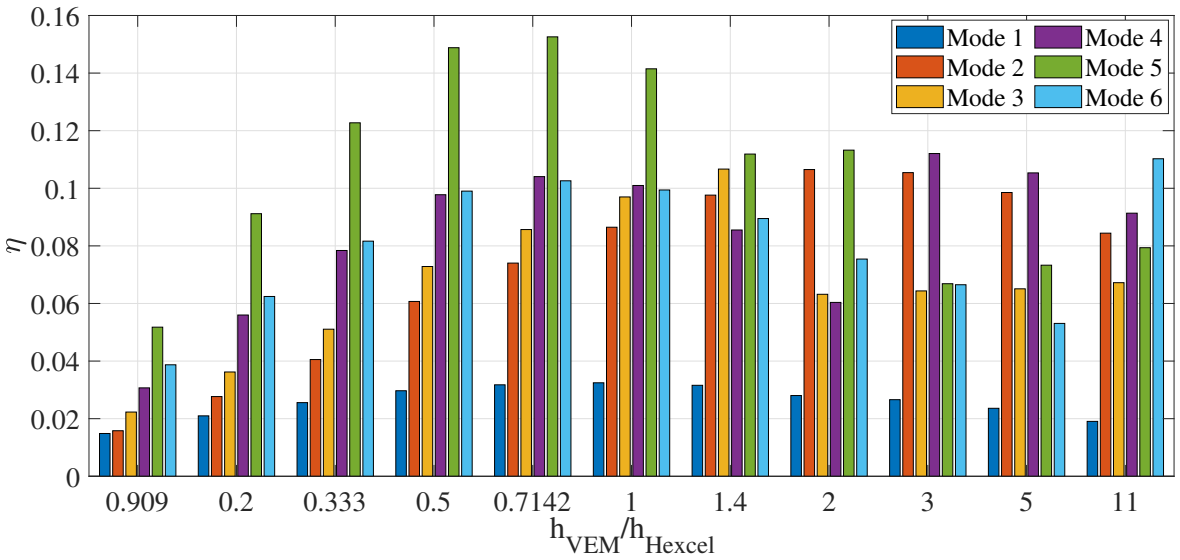


Figure 5.20: Thickness evaluation of thickness ratio, $\frac{h_{VEM}}{h_{Hexcel}}$.

The maximum value considered for the thickness ratio is 11. Before that value, except for the sixth mode of vibration, all the other modes present a maximum value of loss factor. This is not an objective analysis, as there are probably many values of thickness ratio that can present better values of loss factor, although Figure 5.20 shows that all the modes present, in that scenario, satisfactory damping capacities are reached when the thickness ratio takes values between 0.7142 and 1.4.

5.8 Fiber Orientation

Finally, after width, thickness and location, it is time to study the influence of the stacking sequence on the efficiency of the damping treatment. The wide range of configurations for a six-layer symmetric laminate composite plate does not allow an analysis that is similar to those that were carried out for the previous parameters. In order to overcome this difficulty, it is proposed a wise parametric method that simplifies the parametric studies on fiber orientation: the Layerwise Optimization Approach.

5.8.1 Layerwise Optimization Approach

Narita [2003] proposed this method to optimize vibration behavior, namely in order to maximize the fundamental frequency of laminated composite plates.

Several optimization techniques would be acceptable for this task. However, the high amount of design variables as those that are present at a stacking sequence optimization would be difficult for the analysis since it would take a high computation time.

This method is simple and effective. It is based on experimentation and physical observation of the behavior of a laminate composite plate subjected to bending. In laminate bending, the outer layer plays a more decisive role than the inner layer, as it has more stiffening effect, thereby, higher influence on the maximum natural frequency of the plate. Therefore, the fiber orientation of the outer layer is more decisive than the fiber orientation of the inner layer, so, it should be a priority in the design of the stacking sequence. The assumption of LOA is the following:

> *"The optimal stacking sequence for the maximum natural frequency of laminated plate can be determined sequentially in the order from the outermost to the innermost layer."*

Boundary conditions are important for the values of natural frequencies of flat plates, but LOA is independent of the methods for calculating natural frequencies. Thus, it can be applied to any method with no added restrictions.

Algorithm

Here, the design variables are a set of fiber orientation angles, each one corresponding to one of the N layers of the plate. This method requires the plate to be a symmetric laminate plate:

$$[\theta_1/\theta_2/\ldots/\theta_k/\ldots/\theta_N] \tag{5.1}$$

where θ_k is a fiber orientation angle in the k-th layer ($k = 1$ for the outermost layer until $k = N$ for the innermost one).

The algorithm is designed on the previous assumption and takes the following steps:

Initial step: Assume a laminate plate with $2N$ layers in total. There are only considered N layers in the upper or in the lower half of the plate. The elastic constant is $E = E_2$ in every direction.

Step 1: Find θ_1^{opt} in one-dimensional search. It corresponds to the fiber orientation of the outermost layer, $k = 1$, that guarantees the maximum fundamental frequency of the laminated plate with an orthotropic lamina in the outermost layer. The other layers remain with $E = E_2$.

Step 2 to Step N-1: Find each θ_k^{opt} in one-dimensional search. It corresponds to the fiber orientation of the k-th layer that guarantees the maximum fundamental frequency of the laminated plate with an orthotropic lamina in the outermost layer. The other inner layers remain with $E = E_2$.

Step N: Find θ_N^{opt} in one-dimensional search. It corresponds to the fiber orientation of the innermost layer, $k = N$, that guarantees the maximum fundamental frequency of the laminated plate.

This algorithm does not ensure that the final values are the global optimum ones, but it is expected to achieve close values. After an iteration of the algorithm is complete, it is necessary to repeat it until the convergence is verified. The Initial Step of the next iteration presents the stacking sequence from the last step of the last iteration. Thereby, the first step should find the optimal fiber orientation of the outermost layer and the inner layers must keep their properties and fiber orientations. Figure 5.21 illustrates this process.

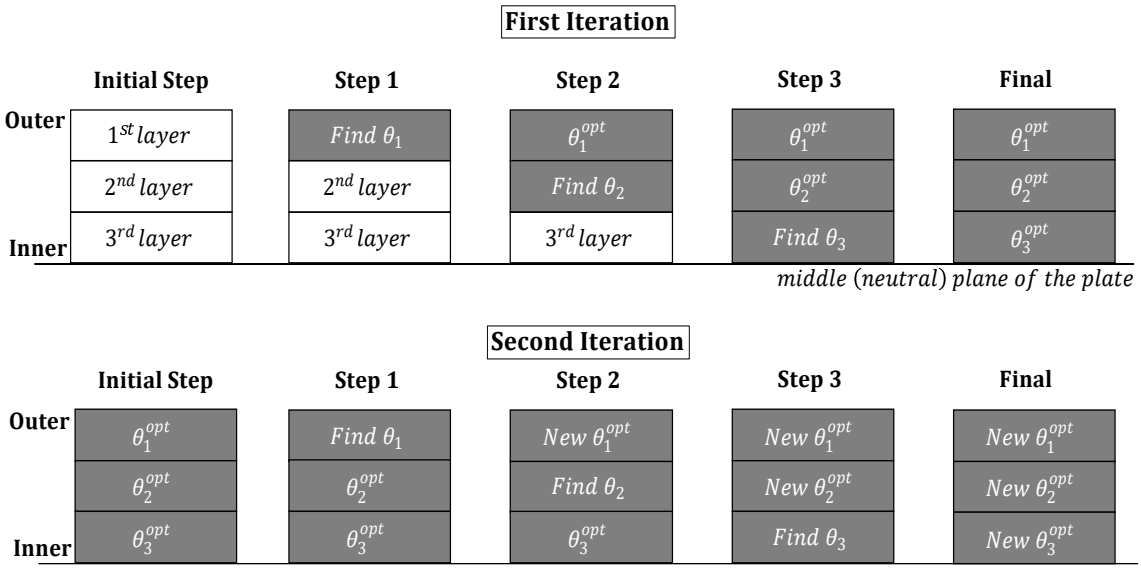


Figure 5.21: Layerwise Optimization Approach for a symmetric six-layered plate.

The shaded areas correspond to orthotropic layers with the properties of the considered orthotropic material (E_1, E_2), while white layers must consider the hypothetical properties (E_1=E_2) [Narita, 2003].

LOA with viscoelastic core

The shear energy of a laminate without viscoelastic core can be calculated as proposed by Li and Narita [2013]. The shear energy of a thin plate represents a small quantity when compared with in-plane energy. So, this last one has a higher influence on the total stored energy in the laminate. Thereby, it is possible to apply LOA with a viscoelastic core, without compromise the accuracy of the method [Li and Narita, 2013].

Results and Discussion

It is easy to understand that each mode has its optimal stacking sequence. Thereby, a stacking sequence provided by LOA does not fit as optimal for all modes. Thus, the FEM model has to give information about the mode of interest.

It was considered that the plate would have 50% of its area covered by viscoelastic material, in SMACWRAP ® 0.2 mm arrangement of Section 5.3.1. Firstly, it is analyzed the first mode of vibration, in order to find the best optimization sequence for the maximum natural frequency. The six fiber orientation angles are design variables, with $-90° \leq \theta_k \leq 90°$. To speed up this process, the method considers changing the fiber orientation angle in steps by 5° increments. For a six-layered symmetric plate:

$$\theta_1 = \theta_6$$
$$\theta_2 = \theta_5$$
$$\theta_3 = \theta_4$$

At the first step of the first iteration, Figure 5.22 represents the natural frequencies for stacking sequence $[\theta_1/0/0/0/0/\theta_6]$.

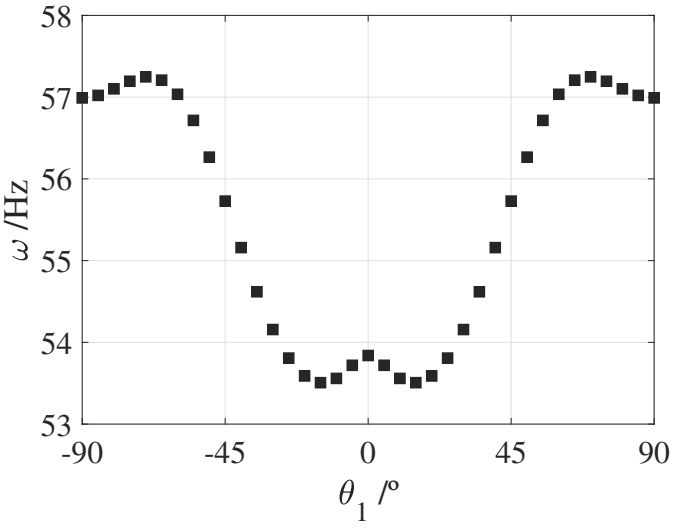


Figure 5.22: First step of the first iteration of Layerwise Optimization Approach.

Here, as the goal is to choose the maximum natural frequency value, the fiber orientation angle of the outermost layer is $\theta_1 = 70°$. This process is repeated until the end of an iteration. Then, a new iteration takes place and the algorithm is also repeated. Table 5.5 summarizes this process until convergence, when the covered area by VEM is 50%.

Table 5.5: Maximization of the fundamental natural frequency.

	Step 1		Step 2		Step 3	
	θ_1	$\omega^{(1)}$ /Hz	θ_2	$\omega^{(2)}$ /Hz	θ_3	$\omega^{(3)}$ /Hz
1^{st} iteration	70°	57.2480	-65°	101.4874	30°	106.1695
2^{nd} iteration	60°	111.4438	-65°	111.4438	20°	112.1303
3^{rd} iteration	60°	112.1303	-65°	112.1303		

Since the first two steps of the third iteration presented similar fiber orientations to the first two steps of the second iteration, the third iteration ends at the second step and the stacking sequence of the second iteration is the optimal one:

$$[60°/-65°/20°/20°/-65°/60°] \tag{5.2}$$

The optimization of the fundamental natural frequency does not guarantee the same for the loss factor. Nevertheless, this stacking sequence was studied and compared with the obtained values in Section 5.3.1 and the final results are on Table 5.6 (these values were obtained following the procedure of Section 5.3.1).

Table 5.6: Comparison of loss factors between original stacking sequence and optimal for natural frequency.

	[90°/0°/90°/90°/0°/90°]	[60°/-65°/20°/20°/-65°/60°]
Mode	η_{max}	η_{max}
1	0.0620	0.1243
2	0.1010	0.0655
3	0.1170	0.1071
4	0.1664	0.2022
5	0.1660	0.1849
6	0.1698	0.2088

Despite positive results in many modes, the second mode of vibration proves that the application of LOA requires an analysis for a specific mode because it is not possible to find a stacking sequence that is the optimal stacking sequence for all the modes. Moreover, it is not guaranteed that this loss factor value is the optimal one.

The algorithm considers the maximization of frequencies instead of the loss factor, even though its a way of searching for the maximum values may help on improving the efficiency of the damping treatment by choosing a proper fiber orientation sequence. Thus, instead of looking for the loss factor that corresponds to the maximum frequency, now, the loss factor is the parameter that is maximized. The basis of the algorithm remains the same. Table 5.7 has the results concerning this new approach, when the covered area by VEM is 50%.

Table 5.7: Maximization of the loss factor for the first mode of vibration.

	Step 1		Step 2		Step 3	
	θ_1	η	θ_2	η	θ_3	η
1st iteration	90°	0.0245	-60°	0.0390	15°	0.0399
2nd iteration	70°	0.0533	-65°	0.0556	20°	0.0556
3rd iteration	65°	0.0583	-65°	0.0583	20°	0.0583

The final stacking sequence is:

$$[65°/-65°/20°/20°/-65°/65°] \tag{5.3}$$

It is possible to say that optimizing the values of natural frequency does not imply a maximum for the loss factor. Table 5.8 shows the results, after the evaluation of both configurations with a width increase of the viscoelastic strips from the edges to the center, as done before.

Table 5.8: Comparison of loss factors between the optimized stacking sequence for maximum natural frequency and optimal stacking sequence for maximum loss factor.

	[60°/-65°/20°/20°/-65°/60°]	[65°/-65°/20°/20°/-65°/65°]
Mode	η_{max}	η_{max}
1	0.1243	0.1259
2	0.0655	0.0585
3	0.1071	0.1082
4	0.2022	0.1945
5	0.1849	0.1823
6	0.2088	0.2674

The analysis consists on the evaluation of the first mode of vibration. However, other modes have other stacking sequences that benefit its maximum loss factor. In that cases, LOA does its job, as it only focuses on the search of the maximum value of the parameter.

A different application of LOA was proposed by Narita [2006]. Here, the hypothetical layers (layers before a fiber optimization is ascribed) of the first iteration should be layers with mass but no stiffness. To verify if there were differences between the two ways of applying this method, a new iterative process was carried out and its results are in Table 5.9. In both cases, density has the same value.

Table 5.9: Maximization of the loss factor for the first mode of vibration, with hypothetical layers with mass but no stiffness.

	Step 1		Step 2		Step 3	
	θ_1	η	θ_2	η	θ_3	η
1st iteration	-45°	0.0294	60°	0.0449	10°	0.0253
2nd iteration	-70°	0.0516	65°	0.0544	-20°	0.0556
3rd iteration	-65°	0.0583	-65°	0.0583	-20°	0.0583

The final stacking sequence is:

$$[-65°/65°/-20°/-20°/65°/-65°] \tag{5.4}$$

There were no significant changes in the final values of the final loss factor, which shows that both considerations are acceptable.

The approach of Narita [2003] produced good results in the loss factor, even though the original purpose was to study maximum frequencies. It is almost sure that the final stacking sequence does not guarantee the highest loss factor. Indeed, its increment of 5° hides several configurations that potentially could offer better damping capacity, although the computational cost increases. This method is easy and fast, especially in a six-layered symmetric plate. However, bigger structures with more layers need improvements that bring an equilibrium between accuracy and computational cost.

5.8.2 Teaching Learning Based Optimization

One of the main concerns regarding the Layerwise Optimization Approach is its accuracy to maximize a parameter such as loss factor. Many optimization methods would give global optimum values for loss factor, but the reduced computational cost of LOA is an important advantage.

The Teaching Learning Based Optimization (TLBO) algorithm was proposed by Rao, R.V. [2011], and it is an evolutionary algorithm of easy comprehension that does not use gradients. It is based on the dynamic between the class and the teacher. The teacher is responsible for sharing the knowledge with the students, as well as guarantee the effectiveness of the message. However, the students learn at their velocity, so, each student catches a different amount of knowledge. Outside the classroom, the students share what they know and try to help their colleagues with less capacity to learn the subject. In the end, the population is evaluated.

Algorithm

In this method, a group of students - from now on, learners - are the population, while the different subjects are considered the design variables. The learner that has the best solution is considered the teacher.

The TLBO algorithm is divided in two parts: the Teacher's Phase where the teacher "exposes" the contents; and the Student's Phase, as a result of the interaction between learners. The algorithm is the following one:

Initial Step: Define the objective function and the restrictions. Define the size of the population - the number of learners - as well as the number of design variables - the number of subjects. It is also important to define the termination criterion (number of iterations, for instance).

The objective function is

$$\max \eta$$

subjected to

$$-90° \leq \theta_k \leq 90°$$

where θ_k, $k = 1, ..., 6$ is the fiber orientation of the k-th layer (k-th subject). The population size is 100, so, there are 100 stacking sequences - the learners. The termination criterion is the number of iterations, 50.

Step 1: Generate a random initial population.

Step 2: Calculate the value of the objective function, for each learner - evaluation of all learners. Here, each stacking sequence is put into test and the loss factor for 50% of covered area is registered.

After the initialization process, a random population is submitted to the Teacher's Phase. At this phase, some of the learners remain the same, as their performance in a certain subject is good, for now:

Teacher's Phase

Step 3: Choose the teacher. The teacher is the learner that provides (in a maximization problem) the maximum value of the objective function (i.e., loss factor).

Step 4: Calculate the mean values of each subject, of all learners - $Mean_k$. For the k-th angle, all the values that it takes in each stacking sequence are summed and then, its average value is calculated.

Step 5: The teacher tries to improve the results of the class, improving as much as possible the knowledge on each subject. For that, the mean difference between the teacher value at k subject and $Mean_k$ is given by:

$$Difference\ Mean_k = r_k \left(\theta_{Teacher,k} - T_F \times Mean_k\right) \tag{5.5}$$

where r_k is a random number in the range [0,1] for each subject k, $\theta_{Teacher,k}$ is the value of the teacher at subject k and T_F is a random teaching factor, given by:

$$T_F = 1 + rand(0, 1) \tag{5.6}$$

that represents the effectiveness of teaching some subject k.

Step 6: For each stacking sequence s (learner), sum the $Difference\ Mean_s$ with the fiber angle θ_k^s:

$$\theta_k^{s,new} = \theta_k^s + Difference\ Mean_s \tag{5.7}$$

Step 7: Calculate the new values of the objective function (i.e., the new values of loss factor) to each learner.

Step 8: Compare the generated population in Step 1 with the population in Step 7. As it is a maximization point, the stacking sequences to keep are the ones that provide, for each learner, the highest loss factor. It marks the end of the Teacher's Phase.

Following the Teacher's Phase, it is the Student's Phase:

Student's Phase

Step 9: Create interactions. At this phase, the students interact between them and exchange knowledge. Each one of the learners has to interact with, at least, one other learner (the learner is not able to interact with itself).

Step 10: Generate random numbers, r_P between [0,1] for each learner.

Step 11: Interactions. The knowledge is about to be exchanged. The learners affect the knowledge of a colleague. Here, each stacking sequence P interact with another stacking sequence Q that may have (or not) a better value for loss factor. At the end, a new group of stacking sequences is created. As it is a maximization problem, the new values for each fiber angle of the stacking sequence s=P are given by:

$$\theta_k^{P,new} = \theta_k^P + r_P \times \left(\theta_k^P - \theta_k^Q\right),\ if\ \eta_P > \eta_Q \tag{5.8}$$

or

$$\theta_k^{P,new} = \theta_k^P + r_P \times \left(\theta_k^Q - \theta_k^P\right),\ if\ \eta_Q > \eta_P \tag{5.9}$$

Step 12: Compare the created population at the end of Step 8 and the generated in Step 11. Again, for each learner, the stacking sequence to keep is the one that provides the highest loss factor. It marks the end of the Students' Phase.

With the end of the Student's Phase, a new iteration begins with the Teacher's Phase. Now, instead of a random population, the population that is going to be evaluated in Step 2 is the chosen population at the end of the Student's Phase of the previous iteration.

The purpose of this method in the current work is to analyze the accuracy of LOA and which adjustments should be done, to get that method closer to the optimal values. The study involved a population of 200 random stacking sequences (learners) with 50 iterations. The stacking sequence that may provide the optimal stacking sequence is:

$$[-60^\circ/68^\circ/71^\circ/71^\circ/68^\circ/-60^\circ] \tag{5.10}$$

Figure 5.23 shows the evolution of the maximum loss factor registered between all the 200 stacking sequences, at the end of each iteration (after Student's Phase).

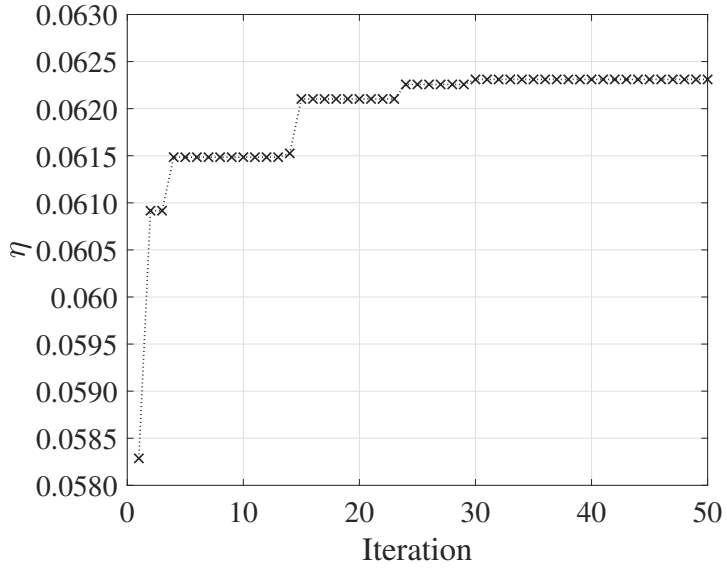


Figure 5.23: Convergence of loss factor with P_n=200 and 50 iterations.

The number of iterations is small, however, the variation between different values of loss factor decreased as the iterative process moved on. Besides that, the only purpose of this process was to validate the results obtained by the Layerwise Optimization Approach. This iterative process allows seeing that LOA provided a stacking sequence that does not give the maximum value. The TLBO method could provide better and more exact values. That process was also analyzed, but it does not have any practical interest, since it is impossible to ensure angles with such exactitude. Therefore, both methods assumed discrete values and it was possible to calculate the error of the process by the following ratio:

$$E_{opt} = \frac{|\eta_{max}^{LOA} - \eta_{max}^{\text{TLBO}}|}{\eta_{max}^{\text{TLBO}}} \times 100 \tag{5.11}$$

$$\therefore E_{opt} = \frac{|0.0583 - 0.0623|}{0.0623} \times 100$$

$$\therefore E_{opt} = 6.42\% \tag{5.12}$$

This error is pretty acceptable. The population size may compromise the accuracy of the results, so, this error may vary a little bit, however, the increment of LOA was 5°, so that the process can be fast. However, as LOA is a fast way to get values, there is enough room for maneuver.

Thus, it is possible to conclude that the differences in computational cost between LOA and TLBO are significant. LOA presented results at the end of the third iteration, while TLBO needed more. Therefore, Layerwise Optimization Approach is a much simple method with profitable results.

5.9 Optimized Stacking Sequence Analysis

LAO and TLBO considered a case where 50% of the plate is affected by a viscoelastic layer and the remaining does not. The aim is to study the effects of the optimization process in

other covered area scenarios. Figure 5.24 presents a comparison between the loss factor of the first mode of vibration.

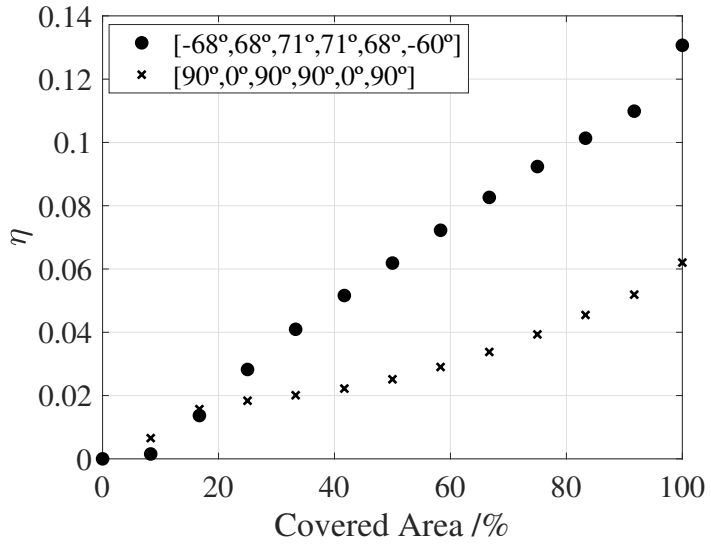


Figure 5.24: Comparison between the optimized configuration and the original configuration regarding loss factor.

The maximum value for the original stacking sequence was achieved with a total damping treatment. A similar loss factor can be now reached with a partial damping treatment with 50% covered area, by only changing the fiber orientation of the layers. Figure 5.25 establishes the relation between the updated and the outdated values of natural frequency.

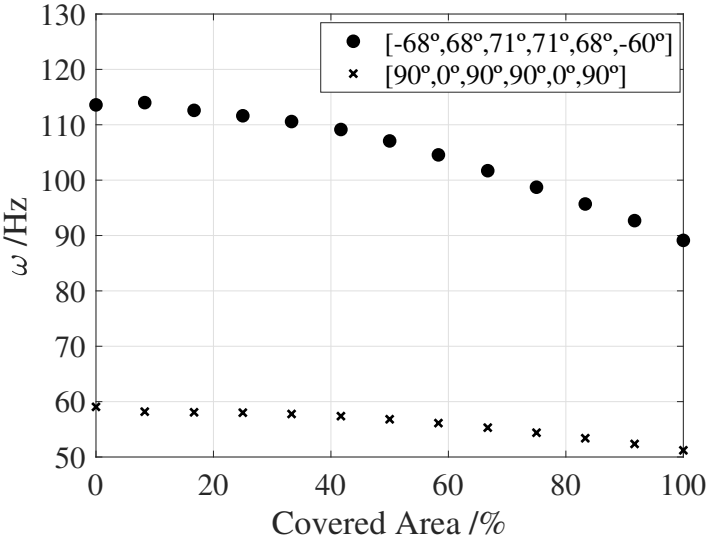


Figure 5.25: Comparison between the optimized configuration and the original configuration regarding natural frequency.

The covered area for which the maximum frequency is reached does not find correspondence in the covered area for the maximum loss factor. Indeed, they are on opposite sides: while the maximum frequency is achieved with 8.3% of covered area, the maximum

loss factor is registered for the total damping treatment. Both graphs are then interesting if a compromise between η and ω is important.

Chapter 6

Conclusion

6.1 Conclusions

Over the years, the use of damping accompanies the expansion of several industries, such as aeronautics, where lightweight structures play a prominent role. Passive damping devices allow the reduction of problems created by noise and vibrations, and viscoelastic damping treatments are a good example of them since they do not add a significant amount of mass to the structure.

According to the objectives, it was developed a dynamical analysis where experimental results are compared with numerical predictions in Chapter 5. This analysis involved seven plates with different types of damping treatments and materials.

Considering a total damping treatment with the plates with SMACWRAP ®, it was found that the 0.1 mm viscoelastic strip arrangement did not promote any significant effect. However, the verification by LAC showed that plates with viscoelastic strips of SMACWRAP ® with 0.1 mm thickness presented a worse correlation with the numerical FRF than those who had a viscoelastic strip of SMACWRAP ® with 0.2 mm thickness. Considering that, besides the thickness of the plate, the other parameter that varied between those plates was the location of the viscoelastic strip in the plate - in plates with SMACWRAP ® with 0.2 mm, the middle plane of the viscoelastic layer coincided with the middle plane of the viscoelastic strip - it is possible to state that next to the middle plane of the plate, the strip is more successful and provides a greater damping capacity to the plate. The higher shear strains next to the middle plane justify this observation.

Regarding partial damping treatments, they presented less satisfactory results. The FRF did not present the appearance of a plateau which may be an indicator of damping treatments, for instance. Instead, a greater number of resonance frequencies was present in the curves. LAC showed that the viscoelastic treatment promoted an increase in the correspondence between numerical FRF and experimental FRF, which was better for thicker plates. The plate with SMACWRAP ® with 0.1 mm partial damping treatment presented results that did not evidence the presence of damping, with a correlation with numerical values as poor as the reference plate's. In fact, the reference plate presented experimental FRF with a poor correlation level, as well as some partially damped plates.

Therefore, the total thickness of the plate influences the correspondence between the predicted and the experimental results, so, it was concluded that a minimum value of thickness should be established, from which the plates would present a better prediction and performance.

The comparison between plates with different viscoelastic materials is difficult, as properties are not identical. The analysis with the KRAIBON ® 0.5 mm plates presented a

worse LAC performance. Besides that, a comparison between SMACWRAP ® and KRAIBON ® configurations did not evidence lower magnitudes for this last one. So, configurations with KRAIBON ®, albeit produce thicker plates if a damping treatment is applied, did not bring advantages in the bandwidth [0,400] Hz.

Another important objective was to study the influence of some parameters in the behavior of the viscoelastic damping treatments: width, location and position of the viscoelastic strips, as well as the stacking sequence of the plate. In Chapter 6, the analysis considered only SMACWRAP ® to simplify the study.

The width variation, together with the location of the viscoelastic strips, configured the first study of the chapter. Two configurations were considered, based on the starting area of the width increase: if at the edge of the plate or at the center of the plate.

Typically, the maximum values of the loss factor occur when the plate presented a total damping treatment, but in some cases, the maximum loss factors were reached for partial damping treatments, when the viscoelastic strip was only partially integrated. Some of those cases coincided with the occurrence of switches, where two different modes, with nearby natural frequencies, within a range of covered area values, exchange their mode shapes between them. Thus, one of the modes assumes the mode shape of the other mode and vice versa. This configuration is kept until the end of the analysis (total damping treatment) or it could change sooner if another switch occurs.

Besides maximum values of loss factor with partial damping treatments, the analysis of natural frequency alongside the variation of the covered area also shows those switches. A "trend line" that united the discrete values of natural frequency, evidenced the evolution of the natural frequency value for all the modes. When the line exchanged its tendency with another line (another mode of vibration), both modes exchanged between them the configurations of their modes of vibration. This is a more accurate symptom of a switch if, in the loss factor, some sudden change in the trend line's slope happened.

As it was said before, configurations with viscoelastic strips next to the middle plane of the plate present better results. In addition, for an equal amount of material, placing the viscoelastic strips in the edges of the plate benefits the partial damping treatments. The reason for such phenomenon would be a greater amount of shear deformation energy that is generated in that areas. Between all the manufactured configurations, SMACWRAP ® 0.2 mm partial damping treatment is the most interesting.

About the efficiency of the damping capacity, it was possible to observe that, in general, and for each mode of vibration, as the percentage of the covered area raised, the mean value of the loss factor increased, as well as the mean value of natural frequency. For higher modes, the higher complexity of the mode shape pattern may promote the increase of the mean loss factor value.

The next study considered the position of the viscoelastic strips concerning the axis of the plate. Unlike a square plate, the direction of application of the viscoelastic strips could potentially bring some differences with impact in the final performance, but it was not the case. Although there are some differences, it was not proved that one direction of application is better than the other one, as the plates are relatively small.

Thickness was also another evaluated parameter. It was concluded that the maximum width values supported the raise of loss factor. However, it was not the case with thickness. The thickness ratio showed that many modes reached their maximum before the viscoelastic thickness was almost equal to the thickness of the plate, within defined geometrical properties. Thereby, an equilibrium between thickness and width would help the efficiency of damping treatments.

The last design parameter in the analysis was the fiber orientation. In fiber orientation

optimization, only the first mode of vibration was taken into account, because the aim was to appraise the evolution of the stacking sequence, instead of the behavior of the modes of vibration. A similar analysis to the previous ones would be cumbersome because there are many possible combinations and lots of time would be spent with no need.

So, a parametric method was used: the Layerwise Optimization Approach. The initial approach was focused on the maximization of the fundamental natural frequency, but it is not guaranteed that this would ensure the maximum loss factor.

It was observed that the maximization of the natural frequency promoted greater values of loss factor, but no considerations would be possible about if the maximum value was reached or not. Another analysis, where the loss factor was the parameter to be maximized (instead of the natural frequency), showed slightly, but not significant, changes in the stacking sequence, which means that this method could be used with the direct maximization of the loss factor.

Since nothing was established in the literature about the efficiency of the method for different approaches that did not consider natural frequencies, it was adopted an evolutionary optimization algorithm, the Teacher Learning Based Optimization, which allowed to study the evolution of the loss factor by an iterative process. The error was 6,42%, which demonstrates that the Layerwise Optimization Approach, after only three iterations, provided a good result to the loss factor, within restrictions, such as the increment of 5°. Indeed, this increment hides many possible stacking sequences. Therefore, lower increments would enable new and more advantageous stacking sequences, and LOA would satisfy the needs without significant computational costs, unlike optimization algorithms.

After all the evaluations, one improved scenario was studied and demonstrated that the loss factor almost doubled its value. The maximum natural frequencies occurred for partial damping treatments with a poor expression, where the loss factor is low. On the other hand, the loss factor reached the greatest values with total (and almost total) damping treatments, where the natural frequency registered its lowest values.

6.2 Future Work

To complement and improve the study hereby developed a few suggestions are proposed:

- Dynamical analysis of the non used halves to increase the robustness of the results;
- Manufacturing of test specimens considering the properties resulting from the efficiency parameter analysis and subsequent dynamical analysis;
- Implementation of the Improved Layerwise Optimization Approach, ILOA, proposed by Akoussan et al. [2017], which integers LOA in an algorithm of optimization, to improve and compare results and reinforce the application of LOA to the maximization of other parameters, besides natural frequency;
- Deepen the analysis about thickness, to get an optimum thickness ratio value that satisfies the needs, as well as find a relation between thickness and width of the viscoelastic strips;
- Manufacturing of a thicker reference plate for experimental validation of the influence of thickness in the coherence of the experimental results with the numerical ones;
- Understand if the direction of application of the viscoelastic strips influences the results in bigger plates;

- Evaluation of the shear deformation energy in the plate, to identify preferable locations of high concentration of energy, in order to improve damping efficiency;
- Study of other geometries, such as square plates, circular plates, or even shells, for instance;
- Analysis of other boundary conditions;
- Analysis with other types of laminates.

References

M. M. Agirre. *Experimental and numerical dynamic analysis of press-formed viscoelastic sandwich structures.* PhD thesis, Universidad de Mondragon, 2011.

A. Akay and A. Carcaterra. Damping mechanisms. In P. Hagedorn and G. Spelsberg-Korspeter, editors, *Active and Passive Vibration Control of Structures*, pages 259–299. Springer, Vienna, 2014.

K. Akoussan, H. Boudaoud, E. M. Daya, Y. Koutsawa, and E. Carrera. Sensitivity analysis of the damping properties of viscoelastic composite structures according to the layers thicknesses. *Composite Structures*, 149:11–25, 2016.

K. Akoussan, M. Hamdaoui, and E. M. Daya. Improved layer-wise optimization algorithm for the design of viscoelastic composite structures. *Composite Structures*, 176:342–358, sep 2017.

V. K. Bankar and A. S. Aradhye. A Review on Active, Semi-active and Passive Vibration Damping. *International Journal of Current Engineering and Technology*, 6(6):2187–2191, 2016.

A. M. Baz. In *Active and Passive Vibration Damping*, pages 1–10. John Wiley & Sons, Ltd, 2019.

D. D. Chung. Review: Materials for vibration damping. *Journal of Materials Science*, 36 (24):5733–5737, 2001.

L. Demasi. Partially layer wise advanced zig zag and HSDT models based on the generalized unified formulation. *Engineering Structures*, 53:63–91, 2013.

D. Granger and A. Ross. Effects of partial constrained viscoelastic layer damping parameters on the initial transient response of impacted cantilever beams: Experimental and numerical results. *Journal of Sound and Vibration*, 321(1-2):45–64, 2009.

Z. Gürdal, R. T. Haftka, and P. Hajela. *Design and optimization of laminated composite materials.* John Wiley & Sons, 1999.

L. Hazard. *Design of viscoelastic damping for vibration and noise control: modelling, experiments and optimisation.* PhD thesis, Université Libre de Bruxelles, 2007.

D. I. G. Jones. *Handbook of Viscoelastic Vibration Damping.* Wiley, 2001.

J. Li and Y. Narita. Analysis and optimal design for the damping property of laminated viscoelastic plates under general edge conditions. *Composites Part B: Engineering*, 45 (1):972–980, 2013.

K. M. Liew, Z. Z. Pan, and L. W. Zhang. An overview of layerwise theories for composite laminates and structures: Development, numerical implementation and application. *Composite Structures*, 216:240–259, 2019.

R. A. S. Moreira. *Modelação e análise de tratamentos viscoelásticos multi-camada para controlo passivo de vibrações*. PhD thesis, Universidade do Porto, 2004.

R. A. S. Moreira. Structural Dynamics and Viscoelastic Passive Damping Treatments. In J. P. Davim, editor, *Modern Mechanical Engineering: Research, Development and Education*, pages 89–107. Springer, Berlin, Heidelberg, 2014.

R. A. S. Moreira, J. D. Rodrigues, and A. J. M. Ferreira. A generalized layerwise finite element for multi-layer damping treatments. *Computational Mechanics*, 37(5):426, 2005.

Y. Narita. Layerwise optimization for the maximum fundamental frequency of laminated composite plates. *Journal of Sound and Vibration*, 263(5):1005–1016, 2003.

Y. Narita. Maximum frequency design of laminated plates with mixed boundary conditions. *International Journal of Solids and Structures*, 43(14-15):4342–4356, 2006.

A. D. Nashif, D. I. Jones, and J. P. Henderson. *Vibration damping*. John Wiley & Sons, 1985.

M. Okereke and S. Keates. *Mathematics of Element Formulation*, pages 187–241. Springer International Publishing, Cham, 2018.

E. Oñate. *Thick/Thin Plates. Reissner-Mindlin Theory*. Springer Netherlands, Dordrecht, 2013.

A. Preumont. *Introduction*, pages 1–19. Springer International Publishing, Cham, 2018.

T. Pritz. Analysis of four-parameter fractional derivative model of real solid materials. *Journal of Sound and Vibration*, 195(1):103–115, 1996.

V. Rao, R.V., Savsani, V.J. Teaching-learning-based optimization: A novel method for constrained mechanical design optimization problems. *Computer-Aided Design*, 43 (3): 303–315., 2011.

J. N. Reddy. *Mechanics of Laminated Composite Plates and Shells: Theory and Analysis, Second Edition*. CRC Press, 2003.

J. N. Reddy. *An Introduction to the Finite Element Method*. McGraw-Hill Education, 2005.

J. D. Rodrigues. *Apontamentos de Vibrações de Sistemas Mecânicos*. Faculdade de Engenharia da U.PORTO, PORTO, 2019 edition, 2019.

C. W. D. Silva. In C. W. D. Silva, editor, *Vibration Damping, Control, and Design*, pages 1–32. CRC Press LLC, 2007.

C. M. a. Vasques. *Vibration control of adaptive structures : modeling, simulation and implementation of viscoelastic and piezoelectric damping technologies*. PhD thesis, Universidade do Porto, 2008.

C. M. A. Vasques and L. C. Cardoso. Viscoelastic Damping Technologies: Finite Element Modeling and Application to Circular Saw Blades. In C. M. A. Vasques and J. Dias Rodrigues, editors, *Vibration and Structural Acoustics Analysis: Current Research and Related Technologies*, pages 207–264. Springer Netherlands, Dordrecht, 2011.

C. Xu, M.-Z. Wu, and M. Hamdaoui. Mixed integer multi-objective optimization of composite structures with frequency-dependent interleaved viscoelastic damping layers. *Computers & Structures*, 172:81–92, 2016.

L. Zhu, N. Li, and P. R. Childs. Light-weighting in aerospace component and system design. *Propulsion and Power Research*, 7(2):103–119, 2018.

Appendix A

Assembly

A.1 Introduction

Typically, each finite element has the same number of degrees of freedom at the nodes and the elementary matrix is a square matrix with as many rows (and columns) as degrees of freedom. The introduction of damping treatments brings extra degrees of freedom, since there are more layers to consider. This question becomes more complex when it comes to partial damping treatments, where each node may have degrees of freedom of two or more elements, without these belonging to all the elements simultaneously. The following example considers a beam, however, an identical scheme is applied to other structures, like plates.

A.2 Assembly

Consider the beam of length L with three linear beam finite elements - see FigureA.1. Element 1 and element 2 have partial damping treatments, while the third element does not have any treatment.

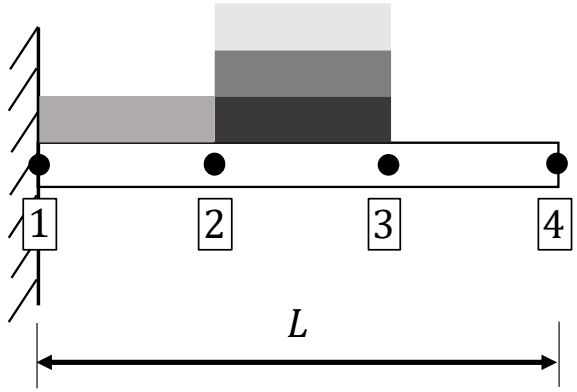


Figure A.1: Beam with partial damping treatments.

For each node i=1,2,3,4, the degrees of freedom are:

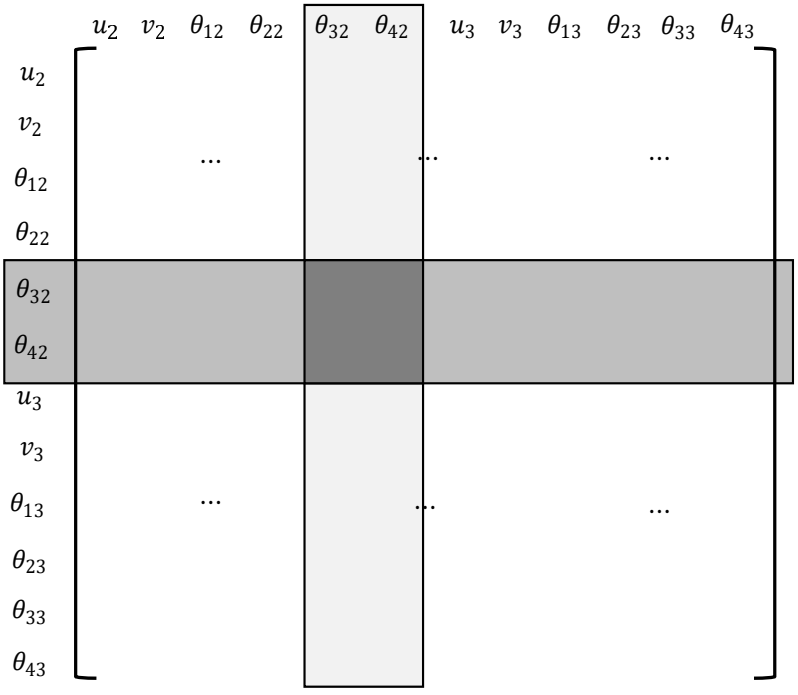
- Node 1: u_1, v_1, θ_{11}, θ_{21};
- Node 2: u_2, v_2, θ_{12}, θ_{22}, θ_{32}, θ_{42};
- Node 2: u_3, v_3, θ_{13}, θ_{23}, θ_{33}, θ_{43};

- Node 4: u_4, v_4, θ_{14}.

In beams, the reference layer have three degrees of freedom: two displacements and one rotation. When a layer is added, an extra rotation is also created. Thus, according to FigureA.1, element 1 has four degrees of freedom on each node. However, node 2 has five degrees of freedom, because this element characterizes a pile of two layers, beside the beam layer. The elementary matrix for element 1 is:

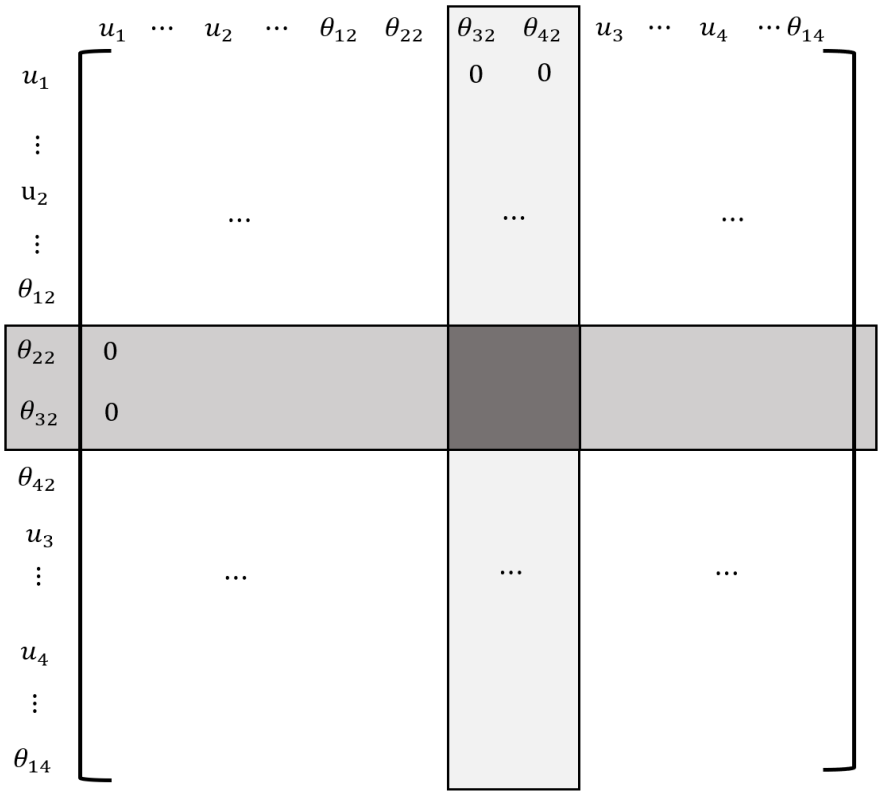
$$\begin{array}{c} \\ u_1 \\ v_1 \\ \theta_{11} \\ \theta_{21} \\ u_2 \\ v_2 \\ \theta_{12} \\ \theta_{22} \end{array} \begin{array}{c} \begin{array}{cccccccc} u_1 & v_1 & \theta_{11} & \theta_{21} & u_2 & v_2 & \theta_{12} & \theta_{22} \end{array} \\ \left[\begin{array}{cccccccc} & & & & & & & \\ & \cdots & & & \cdots & & \cdots & \\ & & & & & & & \\ & \cdots & & & \cdots & & \cdots & \\ & & & & & & & \\ & \cdots & & & \cdots & & \cdots & \\ & & & & & & & \end{array}\right] \end{array} \tag{A.1}$$

and for element 2 is:



(A.2)

Despite sharing node 2, θ_{32} and θ_{42} are not common to elements 1 and 2, since these degrees of freedom appears as a consequence of the number of layers that element 2 represents. Therefore, the assemble of this layers have to consider the existence of degrees of freedom that are not common to consecutive elements, hence, some coefficients are necessarily zero, as there is no interaction between some degrees of freedom:


u_1 ⋯ u_2 ⋯ θ_{12} θ_{22} θ_{32} θ_{42} u_3 ⋯ u_4 ⋯ θ_{14}
u_1
⋮
u_2
⋮
θ_{12}
θ_{22}
θ_{32}
θ_{42}
u_3
⋮
u_4
⋮
θ_{14}
0
0
0
0
...
...
...
...
...
...

(A.3)